Structural and Functional Studies of Peptide and Protein on Engineered Surfaces/Interfaces

by

Yaoxin Li

A dissertation submitted in partial fulfillment
of the requirements for the degree of
Doctor of Philosophy
(Chemistry)
in the University of Michigan
2017

Doctoral Committee:

Professor Zhan Chen, Chair
Professor Ari Gafni
Professor Robert T. Kennedy
Professor E. Neil G. Marsh

yaoxin@umich.edu

2017

ORCID iD: 0000-0002-1610-7326

Dedication

To my family

Acknowledgements

First and foremost, I would like to thank my advisor, Professor Zhan Chen, for his excellent support and guidance during my five-year PhD work. He granted me with enough research freedom by letting me think and work on multiple projects and helping me to build strong confidence and independence towards research discovery. He also provided me with extensive guidance when I had difficult times. His motivation will always inspire me with great enthusiasm. Without his help and support, I wouldn't have been able to finish this difficult journey to purse a doctorate degree and be a better scientist.

I would also like to thank my committee members, professors Neil Marsh, Robert Kennedy, and Ari Gafni. Thank you all for being my thesis committee members. I've gained so much biochemistry knowledge when I had the chance to rotate in professor Neil Marsh's lab. For professors Robert Kennedy, and Ari Gafni, it was a great pleasure for me to be a student in your class, where I learned a great deal.

I'm so grateful for my awesome lab mates. When I first joined the lab, Dr. Xiaofeng Han introduced the background and operation of SFG systems to me, which helped build solid fundamental knowledge. Dr. Chi (Jesse) Zhang gave me an extensive and detailed introduction of the physical background of nonlinear optics and SFG. I still remembered all his handwritings on the white board to make sure that I understood all of what he said. I appreciated the helpful discussion with Dr. Pei Yang, Dr. Lei Shen, and Dr. Bei Ding about data analysis. I'm thankful for Dr. Yuwei Liu's help to start my first project. I also appreciated Dr. Joshua Jasensky's help on

writing and very useful discussion on projects, and his generosity whenever I had a favor to ask for. Very special thanks to Dr. Xiaoxian Zhang both as a mentor and as a friend, who not only guided me on several projects as a senior scientist, but also helped me through very difficult times. I've had such a great time to work with all past and present Chen lab members that I overlapped with. It's a great honor to be a member of this group!

I'm very appreciated the help from all our collaborators outside the lab. A very large part of this thesis wouldn't have been completed without the contributions from professor Neil Marsh's lab in Chapter 2, 3, and 4. I had a wonderful opportunity to learn solid peptide synthesis from Dr. Benjamin Buer and Dr. Bishwajit Paul. Dr. Tadeusz Ogorzalek collaborated with me on the work presented in Chapter 3 and Dr. Somayesadat Badieyan in Chapter 4. Dr. Shuai Wei from professor Charles Brooks group collaborated with me on the coarse grained simulation presented in Chapter 2, and 3. Dr. Kenneth Cheng from professor Joerg Lahann lab provided the CVD surfaces and polymer brush samples in Chapter 5. Dr. Maggie Herron from professor Nicholas Abbott group performed the anti-bacterial tests in air presented in Chapter 4 and 5. Dr. Jianfeng Wu from professor Chuanwu Xi group collaborated with me on the anti-bacterial tests in Chapter 2. Thank you all so much for your contributions.

I'm grateful for the financial support from the Army Research Office (W911NF-11-1-0251), Defense Threat Reduction Agency (HDTRA1-11-1-0019), and National Science Foundation (CHE-1505385).

My undergraduate advisor, professor Weitai Wu, was the first to introduce me into research. I'm so thankful for his sincere support of my decision to study abroad and he granted me with such an opportunity to work on research projects, writing, and giving presentations before I came to

United States. This really helped me lay a good and solid foundation for my graduate work in US. His endless energy towards science encouraged me for further research after college.

Finally, I would like to thank my family; my parents, my parents-in-law, and especially my husband, Hongbo Zhu, for their support and encouragement. I'm so appreciative of my husband's bravery to start a new life in Ann Arbor after spending two years in Nebraska pursuing his master's degree. I always receive support and help from him no matter what the difficult situation I'm facing. He can always make things easier no matter what that is. And he can always cheer me up when I felt disappointed. Thank you so much for always being there for me!

Table of Contents

List of Figures

List of Tables

Abstract

Biomolecular decorated surfaces have shown great potential in many applications ranging from antimicrobial coatings to biosensing and biofuels due to their excellent properties. The performance of such biomolecular functionalized surfaces is largely dependent on the molecular structure of surface immobilized biomolecules, the surfaces used for attachment, and the surrounding environment biomolecules are functioning in. Moreover, maintaining the functions of such biomolecular surfaces in the absence of bulk water is challenging but important for extending the applications of such surfaces to non-aqueous environment. In order to have an in-depth understanding of how such biomolecule immobilized surfaces should be designed with optimized functions, molecular level characterization needs to be done to reveal the structures of interfacial biomolecules. Here my thesis research mainly focuses on the investigations of structures (conformations and orientations) of immobilized peptides and proteins at the molecular level using sum frequency generation vibrational spectroscopy (SFG), supplemented by circular dichroism (CD) and attenuated total reflectance-Fourier transform infrared spectroscopy (ATR-FTIR). The relations of structures and functions of the biomolecular surfaces are elucidated.

I first studied the effect of the immobilization site (e.g., N- or C-terminus) on the structure and activity of surface immobilized antimicrobial peptide (AMP) MSI-78 using a combination of SFG, CD, coarse grained MD simulation, and antibacterial testing. This peptide exhibits similar secondary structure but different orientations when immobilized with different termini, leading to varied antibacterial activity. In order to determine whether a peptide could be engineered to assume

a different orientation (standing up instead of lying down), a combined coarse grained MD simulation/SFG approach was developed to design AMPs with controlled orientations after surface immobilization.

To extend this research into more complicated systems, surfaces immobilized with enzymes were characterized using SFG and coarse grained MD simulation. Results show that not only can the orientation of these immobilized enzymes be controlled by selecting the surface immobilization site, but this surface orientation can dictate the enzymatic activity. The enzymatic activity is also affected by the property of the underlined surface for enzyme immobilization. With a more hydrophilic surface, a better enzymatic activity was observed.

Thirdly, methods of retaining the structure and function of immobilized biomolecules in the absence of bulk water were developed. Both native secondary structure and orientation of surface immobilized biomolecules can be retained and controlled by physically attached sugar coatings and chemically co-immobilized poly-saccharide molecules. Chemically tethered sugar was found to be able to enhance the antibacterial activity of immobilized AMPs in dry conditions.

Lastly, the interfacial structures of protein therapeutics adsorbed at the silicone oil surface are characterized by SFG. SFG signals contributed by both alpha helical and beta sheet structures were observed from proteins at the silicone oil surfaces. Nonionic surfactants are effective on reducing protein aggregations at such surfaces.

This thesis is collaborative in nature. Prof. Neil Marsh's group performed the enzyme engineering, and Prof. Charlie Brooks' group carried out the simulation. The antimicrobial activity measurements were done by Prof. Chuanwu Xi's group and Prof. Nick Abbott's group. The CVD coatings were made by Prof. Joerg Lahann's group.

This thesis provides a detailed and systematic study of how peptides and proteins behave on abiotic surfaces in different chemical environments. Methodologies on how to retain the structure and enhance the activity of surface immobilized peptides and proteins in the absence of bulk water have been developed.

CHAPTER 1 Introduction

The content in Chapter 1.1 has been adapted from the following manuscript which will be submitted in the future: **Li Y**, Jasensky J, Chen Z. Strategies of the Control in Structure and Behavior of Surface-Immobilized Peptides at Buried Interfaces.

1.1 MOTIVATION AND BACKGROUND

Immobilization of biomolecules on solid supports is essential for bio-functionalization of abiotic surfaces, which present versatile applications,[1] including a new generation of antibacterial surfaces,[2-4] antifouling coatings,[5] chemically selective biosensors,[6, 7] biochips,[8, 9] and optimized biofuel cells.[10, 11] Generally, surface immobilized biomolecule behavior and activity are influenced by the immobilized peptide/protein structure (e.g., conformation and orientation), which are mediated by the peptide/protein surface immobilization site, hydrophobicity of surface for immobilization, surface preparation, surrounding environment (e.g., medium to which surface immobilized biomolecules exposed), immobilization method, etc.[12-14] Therefore, a thorough and systematic understanding on peptide/protein immobilization surfaces in different conditions and how they are related to their behaviors and performance is critical. Such a wealth of information will help to design, develop, and control biomolecule immobilization surfaces with better and optimized performance.

Surface immobilized peptides and proteins can be used in many different environments, including those with no bulk water. When immobilized biomolecules are exposed to an environment with no bulk water, their functions are normally affected due

to structural changes.[15] To ensure that surface immobilized biomolecules are still active in the absence of bulk water, methods developed for the retention of protein and peptide conformation and function is extremely important but also very challenging.[11, 16-18] Such method development needs an in depth understanding of biomolecular interactions with surrounding environments,[14, 19-23] which will be investigated in detail in this dissertation.

Biomolecules have great potential in the pharmaceutical industry, since their high biocompatibility allows for the treatment of diseases with little side effects.[24, 25] However, protein tends to aggregate/adsorb at surfaces/interfaces, resulting in activity decrease or loss, especially on silicone oil surface, which is widely encountered by protein therapeutics in drug delivery devices.[26-31] Detailed structural information of protein molecules in this case is missing due to the lack of appropriate characterization methods to probe silicone oil/solution interfaces. Obtaining conformational information of protein aggregated/adsorbed at silicone oil surface *in situ* is very important, which will provide a fundamental and detailed molecular level understanding of protein behaviors at the silicone oil surface/interface. It is also crucial to elucidate the effects of surfactants, widely used in protein drug formulations to prevent and minimize protein aggregation at interfaces.[32-34] It will provide valuable guidance for formulation scientists about how surfactants affect protein adsorption on silicone oil surfaces and help find efficient ways to reduce such aggregations and increase the storage time of such protein therapeutics.

Many analytical tools have been used to study behaviors of biomolecules at surfaces/interfaces. Such surface sensitive techniques include secondary ion mass spectrometry (SIMS), X-ray photoelectron spectroscopy (XPS), atomic-force microscopy (AFM), surface plasmon resonance (SPR), and quartz crystal microbalance (QCM). SIMS

is a technique that uses a focused primary ion beam to sputter the sample surface and characterizes the secondary ions using mass spectrometry. XPS can quantitatively analyze the elemental composition of surface materials by irradiating the sample surface with X-ray beams. Both SIMS and XPS had been utilized to analyze adsorption, conformation, and orientation changes of biomolecules.[35-40] However, both techniques require high vacuum for signal collection, which then limits its application of studies on biomolecules at ambient and native conditions. AFM can probe the surfaces with high spatial resolution profile on the order of nanometers, and had also been applied to study protein adsorption, structure, and morphology.[41, 42] Both SPR and QCM can measure molecular adsorption and were applied to monitor the biomolecule adsorption on different substrate surfaces and biomolecule-substrate interactions *in situ*.[27, 43] However, none of these techniques can provide molecular structural information of biomolecules at surfaces/interfaces at ambient environment *in situ*. Therefore, a surface/interface sensitive technique with monolayer sensitivity and the capability to monitor molecular structural information is required to provide valuable information of biomolecules *in situ*. This technique will be discussed in Section 1.2.

In this thesis, I helped to address five key questions regarding interfacial biomolecule behaviors: (1) does surface immobilization of antimicrobial peptides (AMPs) through different termini affect immobilized peptide activity; (2) how does immobilization site and surface hydrophilicity affect the coverage and activity of surface immobilized enzymes; (3) can hydro mimetic molecules such as hydroxyl-rich polymers and sugars retain/improve the conformation and activity of immobilized AMPs in the absence of bulk water; (4) can surface immobilization of AMPs be extended to more practical surfaces,

such as reactive polymer films prepared using chemical vapor deposition (CVD); (5) how does the behavior of fusion proteins change at silicone oil interfaces, in the absence or presence of surfactants.

1.2 SUM FREQUENCY GENERATION VIBRATIONAL SPECTROSCOPY

Sum frequency generation vibrational spectroscopy (SFG) is the primary analytical tool used in this dissertation to study interfacial peptides and proteins. SFG is a nonlinear optical process, and has been extensively applied and developed to study polymers, lipid, and biomolecules at surfaces/interfaces *in situ*.[44-52] Complicated data analysis methods have also been developed to obtain molecular structural information from SFG spectra.[50, 53] A growing number of research groups have utilized this technique or combined this technique with other analytical methods to study different interfacial systems.

1.2.1 SFG Overview

SFG is a surface-specific second-order nonlinear optical technique that provides a vibrational spectrum of molecules at surfaces/interfaces.[54-56] SFG is a process (Figure 1.1a) in which two laser beams, one with a fixed visible frequency ω_{VIS}, the other one with a tunable IR frequency ω_{IR}, are overlapped spatially and temporally at a surface or interface. A third beam then is generated at a specific direction by phase matching conditions with a frequency at the sum of the two input beams: $\omega_{SFG} = \omega_{VIS} + \omega_{IR}$. The intensity of this generated beam is resonantly enhanced when the frequency of the tunable IR beam matches the vibrational mode of the molecules at the interface (Figure 1.1b). When the frequency of the IR beam is scanned over a defined region, SFG signals can be monitored against IR frequency, generating a vibrational spectrum of molecules at the interface with vibrational

peaks detected.[44] In general, as seen in Figure 1.1b, SFG can be considered as a combination of IR adsorption and Raman scattering. Therefore, only vibrational modes that are both IR- and Raman-active will be SFG-active. SFG can be used to probe a surface or an interface that is accessible to laser light, such as solid/air interface, solid/liquid interface, solid/solid interface, or air/liquid interface.

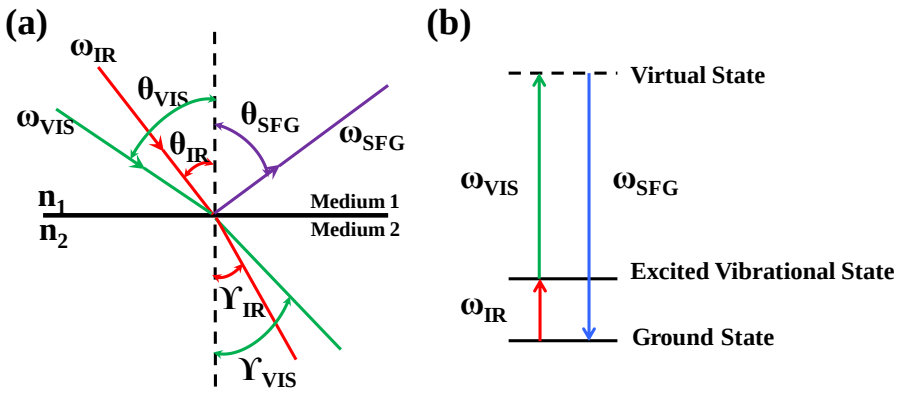

Figure 1.1 (a) The co-propagating non-collinear SFG geometry. (b) SFG energy level diagram of SFG process.

1.2.2 SFG Surface Specificity

The selection rule for the SFG process is different from linear vibrational spectroscopy. For the vibrational modes of molecules to be SFG active, the molecules must be in an asymmetric environment. Such asymmetric environment can be achieved by two methods: (1) an introduction of a surface into a medium breaks the centro symmetry of bulk materials; (2) surface molecules that have a net polar orientation. The physical properties behind can be explained by their selection rule. SFG intensity is proportional to the square of the second order nonlinear susceptibility, $\chi^{(2)}$, under the electric dipole approximation. In a centrosymmetric environment, all directions are equivalent: $\chi^{(2)}(r) = \chi^{(2)}(-r)$; moreover, $\chi^{(2)}$ is third rank tensor: $\chi^{(2)}(r) = -\chi^{(2)}(-r)$. To solve these two

equations, $\chi^{(2)} = 0$. Therefore, SFG is intrinsically surface and interface sensitive where centro symmetry is broken, and is forbidden in the centrosymmetric medium. As a result of this, only the molecules at surface/interface will be able to generate SFG signal, with background signals from the bulk medium effectively removed.

1.2.3 SFG Theory

SFG has been developed and discussed in great details in previous publications.[54, 55, 57-59]

In general, SFG intensity can be expressed as:[55]

$$I_{SFG} \propto \left|\chi_{eff}^{(2)}\right|^2 I_{IR} I_{VIS} \tag{1.1}$$

where I_{IR} and I_{VIS} are intensities of the input IR and visible beams, respectively. $\chi_{eff}^{(2)}$ is the effective second order nonlinear susceptibility.

After recording an SFG spectrum with a specific vibrational peak, $\chi_{eff}^{(2)}$ of the vibrational mode can be obtained by fitting the spectrum using the following equation:[55]

$$\chi_{eff}^{(2)} = \chi_{NR}^{(2)} + \sum_q \frac{A_q}{\omega_{IR} - \omega_q + i\Gamma_q} \tag{1.2}$$

where $\chi_{NR}^{(2)}$ is the nonresonant contribution from the sample or substrate, A_q is the amplitude of the vibrational mode, ω_q is the frequency, and Γ_q is the damping coefficient of the qth vibrational mode.

Each beam (two input beams and one output beam) can be adjusted to either s- or p-polarization, $\chi_{eff}^{(2)}$ with different polarization combinations can be experimentally measured by spectrum fitting.[55] Such SFG experiments with different polarization combinations can be used to deduce the orientation of surface immobilized molecules, which will be discussed later.

For an isotropic interface in the x-y plane (the plane of the interested or tested sample surface), the effective second order nonlinear susceptibility components can be related to the second order nonlinear susceptibility components in the lab-fixed coordinating systems,[55] as below:

$$\chi^{(2)}_{eff,ssp} = L_{yy}(\omega_{SFG})L_{yy}(\omega_{VIS})L_{zz}(\omega_{IR})\sin\theta_{IR}\,\chi^{(2)}_{yyz} \tag{1.3}$$

$$\begin{aligned}\chi^{(2)}_{eff,ppp} = &-L_{xx}(\omega_{SFG})L_{xx}(\omega_{VIS})L_{zz}(\omega_{IR})\cos\theta_{SFG}\cos\theta_{VIS}\sin\theta_{IR}\,\chi^{(2)}_{xxz} - \\ &L_{xx}(\omega_{SFG})L_{zz}(\omega_{VIS})L_{xx}(\omega_{IR})\cos\theta_{SFG}\sin\theta_{VIS}\cos\theta_{IR}\,\chi^{(2)}_{xzx} + \\ &L_{zz}(\omega_{SFG})L_{xx}(\omega_{VIS})L_{xx}(\omega_{IR})\sin\theta_{SFG}\cos\theta_{VIS}\cos\theta_{IR}\,\chi^{(2)}_{zxx} + \\ &L_{zz}(\omega_{SFG})L_{zz}(\omega_{VIS})L_{zz}(\omega_{IR})\sin\theta_{SFG}\sin\theta_{VIS}\sin\theta_{IR}\,\chi^{(2)}_{zzz}\end{aligned} \tag{1.4}$$

where θ_{SFG}, θ_{VIS}, and θ_{IR} are the output angle of SFG signal, input angle of visible beam, and input angle of IR beam relative to the surface normal, respectively. These angles are also labeled in Figure 1.1a. $\chi^{(2)}_{IJK}(IJK = x,y,z)$ s are the nonlinear second order susceptibility components of the material at the surface/interface defined in a lab-fixed coordinate system.[55] For an isotropic surface, only seven non-zero $\chi^{(2)}_{IJK}$ terms exist due to the selection rule. $L_{ii}(i = x,y,z)$'s are the Fresnel coefficients responsible for the local field correction. They are functions of reflected or refracted angles of input/output beams, and refractive indices of the materials forming the interface. Fresnel coefficients can be written as below:

$$L_{xx}(\omega) = \frac{2n_1(\omega)\cos\Upsilon}{n_1(\omega)\cos\Upsilon + n_2(\omega)\cos\theta}$$

$$L_{yy}(\omega) = \frac{2n_1(\omega)\cos\theta}{n_1(\omega)\cos\theta + n_2(\omega)\cos\Upsilon} \tag{1.5}$$

$$L_{zz}(\omega) = \frac{2n_2(\omega)\cos\theta}{n_1(\omega)\cos\Upsilon + n_2(\omega)\cos\theta}\left(\frac{n_1(\omega)}{n'(\omega)}\right)^2$$

where n' is the refractive index of the interfacial layer. In this thesis, we assumed that the interfacial refractive index is the average of the refractive indices of medium 1 and medium 2. Other angles were labeled in Figure 1.1b. Υ is the refractive angle that can be obtained through Snell's law:

$$n_1 \sin\theta = n_2 \sin\Upsilon \tag{1.6}$$

Then for $\chi^{(2)}_{IJK}(IJK = x, y, z)$, the nonlinear second order susceptibility component, can be related to the molecular hyperpolarizability, $\beta^{(2)}_{ijk}(ijk = a, b, c)$, through a coordinate system transformation:[57]

$$\chi^{(2)}_{IJK} = N\sum_{IJK=x,y,z}\langle R_{Ii}R_{Jj}R_{Kk}\rangle\,\beta^{(2)}_{ijk} \quad ijk = a, b, c \tag{1.7}$$

where N is the number of molecules at the surface/interface. R is the transformation matrix from the molecular frame (a, b, c) to lab frame (x, y, z). $\chi^{(2)}_{IJK}$, therefore, is then an ensemble average of the molecular hyperpolarizability with coordinate transformed.

The resonant part of $\beta^{(2)}_{ijk}$ is directly proportional to the product of the IR dipole (μ) derivative and the Raman polarizability (α) derivative of the vibrational mode Q as below:[53]

$$\beta^{(2)}_{ijk} \propto \frac{\partial\mu_i}{\partial Q}\frac{\partial\alpha_{jk}}{\partial Q} \tag{1.8}$$

this is also why in order to be SFG-active, the vibrational modes must be both IR-active and Raman-active.

1.2.4 Orientation Analysis of Peptides

The method of orientation analysis for peptide at surface/interface has been reported in previous publications.[50, 53] This method will be discussed briefly below.

Firstly, a theoretical orientation curve plotting $\chi^{(2)}_{zzz}/\chi^{(2)}_{xxz}$ as a function of tilt angle of immobilized peptides was generated. The tilt angle is defined as the angle between the main axis of a helix relative to the surface normal. Both amide I A mode and E_1 mode are SFG active. The dependence of $\chi^{(2)}_{xxz}$ and $\chi^{(2)}_{zzz}$ on molecular hyperpolarizability is described below:[53]

For the A mode,

$$\chi^{(2)}_{A,xxz} = \frac{1}{2}N_s[(1+r)\langle\cos\theta\rangle - (1-r)\langle(\cos\theta)^3\rangle]\beta_{ccc} \quad (1.9)$$

$$\chi^{(2)}_{A,zzz} = N_s[r\langle\cos\theta\rangle + (1-r)\langle(\cos\theta)^3\rangle]\beta_{ccc} \quad (1.10)$$

For the E mode,

$$\chi^{(2)}_{E,xxz} = -N_s[\langle\cos\theta\rangle - \langle(\cos\theta)^3\rangle]\beta_{aca} \quad (1.11)$$

$$\chi^{(2)}_{E,zzz} = 2N_s[\langle\cos\theta\rangle - \langle(\cos\theta)^3\rangle]\beta_{aca} \quad (1.12)$$

where β_{ccc} and β_{aca} are the molecular hyperpolarizability, N_s is number of tested alpha helices, θ is the angle between the alpha helical axis relative to the surface normal. Because of the limitation of the SFG spectral resolution, A mode and E_1 mode can't be resolved. The effective susceptibility is then assumed to be the sum of the susceptibilities of those two modes. For a perfect alpha helix with 18 residues, molecular hyperpolarizabilities were

deduced as: $r = {\beta_{aac}}/{\beta_{ccc}} = 0.59$ and ${\beta_{aca}}/{\beta_{ccc}} = 0.31$.[53] Therefore, we can deduce a theoretical curve of ${\chi^{(2)}_{zzz}}/{\chi^{(2)}_{xxz}}$ with orientation angle for a perfect alpha helix.

Secondly, ${\chi^{(2)}_{zzz}}/{\chi^{(2)}_{xxz}}$ can be experimentally measured from the tested peptide surfaces. By recording SFG spectra with both ssp (s-polarized SFG, s-polarized visible, and p-polarized IR) and ppp polarizations in amide I region and fitting the spectra using equation 1.2, ${\chi^{(2)}_{eff.ppp}}/{\chi^{(2)}_{eff,ssp}}$ ratios can be deduced.

As discussed in Section 1.2.3, ${\chi^{(2)}_{eff.ppp}}/{\chi^{(2)}_{eff,ssp}}$ can then be used to deduce the experimental ${\chi^{(2)}_{zzz}}/{\chi^{(2)}_{xxz}}$, by taking the Fresnel coefficient into consideration using equation 1.3 and 1.4. Here, by using the near-total-reflection geometry, the contributions from $\chi^{(2)}_{xxz}$, $\chi^{(2)}_{xzx}$, and $\chi^{(2)}_{zxx}$ in $\chi^{(2)}_{eff,ppp}$ can be neglected. Therefore, we assumed that $\chi^{(2)}_{eff,ppp}$ only originates from $\chi^{(2)}_{zzz}$.

The experiment obtained ${\chi^{(2)}_{zzz}}/{\chi^{(2)}_{xxz}}$ can then be used to determine the orientation of peptide at surface/interface by projecting this ratio to the theoretical calculated curve.

1.2.5 SFG Experimental Geometry

The visible beam and tunable IR beam go through one side of the prism, and overlapped spatially and temporally on the bottom side of the prism. The incident angles of visible and IR beam are 58/57° and 55°, separately relative to the surface normal to

achieve the near-total-reflection geometry. An SFG experimental geometry with prism as substrate is shown in Figure 1.2.

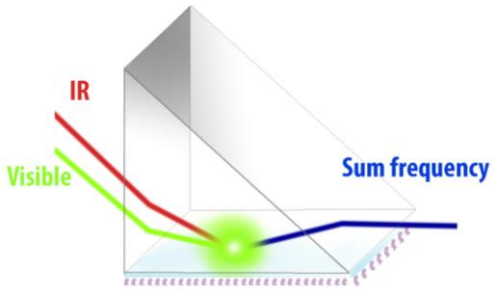

Figure 1.2 SFG experimental geometry using prism. The SFG signals can be collected from prism surface in air, liquid, or solid.

This thesis focuses on the behaviors of biomolecules at surfaces and interfaces. The amide I region, mainly 1500 cm^{-1}-1800 cm^{-1}, is the most important region studied. The substrate for this study should be background-free in this region. CaF_2 prism was chosen for this study because it's transparent for both visible and IR in this frequency region. In order to functionalize the CaF_2 prism surface with a self-assembled monolayer, a 100 nm silica coating was deposited on prism surfaces.

The general cleaning and coating process for substrate is: new CaF_2 prisms are soaked in toluene for 24 h and then sonicated in 1% Contrex AP solution for 10 mins. After this, the prisms are thoroughly rinsed with deionized water, dried under N_2 and then treated with O_2 plasma for 30 s immediately before being coated with SiO_2. A layer of 100 nm of SiO_2 is deposited onto the cleaned CaF_2 prism by an electron-beam deposition process. The SiO_2-cleaned CaF_2 prisms are cleaned under O_2 plasma for 3 min right before sample characterization.

1.3 PRESENTED RESEACH

In this thesis, the behaviors of biomolecules (peptide and protein) at surface/interface will be systematically studied in detail. In Chapter 2, SFG combined with CD, coarse grained simulation, and antibacterial tests will be applied to examine surface immobilized peptides. An understanding of how peptide structure and orientation after immobilization is related to its antibacterial function will be discussed. A coarse grained MD simulation method was developed and will be presented. It will provide valuable guidance on how to design peptide sequence with controlled orientation. Overall, molecular level understanding of interfacial peptide structures and orientations and its functions has been achieved.

More complicated biomolecules, enzymes, will be examined in Chapter 3 by SFG and ATR-FTIR, with the help of coarse grained MD simulation. A combination of SFG and coarse grained MD simulation will be applied to investigate surface-bound β-galactosidase. Studies of how engineering/immobilization site of enzymes and surface properties are related to enzymatic activity will be discussed. Moreover, orientations of immobilized haloalkane dehalogenase, deduced by SFG and ATR-FTIR, will be presented. The work done in Chapter 3 will help better understand the relations of enzyme behavior after surface immobilization and its functions on a molecular level. Additionally, a combination of SFG and ATR-FTIR further confirms that orientation of immobilized enzymes can be controlled by tailoring specific residues on the enzyme.

The development of hydro-mimetic strategies to retain structure, orientation, and function of immobilized biomolecules will be presented and discussed in Chapter 4 and Chapter 5. Understanding how physically attached sucrose by spin-coating influences

structural retention and systematically controlling orientations of immobilized biomolecules will be discussed in detail. Due to limitations of physically attached sugar molecules, new method of chemically tethered maltodextrin was developed and will be presented in Chapter 4. Additionally, a method to chemically tether sugar was also applied to immobilized peptide on polymer surfaces, and its effect on the function of such surfaces will be presented in Chapter 5.

Other than studies of surface immobilized biomolecules, behaviors of protein therapeutics in pharmaceutical industry on silicone oil surfaces will be examined using SFG in Chapter 6. The effects of non-ionic surfactants on the reducing of protein aggregation on silicone oil surface will also be discussed in detail. A molecular level understanding of protein structures on silicone oil surface has been achieved, which will provide important information in designing better delivery devices for such protein therapeutics with minimal structure distortion.

In summary, this thesis presents a detailed and systematical study of biomolecule behaviors on engineered surfaces in different environments. Important information obtained from this work will help better design and develop bio-materials functionalized surfaces with better performance, or optimized activity.

1.4 REFERENCES

1. F. Costa, I. F. Carvalho, R. C. Montelaro, P. Gomes and M. C. L. Martins, *Acta Biomaterialia*, 2011, **7**, 1431-1440.
2. K. Gregory and C. M. Mello, *Applied and environmental microbiology*, 2005, **71**, 1130-1134.
3. J. R. Uzarski and C. M. Mello, *Analytical chemistry*, 2012, **84**, 7359-7366.
4. J. R. Uzarski, A. Tannous, J. R. Morris and C. M. Mello, *Colloids and Surfaces B: Biointerfaces*, 2008, **67**, 157-165.

5. G. Cheng, H. Xue, G. Li and S. Jiang, *Langmuir*, 2010, **26**, 10425-10428.

6. W. H. Scouten, J. H. Luong and R. S. Brown, *Trends in biotechnology*, 1995, **13**, 178-185.

7. K. Hernandez and R. Fernandez-Lafuente, *Enzyme and microbial technology*, 2011, **48**, 107-122.

8. F. Rusmini, Z. Zhong and J. Feijen, *Biomacromolecules*, 2007, **8**, 1775-1789.

9. P. Jonkheijm, D. Weinrich, H. Schröder, C. M. Niemeyer and H. Waldmann, *Angewandte Chemie International Edition*, 2008, **47**, 9618-9647.

10. S. Calabrese Barton, J. Gallaway and P. Atanassov, *Chemical reviews*, 2004, **104**, 4867-4886.

11. S. D. Minteer, B. Y. Liaw and M. J. Cooney, *Current opinion in biotechnology*, 2007, **18**, 228-234.

12. Y. Liu, T. L. Ogorzalek, P. Yang, M. M. Schroeder, E. N. G. Marsh and Z. Chen, *Journal of the American Chemical Society*, 2013, **135**, 12660-12669.

13. L. Shen, M. Schroeder, T. L. Ogorzalek, P. Yang, F.-G. Wu, E. N. G. Marsh and Z. Chen, *Langmuir*, 2014, **30**, 5930-5938.

14. M. Goel, E. N. G. Marsh, Z. Chen and N. L. Abbott, *Langmuir*, 2014, **30**, 7143-7151.

15. P. Ball, *Chemical reviews*, 2008, **108**, 74-108.

16. T. Yagi, M. Tsuda, Y. Mori and H. Inokuchi, *Journal of the American Chemical Society*, 1969, **91**, 2801-2801.

17. S. Lamare and M. D. Legoy, *Biotechnology and bioengineering*, 1995, **45**, 387-397.

18. A. M. Klibanov, *Nature*, 2001, **409**, 241-246.

19. C. Mattos and D. Ringe, *Current opinion in structural biology*, 2001, **11**, 761-764.

20. L. L. Chang, D. Shepherd, J. Sun, D. Ouellette, K. L. Grant, X. C. Tang and M. J. Pikal, *Journal of pharmaceutical sciences*, 2005, **94**, 1427-1444.

21. A. Trivedi, A. Spiess, T. Daussmann and J. Büchs, *Applied microbiology and biotechnology*, 2006, **71**, 407-414.

22. J. H. Crowe, L. M. Crowe, J. F. Carpenter and C. A. Wistrom, *Biochemical Journal*, 1987, **242**, 1.

23. S. B. Leslie, E. Israeli, B. Lighthart, J. H. Crowe and L. M. Crowe, *Applied and environmental microbiology*, 1995, **61**, 3592-3597.

24. M. C. Manning, K. Patel and R. T. Borchardt, *Pharmaceutical research*, 1989, **6**, 903-918.

25. H. J. Lee, A. McAuley, K. F. Schilke and J. McGuire, *Advanced drug delivery reviews*, 2011, **63**, 1160-1171.

26. M. Soderquist and A. Walton, *Journal of Colloid and Interface Science*, 1980, **75**, 386-397.

27. P. Roach, D. Farrar and C. C. Perry, *Journal of the American Chemical Society*, 2005, **127**, 8168-8173.

28. K. Nakanishi, T. Sakiyama and K. Imamura, *Journal of Bioscience and Bioengineering*, 2001, **91**, 233-244.

29. R. K. Bernstein, *Diabetes care*, 1987, **10**, 786-787.

30. L. S. Jones, A. Kaufmann and C. R. Middaugh, *Journal of pharmaceutical sciences*, 2005, **94**, 918-927.

31. R. Thirumangalathu, S. Krishnan, M. S. Ricci, D. N. Brems, T. W. Randolph and J. F. Carpenter, *Journal of pharmaceutical sciences*, 2009, **98**, 3167-3181.

32. S. Mollmann, U. Elofsson, J. Bukrinsky and S. Frokjaer, *Pharmaceutical research*, 2005, **22**, 1931-1941.

33. J. S. Bee, T. W. Randolph, J. F. Carpenter, S. M. Bishop and M. N. Dimitrova, *Journal of pharmaceutical sciences*, 2011, **100**, 4158-4170.

34. N. Dixit, K. M. Maloney and D. S. Kalonia, *International journal of pharmaceutics*, 2012, **429**, 158-167.

35. E. Vanea and V. Simon, *Applied Surface Science*, 2011, **257**, 2346-2352.

36. L. Baugh, T. Weidner, J. Baio, P. C. Nguyen, L. J. Gamble, P. S. Stayton and D. G. Castner, *Langmuir: the ACS journal of surfaces and colloids*, 2010, **26**, 16434.

37. M. Henry, C. Dupont-Gillain and P. Bertrand, *Langmuir*, 2003, **19**, 6271-6276.

38. M. S. Wagner, S. L. McArthur, M. Shen, T. A. Horbett and D. G. Castner, *Journal of Biomaterials Science, Polymer Edition*, 2002, **13**, 407-428.

39. J. J. Gray, *Current opinion in structural biology*, 2004, **14**, 110-115.

40. J. B. Lhoest, E. Detrait, P. Van Den Bosch De Aguilar and P. Bertrand, *Journal of Biomedical Materials Research Part A*, 1998, **41**, 95-103.

41. S. E. Woodcock, W. C. Johnson and Z. Chen, *Journal of colloid and interface science*, 2005, **292**, 99-107.

42. Y.-P. Yang and C.-C. Lin, *Biomedical Engineering: Applications, Basis and Communications*, 2009, **21**, 311-316.

43. H. Mozsolits and M. I. Aguilar, *Peptide Science*, 2002, **66**, 3-18.

44. Z. Chen, Y. Shen and G. A. Somorjai, *Annual review of physical chemistry*, 2002, **53**, 437-465.

45. G. Richmond, *Chemical reviews*, 2002, **102**, 2693-2724.

46. M. Xiao, X. Zhang, Z. J. Bryan, J. Jasensky, A. J. McNeil and Z. Chen, *Langmuir*, 2015, **31**, 5050-5056.

47. X. Zhang, Y. Li, J. M. Hankett and Z. Chen, *Physical Chemistry Chemical Physics*, 2015, **17**, 4472-4482.

48. J. Wang, C. Chen, S. M. Buck and Z. Chen, *The Journal of Physical Chemistry B*, 2001, **105**, 12118-12125.

49. J. A. Mondal, S. Nihonyanagi, S. Yamaguchi and T. Tahara, *Journal of the American Chemical Society*, 2010, **132**, 10656-10657.

50. A. P. Boughton, P. Yang, V. M. Tesmer, B. Ding, J. J. Tesmer and Z. Chen, *Proceedings of the National Academy of Sciences*, 2011, **108**, E667-E673.

51. J. Kim and G. A. Somorjai, *Journal of the American Chemical Society*, 2003, **125**, 3150-3158.

52. S. Ye, H. Li, W. Yang and Y. Luo, *Journal of the American Chemical Society*, 2014, **136**, 1206-1209.

53. K. T. Nguyen, S. V. Le Clair, S. Ye and Z. Chen, *The journal of physical chemistry. B*, 2009, **113**, 12169.

54. Y. Shen, *Nature*, 1989, **337**, 519-525.

55. X. Zhuang, P. Miranda, D. Kim and Y. Shen, *Physical Review B*, 1999, **59**, 12632.

56. C.-S. Hsieh, R. K. Campen, A. C. V. Verde, P. Bolhuis, H.-K. Nienhuys and M. Bonn, *Physical review letters*, 2011, **107**, 116102.

57. A. J. Moad and G. J. Simpson, *The Journal of Physical Chemistry B*, 2004, **108**, 3548-3562.

58. C. Hirose, H. Yamamoto, N. Akamatsu and K. Domen, *Journal of physical chemistry*, 1993, **97**, 10064-10069.

59. C. Hirose, N. Akamatsu and K. Domen, *Applied Spectroscopy*, 1992, **46**, 1051-1072.

CHAPTER 2 Antimicrobial Peptide Immobilization on SAMs

The contents in Section 2.1 have been adapted with permission from the following publication: **Li Y**, Wei S, Wu J, Jasensky J, Xi C, Li H, Xu Y, Wang Q, Marsh ENG, Brooks CL III, Chen Z. Effects of Peptide Immobilization Sites on the Structure and Activity of Surface-Tethered Antimicrobial Peptides. *J. Phys. Chem. C* **2015**, 119:7146–7155. Copyright 2017 American Chemical Society.

The contents in Section 2.2 have been adapted from the following manuscript which will be submitted in the future: Wei S, **Li Y**, Zou X, Chen Z, Brooks CL III. Orientation Control of Surface Immobilized Peptides.

2.1 EFFECTS OF PEPTIDE IMMOBILIZATION SITES ON THE STRUCTURE AND ACTIVITY OF SURFACE-TETHERED ANTIMICROBIAL PEPTIDES

2.1.1 Introduction

Infection is not only the most common problem caused by implanted or indwelling medical devices, but it can be life-threatening to patients.[1] On average, every person in modern society will have a medical implantation at least once in his/her lifetime.[2] Therefore such infections have huge impact and should either be minimized or prevented entirely. Infections resulting from these indwelling or implanted devices occur because bacterial adhesion, growth, and proliferation lead to biofilm formation on the surfaces of these medical devices (such as urinary or venous catheters, contact lenses, orthopedic implants and stents, or even joint replacement and organ substitution).[3-10] The development of antimicrobial surfaces that can resist biofilm formation or kill bacteria adhered to surfaces represents an important approach to the prevention of bacterial adhesion and proliferation on the surfaces of medical implants.

Antibiotics have been widely used to treat infectious diseases over the past decades. Unfortunately, antibiotic resistance has been developed by many bacteria to the point of becoming a major clinical concern.[11] In addition to conventional antibiotics, many other antibacterial agents have been introduced and extensively studied, including polymers, quaternary ammonium salts, silver nanoparticles, and titanium compounds.[12-15] Although each above agent is effective as an antibacterial treatment, they all possess undesirable side-effects, such as high cytotoxicity, short term antibacterial effect, and hypersensitivity.[16] Antimicrobial peptides (AMPs) provide attractive alternative for developing new antibiotics and making antimicrobial coatings.[17-22] AMPs are naturally occurring amphipathic peptides that can selectively target bacteria, fungi, and even human cancer cells through disruption of the cellular membrane.[18, 23] AMPs exhibit many desirable properties such as broad spectrum activity, high structural stability, low toxicity for healthy mammalian cells, and low susceptibility to bacterial resistance.[18, 19, 24]

The first and most widely studied antimicrobial peptides are peptides in the magainin family, which was first isolated from the frog *Xenopus laevis* skin.[25, 26] Our studies focus on MSI-78, or pexiganan, an antimicrobial peptide designed by Genaera Corporation, which is a potent synthetic analog of magainin. It has been reported that MSI-78 adopts an alpha-helical structure when associated with cell membranes and a random coil structure in aqueous buffer solutions.[27, 28] Its short sequence and alpha-helical structure make it a good choice for structural characterization.

Previous studies have shown that AMPs kill bacteria through the initial electrostatic interactions between the positively charged peptides and the negatively charged bacteria cell membrane, and the later disruption of these membranes due to the amphipathic nature

of the peptide.[29] Different killing mechanisms have been proposed, with peptides adopting different orientations associated with cell membranes.[30, 31] We have investigated molecular interactions between MSI-78 and various model cell membranes using sum frequency generation (SFG) vibrational spectroscopy as a function of MSI-78 solution concentration.[30] We found that different MSI-78 bulk concentrations in solution led to varied interaction mechanisms with model cell membranes, resulting from different peptide orientations associated with the model cell membranes. Others have also studied membrane disruption of MSI-78 by NMR.[32-37] All such previous studies were performed using "free" MSI-78 molecules in bulk solutions.

In this chapter, we immobilized MSI-78 through different peptide termini onto surfaces to create antimicrobial coatings. We characterized the surface-immobilized MSI-78 structure using SFG, which was discussed in Chapter 1 and previous publications.[38, 39] SFG has been applied to examine the secondary structures and orientations of various peptides and proteins adsorbed on surfaces.[40-43] The experimentally deduced MSI-78 structure was further validated using circular dichroism (CD) spectroscopy and coarse grained molecular dynamics simulations. In addition, we determined the antimicrobial activities of the surface immobilized peptides to correlate the deduced structural information to the biological efficacy of the AMPs with the hope of understanding the structure-function relationship of surface immobilized AMPs.

2.1.2 Materials and Methods

All chemicals and solvents were purchased from Sigma-Aldrich (St. Louis, MO, USA) and used without further purification unless otherwise stated.

2.1.2.1 Surface Functionalization and SAM Preparation

SiO_2 coated CaF_2 prisms were prepared and cleaned using the method discussed in Chapter 1. After cleaning, prisms were immediately placed into a freshly prepared 1.0 mM alkyne-EG4-silane (Figure 2.1a) solution in anhydrous toluene for 24 h at room temperature. The functionalized prisms were then rinsed with copious toluene and methanol, and were then dried under nitrogen.

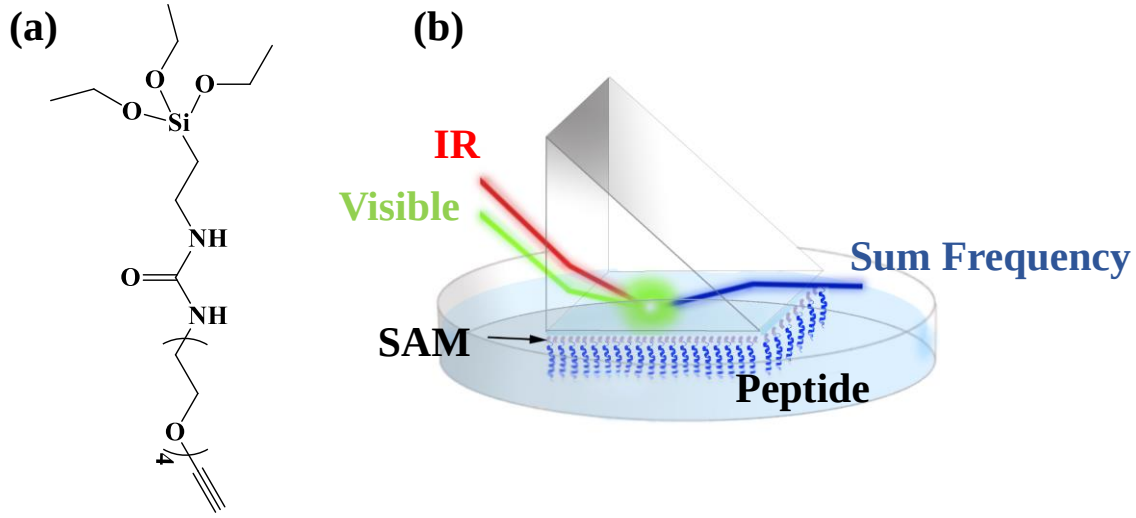

Figure 2.1 a) Molecular formula of alkyne-terminated silane; b) SFG experimental geometry (near-total-reflection geometry) to study immobilized peptide on a right angle CaF_2 prism in contact with phosphate buffer.

2.1.2.2 (-N_3) MSI-78 Surface Immobilization

MSI-78 is a 22-residue antimicrobial peptide with the amino acid sequence: GIGKFLKKAKKFGKAFVKILKK-NH_2. C-terminal amidation of MSI-78 was reported to increase peptide activity.[33] Azido mutated MSI-78 was synthesized using solid phase Fmoc method with one azido-lysine added to the N-terminus (nMSI-78) or C-terminus (MSI-78n) of MSI-78. The nMSI-78 and MSI-78n sequences are shown in Table 2.1.

Peptide stock solutions were prepared by dissolving 2.0 mg peptide powder into 8.0 mL Millipore deionized water (18.2 MΩ cm) and stored in a -30 °C freezer.

Table 2.1 Amino acid sequence of wild type MSI-78, nMSI-78 and MSI-78n

ID	Sequence
MSI-78	GIGKFLKKAKKFGKAFVKILKK-NH_2
nMSI-78	(-N_3)KGIGKFLKKAKKFGKAFVKILKK-NH_2
MSI-78n	GIGKFLKKAKKFGKAFVKILKKK(-N_3)-NH_2

The SAM functionalized prisms were placed into a phosphate buffer solution (pH 8.0, ionic strength 5.0 mM) containing nMSI-78 or MSI-78n (9.5 μM), sodium ascorbate (0.2 M), and copper sulfate (0.5 mM), and reacted overnight. The prisms were first rinsed with phosphate buffer containing EDTA to remove any residue copper ions. They were then rinsed with phosphate buffer and 1.0 mM sodium dodecyl sulfate (SDS) to wash away physically adsorbed peptides, followed by several additional phosphate buffer washes.

2.1.2.3 Circular Dichroism Measurement (CD)

The CD spectra of free MSI-78 in solution and immobilized MSI-78 on surfaces were collected with a J-815 CD spectrometer (Jasco Inc., Japan) using a continuous scanning mode at room temperature. All the spectra were scanned between 190 nm and 240 nm at a 1 nm resolution, 20 nm min^{-1} scan rate and averaged by five successive scans

for each sample. Quartz slides were used as substrates for CD studies to immobilize peptides using the same method described in Section 2.2.1 and 2.2.2.

2.1.2.4 SFG Measurement

In this experimental setup, two laser beams (one 532 nm visible laser beam and one frequency tunable IR beam) pass through one surface of a right angle CaF_2 prism and then overlap spatially and temporally at the other surface (shown in Figure 1b). The incident angles of the 532 nm and IR beams in the SFG setup are 58 and 55 degrees relative to the surface normal respectively before going through the prism. SFG spectra with different polarization combinations of the input and generated signal beams including ssp (s-polarized output SFG signal, s-polarized input visible beam and p-polarized input IR beam) and ppp were collected using the near total internal reflection geometry.[44]

For an alpha-helical structure, the amide I signal is centered at about 1650 cm^{-1}.[45] The orientation of an alpha helix can be deduced from the measured ratio of the effective second-order nonlinear optical susceptibility tensor components detected in ssp and ppp polarizations.[40, 43] This method has been illustrated in detail in Chapter 1 and in previous publications.[30, 46]

SFG spectra are fitted using the following equation:[43]

$$\chi_{eff}^{(2)}(w) = \chi_{NR}^{(2)} + \sum_q \frac{A_q}{w - w_q + i\Gamma_q} \quad \textbf{Equation 2.1}$$

Where ω is the frequency of the IR beam, A_q is the amplitude of the vibrational mode, and Γ_q is the damping coefficient of the q^{th} vibrational mode.

2.1.2.5 Coarse Grained Molecular Dynamics Simulations on Immobilized MSI-78

A previously developed coarse grained surface force field is used in this chapter to study peptide and surface interactions.[47] This model was developed based on the

Karanicolas and Brooks' (KB) Go-like protein model[48, 49] and was well parameterized based on a set of benchmark experimental data for protein adsorption free energies onto SAM surfaces.[50] The KB protein model is used because it has been shown to be able to consistently reproduce protein folding free energy surfaces and folding mechanisms. Using the formation of native contacts defined in the KB protein model, a five-term potential was used to describe the interaction between each residue and a SAM surface (as shown below in Equation 2.2). The first three terms describe the adsorption well and the energy barrier, which are general for any residue and surface type. The last two terms are used to delineate the hydrophobicity of each residue and surface.

$$\boldsymbol{V_{surface} = \sum_i^N \left\{ \pi \rho \sigma_i^3 \epsilon_i \left[\theta_1 \left(\frac{\sigma_i}{z_{is}}\right)^9 - \theta_2 \left(\frac{\sigma_i}{z_{is}}\right)^7 + \theta_3 \left(\frac{\sigma_i}{z_{is}}\right)^3 - (\theta_s(\chi_s - 4.5) + \theta_p \chi_p) \left(\frac{\sigma_i}{z_{is}}\right)^3 \right] \right\}}$$ **Equation 2.2**

All θ's are parameters that were optimized as shown in Table 2.2. An alkyne surface is hydrophobic with χ_s set to be 4.5.[47] The values of χ_p are hydropathy indices of residues that can be found in many biochemistry textbooks.[51] The bond between the alkyne surface and the lysine side chain was simulated through the addition of a harmonic restraint tethering the terminal residue of the peptide to the surface and represented by an interaction potential of the following form:

$$\boldsymbol{U_{restraint} = \frac{1}{2} k_r (r - r_{eq})^2}$$ **Equation 2.3**

where $k_r = 10\ kcal/mol$ is the parameter describing the strength of the restraint and r is the distance of the tethering site from the origin of the surface (0, 0, 0), and $r_{eq} =$ 9.2 Å is the equilibrium distance from the tethering site to the surface origin. The tethering length was used to approximate the distance between the alkyne surface and the C_α of the lysine residue at the tethering site.

Table 2.2 Parameters for the surface model[47]

θ_1	θ_2	θ_3	θ_s	θ_p
0.2340	0.4936	0.1333	0.0067	0.0333

2.1.2.6 Antimicrobial Activity Test of the Immobilized Peptide

Quartz slides were used to grow SAMs and immobilize peptides in the antimicrobial activity test (instead of prisms used in SFG) using the same method presented above.

A LIVE/DEAD BacLight Bacterial Viability kit (L-7007, Invitrogen, Carlsbad, CA) was used to determine bacterial cell viability. A solution of the mixed SYTO 9 and Propidium Iodide (PI) dyes was prepared according to the manufacturer's instruction. *Escherichia coli* ATCC 25922 or *Staphylococcus aureus* ATCC 25923 were grown in Luria Bertani (LB) broth (3 mL, pH 7.2) at 37 °C overnight. The overnight grown bacterial culture was diluted with fresh LB medium to a concentration around 10^8 CFU/mL. 5.0 μL of diluted bacterial culture was mixed with the fluorescent dyes (5.0 μL) and the mixture was dropped onto a peptide-coated quartz slide or an un-treated quartz slide (control), and a glass coverslip (2.5 cm × 2.5 cm) was placed on the droplet. This slide sample was incubated at room temperature in a dark environment for 15 min before being examined using a fluorescence microscope (Olympus 1×71, Center Valley, PA) equipped with Fluorescence Illumination System (X-Cite 120, EXFO) and appropriate filter sets. Images were randomly acquired on different spots by using an oil immersion 60 × objective lens.

2.1.3 Results and Discussions

2.1.3.1 Secondary Structures of (-N_3) MSI-78

Secondary structures of peptides both in bulk and on surfaces were characterized by CD. CD studies on peptides adsorbed/immobilized on substrate surfaces were extensively reported previously.[52-58]

The amino acid sequences of the wild type MSI-78 and terminal azide modified MSI-78s are shown in Table 2.1. Previous studies indicated that wild type MSI-78 adopts a random coil conformation in aqueous buffer solution but forms an alpha-helical conformation in the presence of lipid vesicles.[27] The CD spectra of wild type MSI-78 dissolved in phosphate buffer and azido-derivatives of MSI-78 (nMSI-78 and MSI-78n) after immobilization on surfaces at room temperature are shown in Figure 2.2. Similar to the wild type MSI-78, the azido-derivatives of MSI-78 adopt a random coil conformation in aqueous buffer solution (results not shown). After surface coupling through the reaction of the MSI-78 azido group with the surface alkyne group, the immobilized azido-derivatives of MSI-78 exhibited an alpha-helical conformation, as characterized by the double minima at 207 nm and 222 nm in the CD spectra (Figure 2.2b). The averaged helix contents of the surface bound nMSI-78 and MSI-78n are similar at ~84.5% and ~83.7%, as calculated by CDSSTR, SELCON3, and CONTIN.

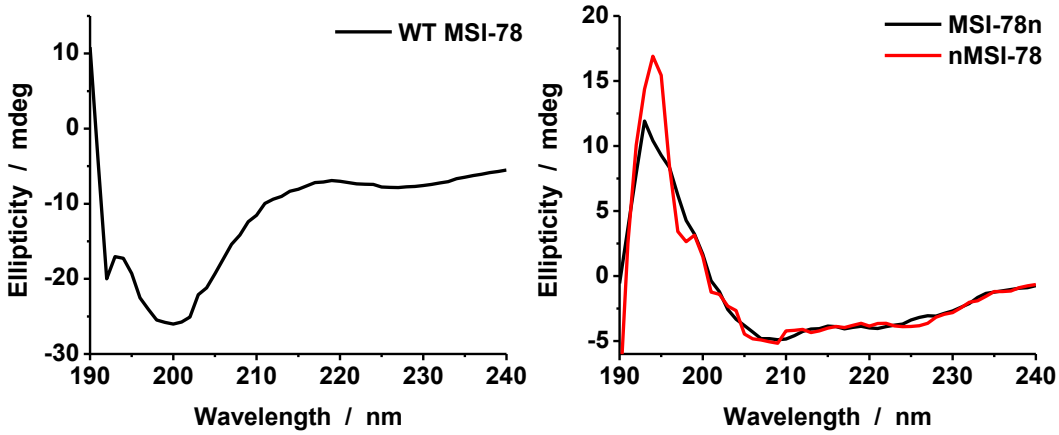

Figure 2.2 CD spectra of a) WT MSI-78 in phosphate buffer; b) surface immobilized nMSI-78 and MSI-78n in phosphate buffer.

The CD spectra shown in Figure 2.2b indicate that a significant conformational change occurred after surface immobilization for both nMSI-78 and MSI-78n. Therefore it appears that surface tethering stabilizes the alpha-helical conformation, even in the absence of lipid vesicles or other membrane mimic species, e. g. 2, 2, 2-trifluoroethanol (TFE).[59] Similar effects have been observed for other peptides upon surface immobilization through cysteine-maleimide coupling.[59-61]

2.1.3.2 Orientations of MSI-78 Molecules Surface-Immobilized through N- and C-Termini

After the structures of the immobilized nMSI-78 and MSI-78n were determined to be alpha-helical using CD, we investigated their surface orientations using SFG. SFG spectra were first recorded from the alkyne-terminated SAM on CaF_2 prism in contact with phosphate buffer in the absence of immobilized peptides (Figure 2.3a). A small peak around 1620 cm^{-1} was detected in the SFG spectrum, which likely originates from the C=O groups in the silane molecules. Therefore the alkyne-terminated SAM does not contribute

large background SFG signals in the 1500-1800 cm^{-1} wavenumber range that would interfere with the amide I signal that should be centered at ~1650 cm^{-1}.

After overnight reaction of the alkyne SAM with either nMSI-78 or MSI-78n, the SAM surface was rinsed using phosphate buffer containing EDTA as a cooper chelator, followed by a rinse using SDS to remove physically adsorbed peptides and phosphate buffer. SFG spectra were then collected from each immobilized peptide on SAM in contact with a phosphate buffer solution. An SFG amide I peak centered at ~1650 cm^{-1} was detected (Figure 2.3b), originating from the alpha-helical conformation of immobilized nMSI-78. The SFG results agree with the conclusion obtained from the CD spectra shown in Figure 2.2. Surfaces derivatized with immobilized nMSI-78 were stable when stored in phosphate buffer at room temperature for at least 2 days and when stored frozen at -30 °C for at least 1 month. SFG spectra collected from the stored samples of immobilized nMSI-78 and showed no noticeable change compared to freshly prepared samples.

The SFG ppp and ssp spectra detected from the immobilized nMSI-78 were fitted using a standard SFG spectral fitting method[43] as shown in Figure 2.3b. The measured χ_{ppp}/χ_{ssp} ratio of the amide I peak at 1650 cm^{-1} is 1.60, which can be used to deduce the orientation of immobilized nMSI-78 and will be discussed further below. We also collected SFG spectra from surface-immobilized MSI-78n, as shown in Figure 2.3c. Differently from nMSI-78, no discernable SFG signal could be detected under either ppp or ssp polarization combination from MSI-78n after surface immobilization. This indicates that either the immobilized peptide molecules have a random coil conformation or that they adopt an alpha helical structure but with the helix axis running parallel to the surface. The CD spectra of MSI-78n immobilized on the surface demonstrate that the immobilized MSI-78n

molecules *do* adopt an alpha helical conformation, implying that the absence of SFG amide I signal is due to a parallel surface orientation of the peptide.

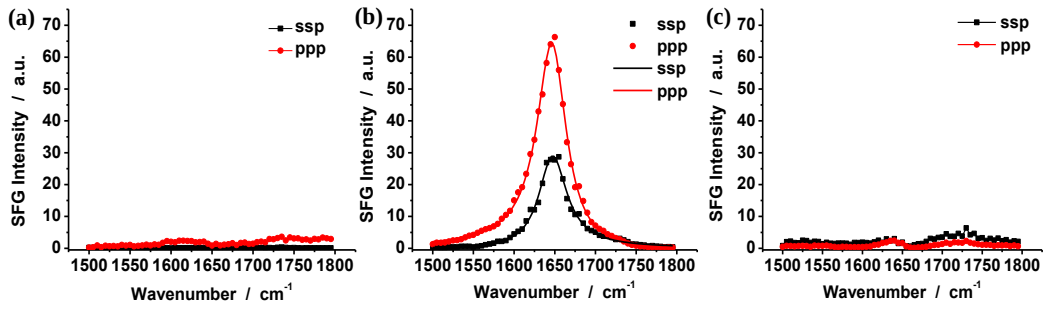

Figure 2.3 SFG ssp (■, black line) and ppp (●, red line) spectra collected from a) alkyne terminated SAM surface; b) nMSI-78 and c) MSI-78n immobilized at the alkyne terminated SAM-phosphate buffer interface.

The orientation of a surface-immobilized alpha-helical peptide can be defined by a tilt angle θ, which represents the angle between the principal axis of the helical peptide and the surface normal. This tilt angle θ can be determined by measuring the χ_{ppp}/χ_{ssp} ratio of the SFG amide I signal of the helix, the details of which have been discussed in Chapter 1 and previous publications.[40, 43] The dependence of the χ_{ppp}/χ_{ssp} ratio on the helix orientation angle for MSI-78 is plotted in Figure 2.4. For the surface immobilized nMSI-78, the measured SFG signal strength ratio χ_{ppp}/χ_{ssp} is 1.60 (fitting parameters shown in Table 2.3). Based on this ratio and the relationship between the χ_{ppp}/χ_{ssp} ratio and the tilt angle shown in Figure 4, the orientation of the surface tethered nMSI-78 is determined to be ~12° relative to the surface normal. Therefore nMSI-78 is approximately perpendicular to the surface, in striking contrast to MSI-78n, which is approximately parallel to the surface as discussed above.

Table 2.3 SFG Fitting Parameters

System	Polarization Combination	Peak Center (cm^{-1})	Peak Width (cm^{-1})	Amplitude
nMSI-78	ppp	1650	25.0±0.1	175.4±0.5
	ssp	1650	25.0±0.2	109.6±1.0

Previously we investigated the surface orientation of immobilized antimicrobial cecropin P1.[59-61] In that study, cecropin P1 was immobilized onto a SAM surface via cysteine-maleimide coupling rather than the click reaction used here. We found that C-terminus cysteine modified cecropin P1 (CP1c) adopted a perpendicular orientation to the surface whereas the N-terminus cysteine modified cecropin P1 (cCP1) adopted a parallel orientation. Therefore we believe that the site-dependent changes in structure we observe for peptides immobilized on surfaces is a general phenomenon.

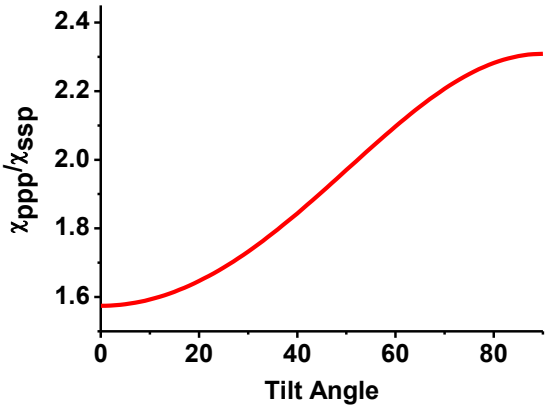

Figure 2.4 Calculated χ_{ppp}/χ_{ssp} SFG susceptibility tensor component ratio plotted as a function of alpha-helix orientation angle with a delta angle distribution.

2, 2, 2-trifluoroethanol (TFE) has the capability to induce the formation of an alpha-helical structure of peptides in solution.[59] In this research, SFG spectra were collected from the immobilized nMSI-78 and MSI-78n at the interface between SAM and 50% TFE in phosphate buffer (Figure 2.5). SFG signals of both immobilized nMSI-78 and MSI-78n increased, indicating that TFE induces a greater helical content for the immobilized peptides. The detection of SFG amide I signal from MSI-78n confirmed the immobilization of MSI-78n on the alkyne-terminated SAM. The SFG spectra in Figure 2.5 were fitted and the measured χ_{ppp}/χ_{ssp} ratios were deduced to be 1.78 and 2.20, respectively, for nMSI-78 and MSI-78n. From these data the tilt angles for immobilized nMSI-78 and MSI-78n were determined to be ~ 34° and ~ 69°, respectively. When the surface is in contact with TFE/phosphate buffer solution, TFE molecules tend to replace the water molecules around the peptides and then interact with the hydrophobic sides of the helices, inducing more alpha helical structure formation. Under this condition, the *inter*-molecular and *intra*-molecular interactions are different, which might change the orientation as discussed further below. The SFG signal intensity from nMSI-78 is stronger than MSI-78n. SFG signal intensity is determined by the surface coverage and orientation of a certain functional group. Assuming a similar structure for immobilized MSI-78n and nMSI-78, based on the fitted amplitude and the deduced orientations (fitting parameters shown in Table 2.4), the coverage of nMSI-78 is about two times that of MSI-78n.

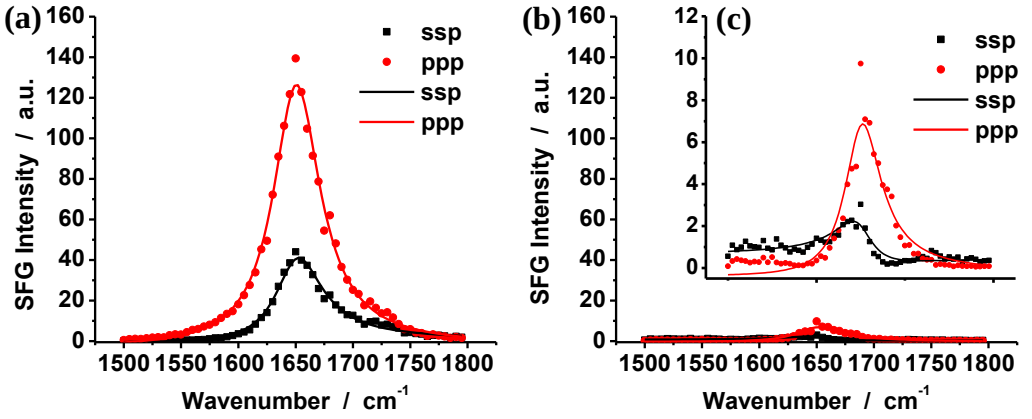

Figure 2.5 SFG ssp (■, black square) and ppp (●, red dot) spectra collected from a) nMSI-78; b) MSI-78n; c) zoomed in spectra of MSI-78n immobilized on the alkyne terminated SAMs-50%TFE/phosphate buffer solution interface. The red/black curve is the fitting curve of the experimental data.

Table 2.4 SFG Spectral Fitting Parameters

System	Polarization Combination	Peak Center (cm^{-1})	Peak Width (cm^{-1})	Amplitude
nMSI-78	ppp	1650	25.0±0.1	284.2±1.1
	ssp	1650	25.0±0.1	159.3±0.7
MSI-78n	ppp	1650	25.0±0.3	66.6±0.6
	ssp	1650	25.0±0.5	30.2±0.5

2.1.3.3 Coarse Grained Molecular Dynamics Simulation of Immobilized (-N_3) MSI-78

As discussed above, we previously observed that CP1c and cCP1 immobilized at a maleimide-terminated SAM surface via different termini exhibit different orientations. It was found in these studies that the observed trends from SFG experiments were well

reproduced with the simulations and additionally, the models provided insights into the origin of structural differences caused by the alternative tethering configurations.[61]

To provide a more detailed understanding of origins of different orientations of immobilized nMSI-78 and MSI-78n observed in this research, we performed coarse grained molecular dynamics simulations. As stated above, we used χ_s of 4.5 for the hydrophobic alkyne SAM surface and the tethering length was approximated to be 9.2 Å based on the length of the side chain of the lysine residue. In this simulation, no external force to constrain the helical structure was used other than the native contacts of the initial helical structure which are defined by the Go-like protein model. As shown in Figure 2.6, the MSI-78 peptide is colored in blue for hydrophilic residues and orange for hydrophobic residues. Generally the MSI-78 hydrophobic residues are more likely to be adsorbed onto the alkyne surface. Thus the orange residues tend to face to the surface. Comparing to CP1,[61] the hydrophobic residues in MSI-78 are more symmetrically distributed with a small cluster of hydrophobic residues gathered near the C-terminus. Furthermore, the lysine (or charged) residues are equally dispersed with the hydrophobic residues throughout the sequence.

As observed in Figure 2.6b, the hydrophobic residues clustered near the C-terminus of MSI-78n adsorbed to the surface first, forcing the entire peptide to lie down. In contrast, as shown in Figure 2.6a, only several hydrophobic residues of nMSI-78 close to the surface were adsorbed, however, the rest of the peptide was still well accommodated in the solution and did not lie down on the surface. This result suggests that the N-terminus tethered nMSI-78 peptide on the surface should generate SFG signals due to the standing-up pose, while the C-terminus tethered peptide with a lying-down pose should not. From the above

observation, it can be seen that due to the unfavorable interactions between the hydrophobic segments of MSI-78 and the surrounding water, they liked to be adsorbed to the surface. This was the case for MSI-78n, which adopted a lying down orientation. Then why did the hydrophobic residues near the C-terminus of the immobilized nMSI-78 remain in the solution instead of being adsorbed to the surface? We believe that this is due to the four lysine residues which are located near the hydrophobic residues close to the C-terminus. When this region of the peptide was far away from the surface (as the case with N-terminus tethered MSI-78), the charged lysine residues preferred to stay in aqueous solution, overcoming the unfavorable interactions between the hydrophobic residues and water, leading the peptide to adopt a tilted orientation relative to the surface and remain solvated in the phosphate buffer. At the same time, it was less probable for the hydrophilic end of nMSI-78 (N-terminus) to interact with the hydrophobic surface. As we observed, nMSI-78 was standing-up, only slightly tilting from the surface normal. Therefore, due to the overall effects of the hydrophobic and lysine residues, as the hydrophobic C-terminus of MSI-78 was immobilized, the peptide tended to lie down on the surface; but when the hydrophilic N-terminus was tethered to the surface, MSI-78 stood up on the surface.

As we discussed above, when the aqueous phosphate buffer was replaced by a more hydrophobic TFE-phosphate buffer mixture, the interaction between TFE and peptide should be considered. With a different solvent, the orientation of immobilized MSI-78 peptide here also changed. The immobilized nMSI-78 via the N-terminus tilted more towards the surface – as we observed, the orientation changed from ~12° to ~34° relative to the surface normal. With a more hydrophobic solvent, the “free” C-terminus of nMSI-78 is still stable in the TFE-phosphate buffer mixture. However, it becomes easier for the

hydrophobic residues at the N-terminus of nMSI-78 to find the hydrophobic alkyne surface. Therefore, nMSI-78 was tilting a bit more in TFE than in water. The opposite effect was observed for MSI-78n. When the phosphate buffer was replaced by a more hydrophobic TFE-buffer mixture, MSI-78n stood up more, as we observed using SFG.

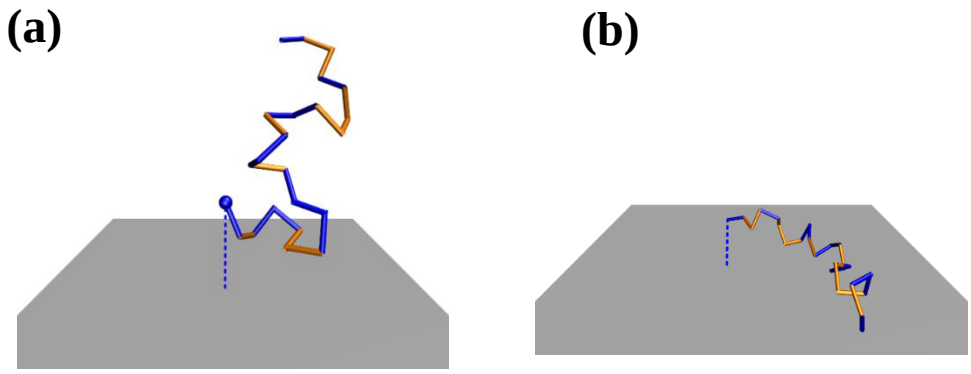

Figure 2.6 Coarse grained simulation results of a) nMSI-78 and b) MSI-78n immobilized on alkyne-terminated SAMs exposed to phosphate buffer solution. The simulated results well recapitulate the experimentally deduced peptide orientations.

2.1.3.4 Antimicrobial Activity Tests of Surface Immobilized MSI-78

We investigated whether the different orientations of immobilized nMSI-78 and MSI-78n result in different antimicrobial activities as well. Antimicrobial activity tests were performed on the immobilized nMSI-78 and MSI-78n against both *Escherichia coli* (*E. coli*) and *Staphylococcus aureus* (*S. aureus*) to examine the relationship between the surface orientation of immobilized MSI-78 and its antimicrobial activity. The bacteria were stained with the Bacterial LIVE/DEAD dyes and characterized by fluorescence microscopy. Figure 2.7 displays the fluorescence images of live cells (green channel) and dead cells (red channel) on either the nMSI-78 or MSI-78n immobilized surface and the merged images. Initially, live bacteria stained with SYTO-9, generating a green fluorescence signal.

When the bacteria died or their membranes were compromised, they stained with PI, red fluorescent dye. Thus, in a merged image damaged or dead cells appear yellow.

a) Against *E.coli* by MSI-78n in 30 min

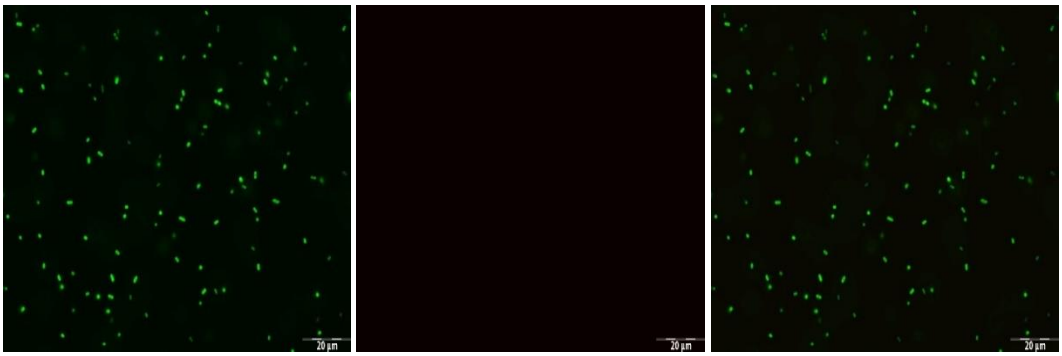

b) Against *E.coli* by MSI-78n in 60 min

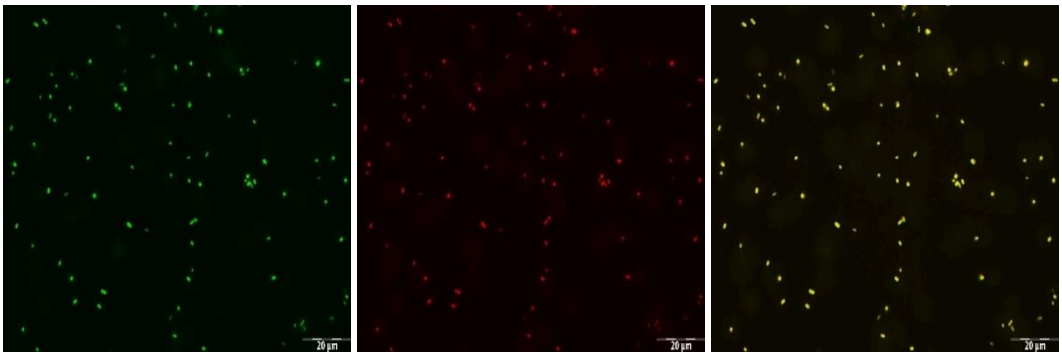

c) Against *E.coli* by nMSI-78 in 30 min

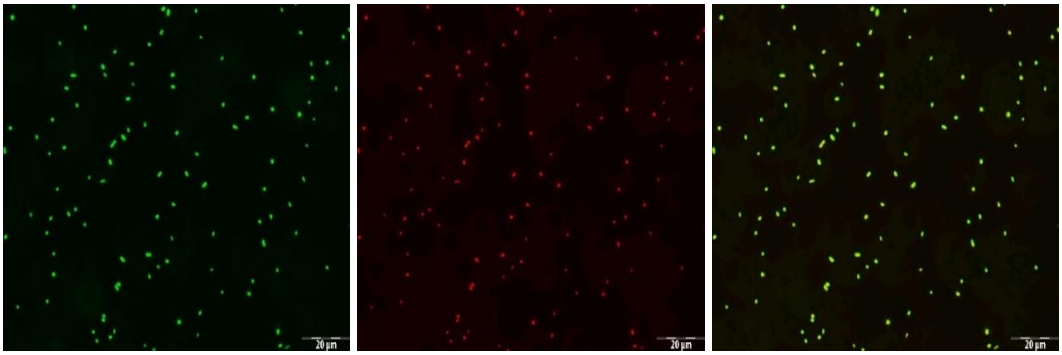

d) Against *E.coli* by nMSI-78 in 60 min

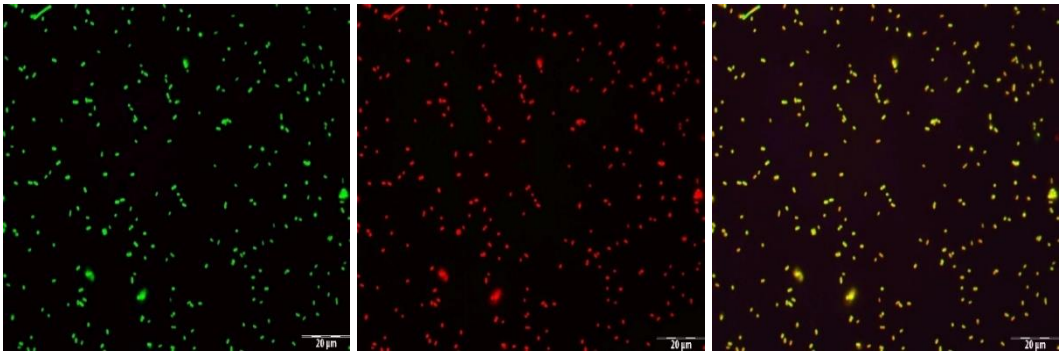

Figure 2.7 Representative micrographs of antibacterial test results of surface immobilized MSI-78n against *E. coli* for a) 30 min and b) 60 min; antibacterial test results of surface immobilized nMSI-78 against *E. coli* for c) 30 min and d) 60 min.

The antibacterial properties of the nMSI-78 and MSI-78n immobilized surfaces were found to be very different (Figures 2.7 and 2.8). Figure 2.7a shows that the surface with MSI-78n immobilized adsorbs some *E. coli* (green fluorescence signals were observed) after 30 min, but no dead bacteria were observed (no red fluorescence signal was observed). Figure 2.7b shows that after 60 min, the adsorbed bacteria on the surface with immobilized MSI-78n were dead; the red and green fluorescence images overlaid, indicating that all the originally adsorbed bacteria were killed. In contrast, Figure 2.7c shows that immobilized nMSI-78 killed most *E. coli* cells after only 30 min, with red and green fluorescence signals coinciding. After 60 min, more bacteria were adsorbed onto the surface with immobilized nMSI-78, and again all the adsorbed bacteria were killed. The quantitative results were also shown in Figure 2.8a. As we discussed above, the immobilized nMSI-78 adopts an alpha-helical conformation and a "standing up" orientation. Differently, the immobilized MSI-78n lies down. Therefore, very likely peptides with a "standing up" orientation initially have a quicker antimicrobial activity towards *E. coli*.

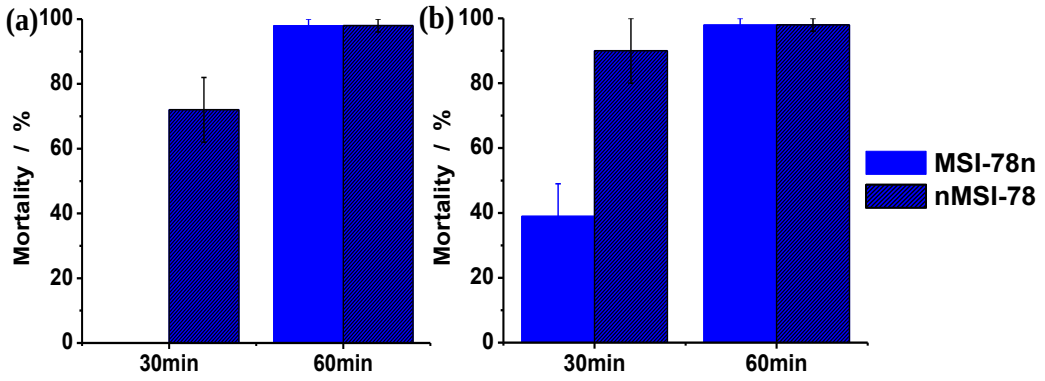

Figure 2.8 Antimicrobial activities of surface immobilized peptides immobilized against a) *E. coli*; b) *S. aureus*. (The presented data are the averaged data measured in three spots at each time on the same surface.)

The initial different orientations of nMSI-78 and MSI-78n likely affect the electrostatic interactions between the negative charged bacterial cell membrane and the cationic peptide, resulting in a change in the activity efficacy of the peptide. According to previous studies,[18, 29] for free antimicrobial peptides in solution, as the bacteria attached to peptides, peptide can interact with the lipid bilayers in several different models. In these models, toroidal pore is the accepted mechanism model for MSI-78 in bulk solution.[34] Here the peptides were immobilized on surfaces, and therefore they would unlikely form toroidal pores. Also, to directly interact with the bacterial inner membrane, the peptides need to penetrate through the bacteria outer membrane, which is unlikely for the peptides immobilized on a surface. Therefore the detailed interaction mechanism between bacteria and surface immobilized antimicrobial peptides is still an open question. Our recent studies on cysteine modified MSI-78 provides more information on its mechanism. Due to the significant number of lysine residues of MSI-78, surface immobilized peptides may present a strong positive charge on the surface and can interact with bacteria membranes more

effectively. This could be true for peptides that are more solvent exposed (such as nMSI-78). Nevertheless, here we showed that the different initial orientations and distributions of charged residues of surface immobilized peptides influenced their antimicrobial activity, which must be due to the differed peptide-bacteria interactions and will be investigated further in details in the future.

Similar results of the antimicrobial activity against *S. aureus*, Gram-positive bacteria, were shown in Figure 2.8b. With more negative surface charge,[62] *S. aureus* may have a stronger electrostatic interaction with cationic peptide, resulting in a slightly higher antimicrobial efficacy.

2.1.4 Conclusion

We have demonstrated that MSI-78 molecules immobilized on a SAM surface via "click" reactions adopt alpha-helical conformations using a combination of CD and SFG spectroscopic studies. SFG results indicated that the peptides immobilized through the N- and C-termini adopt different orientations on the surface due to different interactions between the peptides and the hydrophobic surface. SFG results were validated by coarse grained molecular dynamics simulations. The MSI-78 immobilized through the N-terminus adopts a nearly perpendicular orientation with respect to the surface after covalent attachment to the alkyne terminated SAM surface. In contrast, the C-terminal-immobilized MSI-78 peptide appears to adopt a parallel orientation with respect to the surface. The antimicrobial activity of the immobilized MSI-78 derivatives was found to be dependent on whether the peptide was tethered through the N- or C-terminus, with nMSI-78 exhibiting significantly better antimicrobial activity than MSI-78n. This chapter provides

fundamental and in-depth insights into understanding the structure-function relationship of immobilized peptides on abiotic surfaces that may aid in the design and development of antimicrobial coatings and devices.

2.2 ORIENTATION CONTROL OF SURFACE IMMOBILIZED PEPTIDES

2.2.1 Introduction

Understanding peptide-surface interactions is a main challenge for the optimal design of protein-based biosensors due to the complexity of peptide/protein behavior at the solid/liquid interface.[63-68] A change in either conformation or orientation of the peptide/protein may affect its activity and consequently the performance of the biosensor. The surface chemistry, solvent condition, and the inherent stability and shape of the protein can all be responsible for triggering the loss of native structure or expected orientation of a peptide/protein, like what we discussed in Chapter 2.1. Many studies have been involved in determining the importance of each factor on the behavior of globular proteins on surfaces. For instance, both Latour's and Belfort's lab performed thorough studies to discuss how solid surface properties are able to affect protein adsorption free energies using both experimental and simulation methods.[50, 65, 66, 69, 70] Jiang et al. developed and thoroughly studied surfaces that minimize the protein conformation disruption.[71, 72] On the other hand, simulation methods are widely developed and implemented to study protein orientation and stability with respect to different surface chemistry and protein properties.[66, 73-79]

Despite the success of understanding globular protein behavior on different surfaces, to predict the secondary structure and orientation of a simple peptide with residue-

level structural details can be difficult due to the inherent flexibility that can cause tethered peptides to have more conformational changes than a typical globular protein. Using sum frequency generation spectroscopy accompanied with all-atom and coarse grained simulations,[80-84] success has been achieved in several cases to measure the peptide orientation on different SAM surfaces. A more challenging question asked here is how to improve the potential performance of the biosensor by controlling peptide orientation on such surfaces.

To address this point, a collaboration work with Dr. Shuai Wei from Prof. Charles Brooks group at the University of Michigan was performed by combining coarse grained simulation and SFG studies. A recently developed coarse grained simulation model of protein-surface interactions is used. This model, as validated by previous studies on similar peptide-surface systems,[84, 85] is able to capture the detailed peptide structure, orientation, and thermal stability on a SAM surface. More importantly, the residue-level structural details of the peptide that interacts with the SAM surface are able to provide directive suggestion of how mutations could affect the peptide orientation.

Previous studies have been done to predict the thermal stability and orientation distribution of wild-type and mutated peptides on self-assembled monolayer surface by a coarse grained simulation method alone.[85] In that work, another antimicrobial helical peptide, cecropin P1, was studied by applying mutations to certain residues for a better standing-up pose as opposed to the wild-type peptide. As shown in the previous study of this wild-type MSI-78 peptide,[84] the specific positions of several hydrophobic residues were identified by simulation to be important in contributing to the adsorption of the peptide to an alkyne SAM surface. Accordingly, mutations of only a few key hydrophobic

residues in MSI-78 are suggested in this work that contribute largely to the adsorption. Since hydrophobic amino acids are likely to contact the hydrophobic surface to enable the peptide to lie down on the surface, the mutated residues are proposed with less hydrophobicity but higher helical propensity. Then the structure of the redesigned sequence is expected to be the least deviated from the original structure but has a greater propensity to exhibit a perpendicular pose with either N-/ C-terminus tethered. To validate this prediction from simulations, experimental methods are employed to learn both the structure and orientation of the redesigned peptides on the alkyne SAM surface. The redesigned peptide is incorporated with an extra lysine residue in either terminus. CD is used in this chapter to determine the helical structure of the peptide and the SFG is used to measure the orientation of the peptide tethered on the SAM surface.

2.2.2 Materials and Methods

2.2.2.1 Simulation Model

In this Section, we still use the Karanicolas and Brooks's (KB) Go-like model[86-88] to represent the peptide structure. Details of this model have been presented in section 2.1 and will not be repeated here. A perfect α-helical structure is used as the initial template for the redesigned MSI-78 peptide with an extra lysine residue on both N- and C-terminus. Each initial structure of the redesigned MSI-78 is relaxed with energy minimization using CHARMM in implicit solvent. The relaxed structure is then submitted to the Go model builder on the MMTSB website (http://www.mmtsb.org) to generate input file for the coarse grained simulations.

To measure the peptide orientation on the surface, MD simulations are performed within the canonical ensemble (NVT) at a specific temperature (compared to the replica exchange sampling method). Each simulation was performed with 10 million steps of equilibrium and 30 million steps of production with the time step of 5 fs. This coarse grained model and most other similar models are not accurate in providing the absolute melting temperature of proteins. The KB coarse grained model was scaled so that most proteins have the melting temperature around 350 K. Therefore, as discussed in previous studies of the surface force field parameterization and application on the same peptide interacting with a different SAM surface, the simulation temperature is set to be 215 K to represent the experimental temperature of 298 K.[47, 84, 85]

The percentage of helical motif in this small peptide is measured from the simulation using a novel developed secondary structure assignment method PCASSO by Law et, al.[89] This method is fast, efficient, and specific to C_α only structures, which is an ideal method in analyzing structures from the KB Go-like model.

By assuming the peptide forms a single helix on the surface, the angle (ξ) formed by the helical sequence and the surface normal is measured throughout the simulation. This result will be compared to the angle retrieved by the theoretical correlation of χ_{ppp}/χ_{ssp} ratio from SFG and angle of alpha-helix on the surface as discussed in previous studies.[40] The orientation of the helix will be calculated as

$$\boldsymbol{\xi = acos\left(\frac{\bar{z}.*\overline{z_0}}{|\bar{z}.*\overline{z_0}|}\right)} \quad \textbf{Equation 2.4}$$

where $\overline{z_0}$ is the vector of surface normal and $\bar{z}$ is the vector of the helix.

As will be shown, the peptide may form a bent helical structure. In this case, we measure both the angle formed by the first helix (which is the one close to the surface) and the surface normal (ξ) and the angle between two helices (ς). Using the averaged values of ξ and ς, the χ_{ppp}/χ_{ssp} ratio from SFG is predicted theoretically.

2.2.2.2 Experiment

Azide terminated MSI-78 mutants (N-terminus MSI-78 mutant: nMSI-78m, C-terminus MSI-78 mutant: MSI-78mn) with the amino acid sequence: GIGKFLKKAKKFGKAFAKQLKK-NH_2 were synthesized by Peptide 2.0 Inc. The peptides were immobilized onto a SAM surface using the same method presented above. CD and SFG measurements were performed to study such immobilized peptides using the same method as discussed above.

2.2.3 Results and Discussions

2.2.3.1 Redesigning the MSI-78 Peptide Sequence

As shown above, surface immobilized MSI-78 on an alkyne SAM has a lying-down pose with the C-terminus tethered, while it exhibits a perpendicular pose to the surface with the N-terminus tethered. This result was confirmed by both the SFG data and the structural analysis by the coarse grained simulations. The simulation results indicated that two key residues (V17 and I19), which form strong hydrophobic interactions with the alkyne SAM surface, contribute largely to the lying-down pose when the C-terminus tethered. Here we want to design a new peptide based on the MSI-78 structure so that it will exhibit a standing-up orientation immobilized by either the C- or the N-terminus.

To obtain a potentially perpendicular orientation of a redesigned peptide after immobilization to the surface, we decided to mutate the above two residues (V17 and I19)

to reduce the hydrophobic interactions between the peptide and the surface. We hope that the peptide could keep the helical structure, and therefore propose the mutations using new amino acid residues with a lower hydropathy index and higher helical propensity (with a lower index value). Table 2.7 lists the sequences of the wild-type MSI-78 and the new peptide, with the amino acids involved in mutation marked in red. Mutations V17A and I19Q will lead to lower hydrophobicity (4.2 to 1.8 and 4.5 to -3.5) and better helical propensity (0.61 to 0.0 and 0.41 to 0.39).

Table 2.5 Wild-type and redesigned MSI-78: alpha-helical propensity and hydropathy index of each residue

Wild-type MSI-78											
Resi #	1	2	3	4	5	6	7	8	9	10	11
Residue	G	I	G	K	F	L	K	K	A	K	K
Hydro	-0.4	4.5	-0.4	-3.9	2.8	3.8	-3.9	-3.9	1.8	-3.9	-3.9
Helix	1.0	0.41	1.0	0.26	0.54	0.21	0.26	0.26	0.0	0.26	0.26
Resi #	12	13	14	15	16	17	18	19	20	21	22
Residue	F	G	K	A	F	V	K	I	L	K	K
Hydro	2.8	-0.4	-3.9	1.8	2.8	4.2	-3.9	4.5	3.8	-3.9	-3.9
Helix	0.54	1.0	0.26	0.0	0.54	0.61	0.26	0.41	0.21	0.26	0.26
Redesigned MSI-78											
Resi #	1	2	3	4	5	6	7	8	9	10	11
Residue	G	I	G	K	F	L	K	K	A	K	K
Hydro	-0.4	4.5	-0.4	-3.9	2.8	3.8	-3.9	-3.9	1.8	-3.9	-3.9
Helix	1.0	0.41	1.0	0.26	0.54	0.21	0.26	0.26	0.0	0.26	0.26
Resi #	12	13	14	15	16	17	18	19	20	21	22
Residue	F	G	K	A	F	A	K	Q	L	K	K
Hydro	2.8	-0.4	-3.9	1.8	2.8	1.8	-3.9	-3.5	3.8	-3.9	-3.9

Helix	0.54	1.0	0.26	0.0	0.54	0.0	0.26	0.39	0.21	0.26	0.26

Figure 2.11 shows the two snapshots of the typical structure and orientation of the new mutated MSI-78 on the surface obtained in MD simulation. Residues in the peptide are colored based on their hydrophobicity with blue for hydrophilic residues and orange for hydrophobic ones. The two residues that are mutated are represented by lime colored Van der Waals spheres. With the N-terminus tethered, the peptide exhibits a single helical structure and a generally perpendicular pose to the surface. With the C-terminus tethered, the peptide is also able to form a standing-up pose on the surface, but with a non-continuous bent helical structure. Compared to the wild-type cases, it is as expected that the redesigned peptide has a better capability in accommodating the solvent environment with a standing-up pose on the surface, which is due to the lower hydrophobicity of the mutated residues. Meanwhile, the helical property of the peptide is also well maintained with the mutation to a better helical propensity. The secondary structure motif, the specific orientation of the single helical structure with N-terminus tethered, and the predicted χ_{ppp}/χ_{ssp} ratio from SFG for the bent helical structure with C-terminus tethered are calculated theoretically from the simulation trajectories, which are validated by the following CD and SFG experiments.

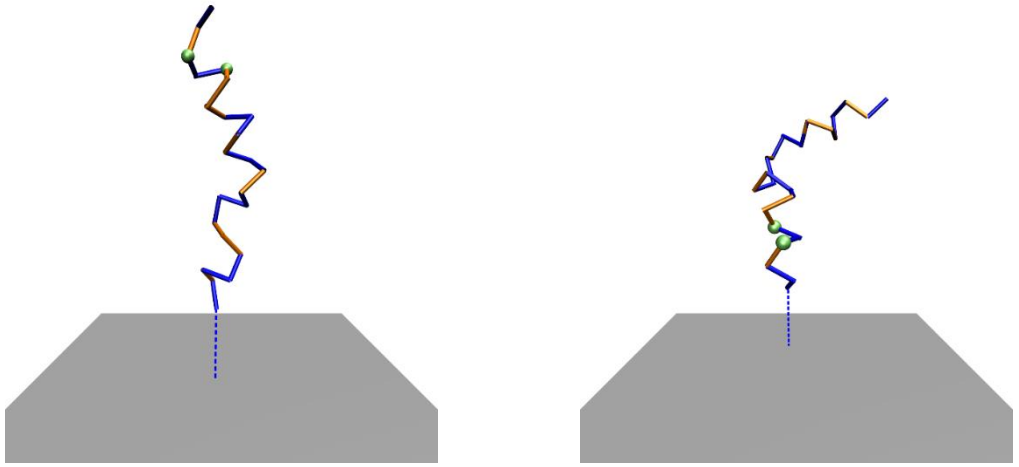

(a) N-terminus tethered (nMSI-78m)

(b) C-terminus tethered (MSI-78mn)

Figure 2.9 Typical snapshots of N-/C-terminus tethered redesigned MSI-78.

2.2.3.2 Secondary Structure of the Redesigned MSI-78 Peptide

Figure 2.12 shows the percentage of the helical motif formation of each residue for the re-designed peptide with N- and C-terminus tethered, calculated by the PCASSO.[89] The residue is considered to be part of the helical structure if it forms more than 50% of the simulation time. With the N-terminus tethered, a single helix is formed from residue number 9 to 19. The very short helical sequence from residue number 2 to 3 is ignored because the length is too small to contribute to the SFG or barely to CD signal. With the C-terminus tethered, both the helical sequence from residue number 11 to 19 (Helix I) and the one from residue number 2 to 6 (Helix II) are long enough to affect the SFG and CD signal.

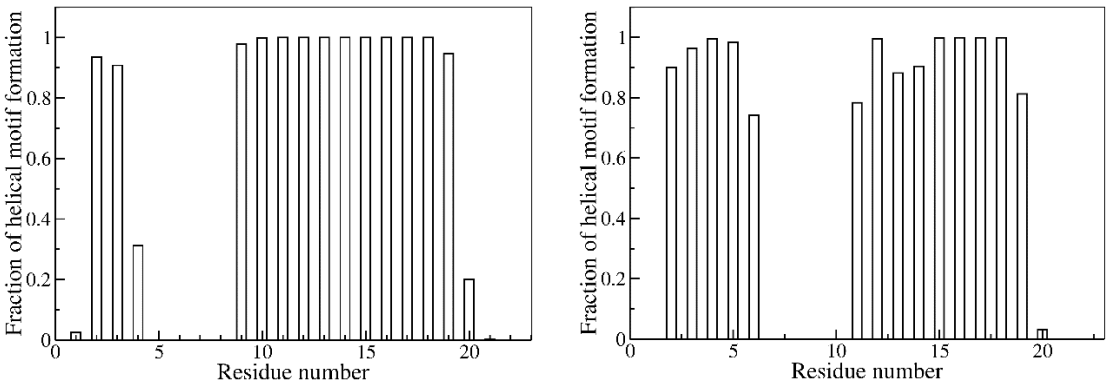

(a) Helical motif of nMSI-78m

(b) Helical motif of MSI-78mn

Figure 2.10 The fraction of helical motif formation for each residue of the redesigned MSI-78 with N-/C-terminus tethered.

To validate the predicted structure of the redesigned peptide on the surface, the CD spectra on surface with both N-terminus and C-terminus immobilized MSI-78 mutants on quartz surface in aqueous phosphate buffer were collected (shown in Figure 2.13b). After surface immobilization, both nMSI-78m and MSI-78mn exhibited alpha helical conformation evidenced by the two negative peaks at 207 nm and 222 nm in the CD spectra.

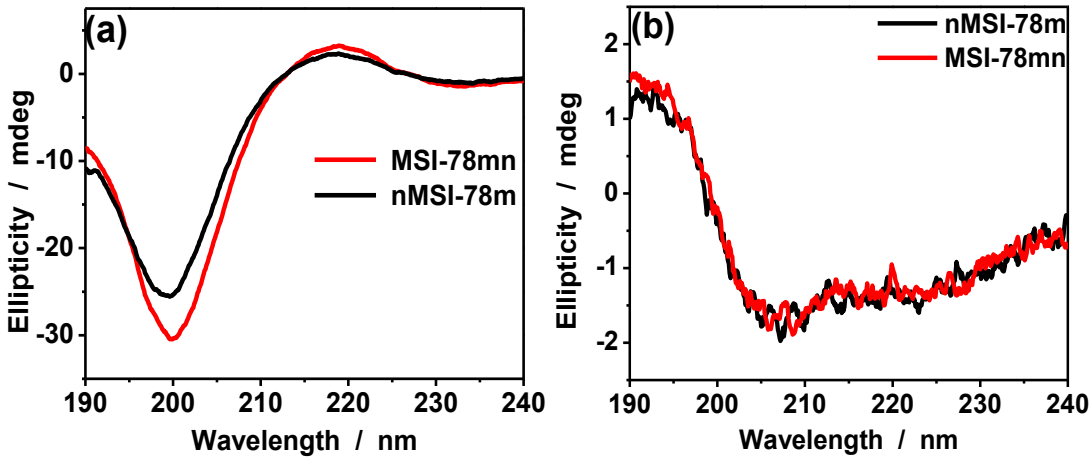

Figure 2.11 CD spectra of free (a) and immobilized (b) nMSI-78m and MSI-78mn in aqueous phosphate buffer.

2.2.3.3 Redesigned Peptide Orientation on the SAM Surface

Since the N-terminus tethered peptide has a single helical structure, we measure the angle ξ formed by the helix and the surface normal using the simulation results. The density distribution of angle ξ as shown in the panel (a) of Figure 2.14 exhibits a tall single peak at the position of around 18°. The density distributions of angle ξ (formed by the first helix and the surface normal) and the angle ς (between two helices) are plotted in panel (b) of Figure 2.14 with blue and red curves, respectively. As shown, the angle ξ has a single tall peak with a small angle with respect to the surface normal and a very narrow angle distribution (<5°) suggesting that the helix I (the one close to the surface) is uniformly perpendicular to the surface for a majority of the simulation time. Interestingly, angle ς has a much broader distribution indicating that the helix II (the one far from the surface) is more flexible to rotate.

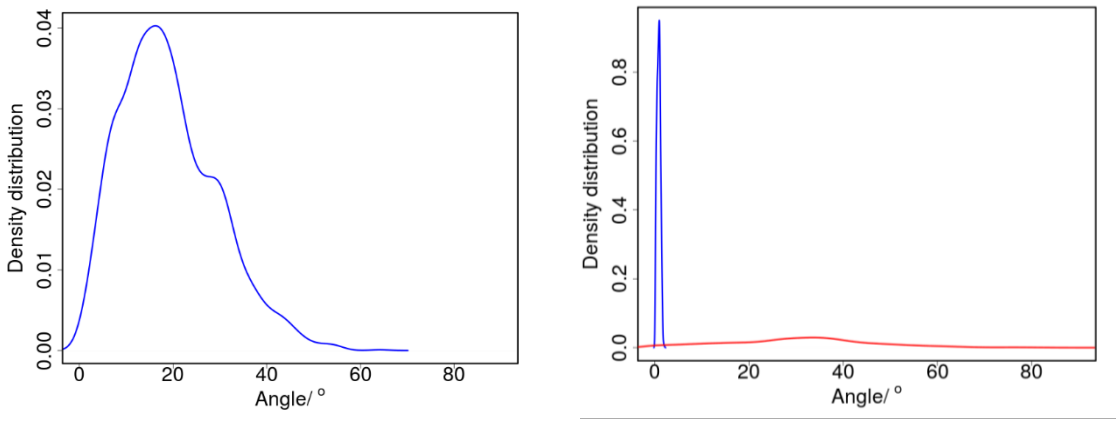

(a) Helix angle (ξ) density distribution of nMSI-78m

(b) Helix angle ξ (blue) and ς (red) density distributions of MSI-78mn

Figure 2.12 Angle distribution of ξ and ς (if needed) for N-/C-terminal tethered peptide deduced by simulation.

As discussed, the single helical structure assumption is not satisfied for the C-terminal tethered peptide so that we cannot compare the angle measured by simulations to the one retrieved from SFG experiments. Instead, the χ_{ppp}/χ_{ssp} ratio from SFG experiment can be predicted according to the developed theoretical method mentioned in Chapter 1 using the average length of helices and the orientation angles calculated using simulation. Here the χ_{ppp}/χ_{ssp} ratio is predicted to be 1.58 for the C-terminal tethered MSI-78 based on the simulated orientation angle distribution shown in Figure 2.12b. To validate the orientation angle measured by simulations for the N-terminal tethered peptide and the predicted χ_{ppp}/χ_{ssp} ratio for the C-terminal tethered peptide, SFG spectra were measured from the immobilized MSI-78 mutants.

As mentioned in Section 2.1, the alkyne SAM we used does not generate background signals in SFG.[84] After surface immobilization, SFG spectra with both ssp and ppp polarization combinations were collected from either nMSI-78m or MSI-78mn in contact with aqueous phosphate buffer solution. A single peak at 1648 cm^{-1} was detected (shown in Figure 2.13), coming from alpha helical conformation of surface immobilized MSI-78 mutants. It further confirms the CD results and indicate that both nMSI-78m and MSI-78mn exhibit ordered alpha helical conformation after surface immobilization.

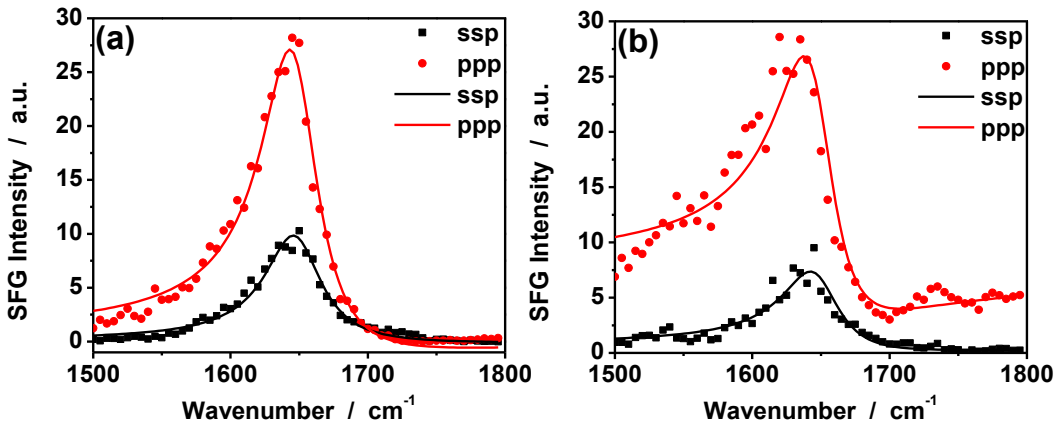

Figure 2.13 SFG spectra and fitting curve of ssp (black square and curve) and ppp (red dot and curve) from a) nMSI-78m and b) MSI-78mn immobilized at alkyne SAM surface in contact with aqueous phosphate buffer.

In order to study the orientation of MSI-78 mutants immobilized on surfaces, SFG spectra of both ssp and ppp were fitted.[40] The measured χ_{ppp}/χ_{ssp} ratio of amide I peak of nMSI-78m is 1.62 and the ratio of MSI-78mn is 1.59 (fitting parameters are shown Table 2.8). Different from azido derivatives of wild type MSI-78, both N- and C-terminus of MSI-78 mutants generate signals in the amide I range. A tilt angle θ, which is determined

from measured χ_{ppp}/χ_{ssp} ratio, can be used to define the orientation angle of the axis of alpha helix relative to the surface normal, as shown in Figure 2.14a. A measured χ_{ppp}/χ_{ssp} ratio of tethered MSI-78 mutants as a function of tilt angle relative to the surface normal was plotted in Figure 2.14b. Since the measured χ_{ppp}/χ_{ssp} ratio is 1.62, the tilt angle of surface immobilized nMSI-78m is 16°, which is close to the angle of 18° measured by simulations. Similar to nMSI-78m, the measured χ_{ppp}/χ_{ssp} ratio of MSI-78mn is 1.59, which is close to the simulation predicted value of 1.58. In sum, after mutation of wild type MSI-78, both N-terminus and C-terminus of MSI-78 mutants tilt a very small angle relative to the surface normal as predicted by the simulation.

Table 2.6 Fitting Parameters for the SFG spectra in Figure 2.13

System	Polarization Combination	Peak Center (cm^{-1})	Peak Width (cm^{-1})	Amplitude
nMSI-78m	ppp	1648	25.0 ± 0.2	126.7 ± 0.9
	ssp	1648	25.0 ± 0.3	78.1 ± 0.6
MSI-78mn	ppp	1648	25.0 ± 0.6	100.3 ± 2.0
	ssp	1648	25.0 ± 0.5	63.2 ± 1.1

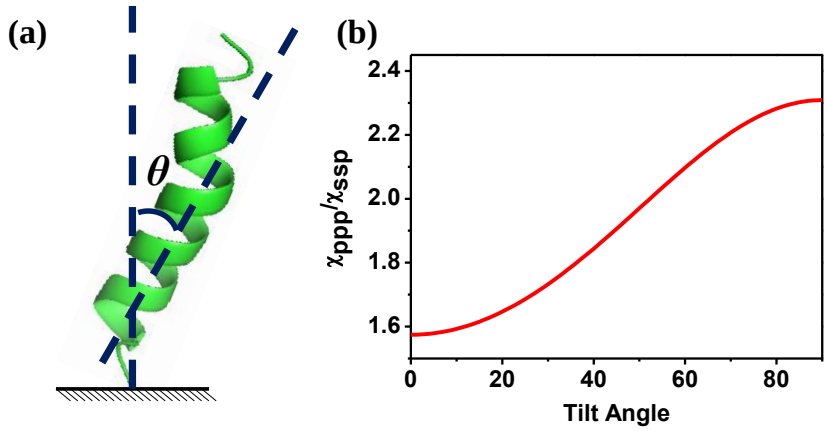

Figure 2.14 a) Scheme of a surface immobilized alpha helical peptide with a tilt angle of θ; b) Calculated χ_{ppp}/χ_{ssp} ratio plotted as a function of the tilt angle of an interfacial helical peptide with a delta distribution.

2.2.4 Conclusion and Discussion

This section develops a new methodology to design a peptide that can adopt controlled orientation after surface immobilization using coarse grained MD simulations. Previously we have shown that surface immobilized MSI-78 adopts different orientations when immobilized with different termini. By mutating two amino acids in MSI-78, this re-designed peptide can adopt a standing-up pose after immobilized on a surface via either terminus. The two mutations are proposed to residues with more hydrophilic properties and with greater helical structure propensity so that the peptide is expected to form a helical structure and perpendicular pose on the surface. The positions of the two redesigned residues are chosen because they were shown in the previous study to contribute largely to the peptide adsorption to the surface.[84] As shown in simulation, the redesigned peptide with only two amino acids mutated is indeed expected to form a helical structure when tethered with either terminus. The simulations result also indicated that the helical structure formation is different for the N- and C-terminal tethered peptide. For the former case, a

peptide is generally found to be a single helix. While for the latter case, the helical structure contains a single bend.

The previous predictions by molecular dynamics simulations were validated by experimental data. The helical structure was confirmed by the CD results. SFG signals were collected from the mutant peptide immobilized via the N-terminus as well as the C-terminus using different polarization combinations. The orientation angle retrieved by the SFG signals for the single helix structure matches the angle deduced from the simulation. Also, for the bent helical structure, the predicted SFG χ_{ppp}/χ_{ssp} ratio based on the averaged helical lengths and orientations from the simulation is consistent with measurements from SFG experiments.

It has been shown that the coarse grained simulation method is capable to predict the behavior of a peptide on a SAM surface in this research and many previous studies.[84, 85] Here for the first time, the simulation prediction was successfully used to design an α-helical MSI-78 mutant for controlled orientations and conformation on a SAM surface, which was further validated by experimental methods. This research demonstrated the power for combining experimental techniques and MD simulations in research. Such a combined approach can be used to design peptides with optimal conformation and orientation after surface immobilization to maximize antimicrobial activity.

2.3 REFERENCES

1. A. Vertes, V. Hitchins and K. S. Phillips, *Analytical Chemistry*, 2012, **84**, 3858-3866.
2. A. G. Gristina, *Science*, 1987, **237**, 1588-1595.

3. L. Hall-Stoodley, J. W. Costerton and P. Stoodley, *Nature Reviews Microbiology*, 2004, **2**, 95-108.

4. J. Nickel, I. Ruseska, J. Wright and J. Costerton, *Antimicrobial Agents and Chemotherapy*, 1985, **27**, 619-624.

5. R. M. Donlan and J. W. Costerton, *Clinical Microbiology Reviews*, 2002, **15**, 167-193.

6. L. McLaughlin-Borlace, F. Stapleton, M. Matheson and J. Dart, *Journal of Applied Microbiology*, 1998, **84**, 827-838.

7. D. Campoccia, L. Montanaro and C. R. Arciola, *Biomaterials*, 2006, **27**, 2331-2339.

8. E. Guaglianone, R. Cardines, C. Vuotto, R. Di Rosa, V. Babini, P. Mastrantonio and G. Donelli, *FEMS Immunology & Medical Microbiology*, 2010, **59**, 410-420.

9. S. Noimark, C. W. Dunnill, M. Wilson and I. P. Parkin, *Chemical Society Reviews*, 2009, **38**, 3435-3448.

10. R. O. Darouiche, *New England Journal of Medicine*, 2004, **350**, 1422-1429.

11. P. S. Stewart and J. William Costerton, *The Lancet*, 2001, **358**, 135-138.

12. E.-R. Kenawy, S. Worley and R. Broughton, *Biomacromolecules*, 2007, **8**, 1359-1384.

13. G. McDonnell and A. D. Russell, *Clinical Microbiology Reviews*, 1999, **12**, 147-179.

14. V. K. Sharma, R. A. Yngard and Y. Lin, *Advances in Colloid and Interface Science*, 2009, **145**, 83-96.

15. S. A. Onaizi and S. S. Leong, *Biotechnology Advances*, 2011, **29**, 67-74.

16. M. Bagheri, M. Beyermann and M. Dathe, *Antimicrobial Agents and Chemotherapy*, 2009, **53**, 1132-1141.

17. H. Jenssen, P. Hamill and R. E. Hancock, *Clinical Microbiology Reviews*, 2006, **19**, 491-511.

18. M. R. Yeaman and N. Y. Yount, *Pharmacological Reviews*, 2003, **55**, 27-55.

19. R. E. Hancock and R. Lehrer, *Trends in Biotechnology*, 1998, **16**, 82-88.

20. K. Gregory and C. M. Mello, *Applied and environmental microbiology*, 2005, **71**, 1130-1134.

21. J. R. Uzarski and C. M. Mello, *Analytical Chemistry*, 2012, **84**, 7359-7366.

22. J. R. Uzarski, A. Tannous, J. R. Morris and C. M. Mello, *Colloids and Surfaces B: Biointerfaces*, 2008, **67**, 157-165.

23. M. Zasloff, *Nature*, 2002, **415**, 389-395.

24. R. E. Hancock and H.-G. Sahl, *Nature Biotechnology*, 2006, **24**, 1551-1557.

25. Y. Ge, D. L. MacDonald, K. J. Holroyd, C. Thornsberry, H. Wexler and M. Zasloff, *Antimicrobial Agents and Chemotherapy*, 1999, **43**, 782-788.

26. M. Zasloff, *Proceedings of the National Academy of Sciences*, 1987, **84**, 5449-5453.

27. A. Ramamoorthy, S. Thennarasu, D.-K. Lee, A. Tan and L. Maloy, *Biophysical Journal*, 2006, **91**, 206-216.

28. B. C. Buer, J. Chugh, H. M. Al-Hashimi and E. N. G. Marsh, *Biochemistry*, 2010, **49**, 5760-5765.

29. K. A. Brogden, *Nature Reviews Microbiology*, 2005, **3**, 238-250.

30. P. Yang, A. Ramamoorthy and Z. Chen, *Langmuir*, 2011, **27**, 7760-7767.

31. H. Sato and J. B. Feix, *Biochimica et Biophysica Acta (BBA)-Biomembranes*, 2006, **1758**, 1245-1256.

32. D.-K. Lee, J. R. Brender, M. F. Sciacca, J. Krishnamoorthy, C. Yu and A. Ramamoorthy, *Biochemistry*, 2013, **52**, 3254-3263.

33. L. M. Gottler and A. Ramamoorthy, *Biochimica et Biophysica Acta (BBA)-Biomembranes*, 2009, **1788**, 1680-1686.

34. K. J. Hallock, D.-K. Lee and A. Ramamoorthy, *Biophysical Journal*, 2003, **84**, 3052-3060.

35. Y. Suzuki, B. C. Buer, H. M. Al-Hashimi and E. N. G. Marsh, *Biochemistry*, 2011, **50**, 5979-5987.

36. E. N. G. Marsh, B. C. Buer and A. Ramamoorthy, *Molecular BioSystems*, 2009, **5**, 1143-1147.

37. L. M. Gottler, H. Y. Lee, C. E. Shelburne, A. Ramamoorthy and E. N. G. Marsh, *ChemBioChem*, 2008, **9**, 370-373.

38. X. Zhu, H. Suhr and Y. Shen, *Physical Review B*, 1987, **35**, 3047-3050.

39. A. G. Lambert, P. B. Davies and D. J. Neivandt, *Applied Spectroscopy Reviews*, 2005, **40**, 103-145.

40. K. T. Nguyen, S. V. Le Clair, S. Ye and Z. Chen, *The Journal of Physical Chemistry B*, 2009, **113**, 12169-12180.

41. Y. Liu, T. L. Ogorzalek, P. Yang, M. M. Schroeder, E. N. G. Marsh and Z. Chen, *Journal of the American Chemical Society*, 2013, **135**, 12660-12669.

42. P. Yang, A. Glukhova, J. J. Tesmer and Z. Chen, *PloS One*, 2013, **8**, e82072.

43. K. T. Nguyen, S. V. Le Clair, S. Ye and Z. Chen, *The Journal of Physical Chemistry B*, 2009, **113**, 12358-12363.

44. J. Wang, M. A. Even, X. Chen, A. H. Schmaier, J. H. Waite and Z. Chen, *Journal of the American Chemical Society*, 2003, **125**, 9914-9915.

45. X. Chen, J. Wang, J. J. Sniadecki, M. A. Even and Z. Chen, *Langmuir*, 2005, **21**, 2662-2664.

46. B. Ding and Z. Chen, *The Journal of Physical Chemistry B*, 2012, **116**, 2545-2552.

47. S. Wei and T. A. Knotts IV, *The Journal of Chemical Physics*, 2013, **139**, 095102.

48. J. Karanicolas and C. L. Brooks, *Proceedings of the National Academy of Sciences*, 2004, **101**, 3432-3437.

49. J. Karanicolas and C. L. Brooks, *Proceedings of the National Academy of Sciences*, 2003, **100**, 3954-3959.

50. Y. Wei and R. A. Latour, *Langmuir*, 2009, **25**, 5637-5646.

51. D. L. Nelson, A. L. Lehninger and M. M. Cox, *Lehninger Principles of Biochemistry*, Macmillan, 2008.

52. C. R. Mcmillin and A. G. Walton, *Journal of Colloid and Interface Science*, 1974, **48**, 345-349.

53. M. Shimizu, K. Kobayashi, H. Morii, K. Mitsui, W. Knoll and T. Nagamune, *Biochemical and Biophysical Research Communications*, 2003, **310**, 606-611.

54. S. E. Blondelle, J. M. Ostresh, R. A. Houghten and E. Perez-Paya, *Biophysical Journal*, 1995, **68**, 351-359.

55. N. Keegan, N. G. Wright and J. H. Lakey, *Angewandte Chemie International Edition*, 2005, **44**, 4801-4804.

56. K. P. Fears, D. Y. Petrovykh, S. J. Photiadis and T. D. Clark, *Langmuir*, 2013, **29**, 10095-10101.

57. B. Sivaraman, K. P. Fears and R. A. Latour, *Langmuir*, 2009, **25**, 3050-3056.

58. S. J. White, S. D. Johnson, M. A. Sellick, A. Bronowska, P. G. Stockley and C. Wälti, *Angewandte Chemie*, 2015, **127**, 988-992.

59. X. Han, L. Soblosky, M. Slutsky, C. M. Mello and Z. Chen, *Langmuir*, 2011, **27**, 7042-7051.

60. X. Han, J. R. Uzarski, C. M. Mello and Z. Chen, *Langmuir*, 2013, **29**, 11705-11712.

61. X. Han, Y. Liu, F.-G. Wu, J. Jansensky, T. Kim, Z. Wang, C. L. Brooks III, J. Wu, C. Xi and C. M. Mello, *The Journal of Physical Chemistry B*, 2014, **118**, 2904-2912.

62. A. Peschel, M. Otto, R. W. Jack, H. Kalbacher, G. Jung and F. Götz, *Journal of Biological Chemistry*, 1999, **274**, 8405-8410.

63. M. Friedel, A. Baumketner and J. E. Shea, *Journal of Chemical Physics*, 2007, **126**, 095101.

64. T. A. Knotts IV, N. Rathore and J. J. d. Pablo, *Biophysical Journal*, 2008, **94**, 4473-4483.

65. G. Anand, S. Sharma, S. K. Kumar and G. Belfort, *Langmuir*, 2009, **25**, 4998-5005.

66. R. A. Latour, *Colloids Surf B Biointerfaces*, 2014, **124**, 25-37.

67. T. Joos and J. Bachmann, *Front Biosci (Landmark Ed)*, 2009, **14**, 4376-4385.

68. J. J. Gray, *Curr Opin Struct Biol*, 2004, **14**, 110-115.

69. G. Anand, S. Sharma, A. K. Dutta, S. K. Kumar and G. Belfort, *Langmuir*, 2010, **26**, 10803-10811.

70. Y. Wei and R. A. Latour, *Langmuir*, 2010, **26**, 18852-18861.

71. L. Li, S. Chen, J. Zheng, B. D. Ratner and S. Jiang, *The Journal of Physical Chemistry B*, 2005, **109**, 2934-2941.

72. S. Chen, J. Zheng, L. Li and S. Jiang, *Journal of the American Chemical Society*, 2005, **127**, 14473-14478.

73. J. I. Lewis, D. J. Moss and T. A. Knotts, *The Journal of Chemical Physics*, 2012, **136**, 245101.

74. B. K. Loong and T. A. Knotts IV, *The Journal of Chemical Physics*, 2014, **141**, 051104.

75. J. Zhou, J. Zheng and S. Jiang, *The Journal of Physical Chemistry B*, 2004, **108**, 17418-17424.

76. J. Zhou, S. Chen and S. Jiang, *Langmuir*, 2003, **19**, 3472-3478.

77. G. Yu, J. Liu and J. Zhou, *The Journal of Physical Chemistry B*, 2014, **118**, 4451-4460.

78. Z. Wu, Q. Cui and A. Yethiraj, *Journal of Chemical Theory and Computation*, 2011, **7**, 3793-3802.

79. Z. Wu, Q. Cui and A. Yethiraj, *The Journal of Physical Chemistry B*, 2010, **114**, 10524-10529.

80. Z. Wang, X. Han, N. He, Z. Chen and C. L. Brooks, 3rd, *J Phys Chem B*, 2014, **118**, 12176-12185.

81. Z. Wang, X. Han, N. He, Z. Chen and C. L. Brooks, 3rd, *J Phys Chem B*, 2014, **118**, 5670-5680.

82. X. Han, J. R. Uzarski, C. M. Mello and Z. Chen, *Langmuir*, 2013, **29**, 11705-11712.

83. X. Han, Y. Liu, F. G. Wu, J. Jansensky, T. Kim, Z. Wang, C. L. Brooks, 3rd, J. Wu, C. Xi, C. M. Mello and Z. Chen, *J Phys Chem B*, 2014, **118**, 2904-2912.

84. Y. Li, S. Wei, J. Wu, J. Jasensky, C. Xi, H. Li, Y. Xu, Q. Wang, E. N. G. Marsh, C. L. Brooks and Z. Chen, *The Journal of Physical Chemistry C*, 2015, **119**, 7146-7155.

85. S. Wei and C. L. Brooks III, *Chinese Chemical Letters*, 2015, DOI: http://dx.doi.org/10.1016/j.cclet.2015.03.020.

86. J. Karanicolas and C. L. Brooks III, *Proc Natl Acad Sci U S A*, 2003, **100**, 3954-3959.

87. J. Karanicolas and C. L. Brooks III, *J Mol Biol*, 2003, **334**, 309-325.

88. J. Karanicolas and C. L. Brooks III, *Proc Natl Acad Sci U S A*, 2004, **101**, 3432-3437.

89. S. M. Law, A. T. Frank and C. L. Brooks, *Journal of Computational Chemistry*, 2014, **35**, 1757-1761.

CHAPTER 3 Enzyme Immobilization on SAMs Through Different Sites and on Different Substrate

The contents in Section 3.1 have been adapted from the following manuscript which has been submitted recently: **Li Y**, Ogorzalek TL, Wei S, Zhang X, Yang P, Jasensky J, Brooks CL III, Marsh ENG, Chen Z. Effects of Mutation Sites on the Orientation and Activity of Surface-Tethered Enzymes.

3.1 EFFECTS OF MUTATION SITES ON THE ORIENTATION AND ACTIVITY OF SURFACE-TETHERED ENZYME, β-GALACTOSIDASE (β-GAL)

3.1.1 Introduction

Enzymes and proteins are often immobilized on solid surfaces for use in applications such as antibacterial and/or antifouling coatings,[1, 2] industrial catalysis,[3] drug delivery,[4] biosensors,[5, 6] and biofuel cells.[7] The immobilization of enzymes on surfaces can dramatically improve the stability, reusability, and the lifetime of enzymes.[8, 9] Moreover, surface immobilization can also broaden the application of enzymes by improving stability under harsh conditions.[10] Despite these benefits, when enzymes are immobilized on abiotic surfaces, the activity often significantly decreases.[11] The molecular mechanisms underlying this decrease are still not well understood.

Different methods have been used to immobilize enzymes on abiotic surfaces, including physical adsorption and covalent attachment.[8, 9, 12-17] Physical adsorption can be accomplished through hydrophobic or ionic interactions between the enzyme molecules and the surface. Since immobilizing enzymes on a surface via non-covalent interactions requires little or no modification of the enzymes, this approach is widely used; however, the physically adsorbed enzymes may leach from the solid support thereby decreasing device activity over time. In addition, physical adsorption randomly orients the enzyme molecules with respect to the surface,[8] with the result that many enzymes may be immobilized in inactive orientations.

Covalent attachment provides greater control over immobilization and prevents enzyme leaching from the surface. A common approach is to cross-link enzymes to a surface functionalized with amine-reactive moieties, such as N-hydroxysulfosuccinimide (sulfo-NHS). This takes advantage of the prevalence of surface lysine residues in most proteins to chemically immobilize the enzyme on the surface. However, analogous to physical adsorption, non-specific cross-linking leads to enzymes immobilized in many different orientations, many of which may be inactive. [18-20]

The stability and activity of enzymes tethered on solid surfaces is also strongly dependent on the properties of the substrate surfaces.[21] However, a detailed understanding of the relationship between the protein attachment site, the chemical properties of the abiotic surface, and enzyme activity remains elusive.

Site-specific surface immobilization of proteins has been investigated previously *in situ* using a combination of surface/interface-sensitive second-order nonlinear sum

frequency generation vibrational spectroscopy (SFG) and attenuated total reflectance Fourier transform infrared spectroscopy (ATR-FTIR).[22-28] By using different polarizations of the input/output beams of SFG or ATR-FTIR, orientation of surface immobilized enzymes can be deduced. Previously, we studied the orientation of surface-tethered 6-phospho-β-galactosidase (β-gal) and nitroreductase (NfsB) on pure maleimide-terminated SAM surfaces using a combination of SFG and ATR-FTIR.[22, 24]

In this section, we engineered two variants of β-galactosidase (β-gal) (E227C and D308C), each containing a unique, solvent exposed cysteine residue through which the enzyme could be tethered to a maleimide-terminated SAM surface in a chemically well-defined manner. Previously we examined the properties of β-gal tethered to a maleimide-terminated SAM surface through a position such that the active site was fully exposed to the bulk solvent. In this case the cysteinyl groups of both the β-gal mutants were introduced into loops close to the active site with the intention of bringing the active site close to the surface (Figure 3.1). We examined effect of re-orienting the enzyme with respect to the surface on enzyme activity and on enzyme structure using a combination of SFG and coarse grained MD simulations. We also examined how the properties of β-gal-D308C varied when immobilized on maleimide/hydroxyl mixed SAM surfaces.

3.1.2 Materials and Methods

All chemicals were purchased from Sigma-Aldrich (St. Louis, MO, USA) and used without further purification unless otherwise stated. O-(propargyl)-N-(triethoxysilylpropyl) carbamate (alkyne-silane) was obtained from Gelest (Arlington, VA). Azido-PEG_3-

maleimide linker was obtained from Click Chemistry Tools (Bioconjugate Technology Company, Scottsdale, AZ). Azido-PEG$_3$-alcohol linker was obtained from Conju-Probe (San Diego, CA).

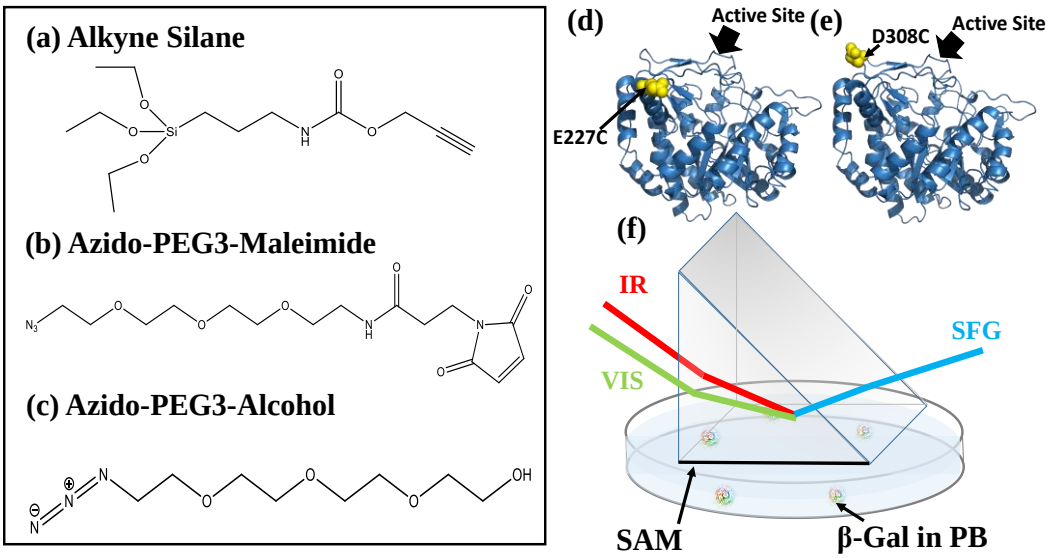

Figure 3.1 Molecular formulas of (a) alkyne silane, (b) azido-PEG3-maleimide linker, and (c) azido-PEG3-alcohol linker; crystal structures (with active site shown) of (d) β-gal-E227C and (e) β-gal-D308C; (f) SFG experimental geometry (near total reflection geometry) used to study surface immobilized enzymes in phosphate buffer.

3.1.2.1 Surface Functionalization

SiO_2 coated right-angle CaF_2 prisms were cleaned and prepared as discussed in Chapter 1. After cleaning, prisms were immediately placed into a freshly prepared 1.0 mM alkyne-silane (molecular structure shown in Figure 3.1a) in anhydrous toluene for 24 h at room temperature. The functionalized prisms were then rinsed with copious amounts of toluene and methanol, and then were dried under nitrogen gas.

Azido-PEG_3-maleimide linker (molecular structure shown in Figure 3.1b) was prepared according to the manufacturer's instruction. The alkyne functionalized prisms were placed into an aqueous solution containing azido-PEG_3-maleimide linker (1 mM), sodium ascorbate (0.2 M), and copper sulfate (0.5 mM), and reacted overnight. The prisms were then rinsed with water, EDTA, and water to remove the residual copper ions. In addition to the pure maleimide-terminated SAM surface, a mixed SAM surface of maleimide and hydroxyl groups (1:10) was also prepared. The alkyne-functionalized prisms were placed into a water solution containing sodium ascorbate (0.2 M), copper sulfate (0.5 mM), azido-PEG_3-maleimide linker, and azido-PEG_3-alcohol linker (molecular structure shown in Figure 3.1c) (molar ratio = 1:10), and reacted overnight. The prisms were then rinsed with water, EDTA, and water again.

3.1.2.2 SFG Measurement

SFG theory and optical setup have been described in Chapter 1 and previous publications.[29-45] SFG has been widely used to study polymers,[31, 46-49] lipids,[50-53] and biomolecules at surfaces/interfaces.[26, 54-60] The incident angles of the 532 nm visible beam and wavelength-tunable infrared beam for the SFG experiments performed in this Section (Figure 3.1f) are 57 and 55 degrees relative to the surface normal respectively before traveling through the prism. All SFG spectra were collected in the ssp (s-polarized output SFG signal, s-polarized input visible beam and p-polarized input IR beam) and ppp polarization combinations using the near total internal reflection geometry (Figure 3.1f). 10 μL of 100 mM Tris(2-carboxyethyl) phosphine hydrochloride solution (TCEP) was added into the β-Gal stock solution and incubated at room temperature for 30 min to reduce

disulfide bonds formed between cysteinyl residues. SFG spectra were then collected from the maleimide-terminated SAM surface in contact with the subphase 5 mM phosphate buffer (pH = 7.4) in a 2 mL reservoir. After that, the stock enzyme solution (with TCEP) was added into the subphase buffer to reach a final concentration of 5 μM. SFG time dependent signal was immediately collected until the system was equilibrated (the signal reached a plateau). Before the collection of any SFG amide I spectra from the immobilized enzymes, the SAM/enzyme solution interface was washed by detergent, Tween 20, to remove any physically adsorbed β-gal molecules. Then SFG spectra with different polarization combinations were collected from the SAM surface in contact with phosphate buffer (which replaced enzyme solution) and analyzed.[23, 26]

3.1.2.3 Design and Expression of Modified β-Galactosidase Constructs

The design and expression of variants of *Lactobacillus lactis* derived 6-phospho-β-galactosidase (PDB entry 2PBG) have been described previously,[24, 61] and carried out by Prof. Neil Marsh's group at the University of Michigan. Briefly, all cysteinyl residues of the native protein were mutated to alanine. To introduce a unique surface-exposed cysteinyl residue within a loop region near the active site, two constructs were produced. One construct mutated Asp-308 to cysteine, while the other construct mutated Glu-227 to cysteine. The specific activity of these mutants in solution was measured using the commercially available chromogenic substrate 2-nitrophenyl-β-galactopyranoside, and found to be within error of that reported for wild type enzyme.[24] Enzymes were stored at concentrations of 50-100 μM at -80 ^{o}C. The presence of exposed reduced cysteinyl residues was verified using the DNTB assay described previously.[24]

3.1.2.4 Enzyme Assay

Enzyme activity was measured using a procedure that was described previously,[24] and carried out by Prof. Neil Marsh's group at the University of Michigan. Briefly, 18-20 mg of beads deriviatized with surface tethered β-gal was suspended into 100 μL of 100 mM potassium phosphate, pH 7.6, 1% DMSO. Assays were initiated by the addition of resorufin β-D-galactopyranoside to a final concentration of 50 μM. Activity was determined by measuring the formation of resorufin with an excitation at 571 nm and recording emission at 584 nm. Typically, ten 1-minute time points were collected for each rate measurement. The surface density of the immobilized protein was determined using the bicinchoninic acid assay described previously.[24]

3.1.2.5 Molecular Dynamics (MD) Simulations

Protein conformations and orientations were measured by employing MD simulation utilizing a coarse-grained method and performed by Prof. Charles Brooks's group at the University of Michigan. This model was building upon Karanicolas and Brooks Go-like protein model by incorporating with a well-parameterized solid surface force field developed previously.[62-66] The key feature of this modeling method is that it quantitatively accounts for the protein-surface hydrophobic interactions between different protein residues and solid materials. This advantage of the model has been successfully applied and validated in thermodynamic studies of the same enzyme system.[67] The details of the model and simulations were described in our previous study except the enzyme tethering sites.[67] As for the mixed maleimide/hydroxyl SAM surface, we accounted for the combined effects of the two types of surface functional groups by mixing weighted

hydrophobic terms. The protein orientation was quantified by calculating the tilt and twist angle with respect to a pre-defined (0,0) pose, for each mutant during the course of the simulations. The orientations (defined by the tilt and twist angles) of the protein on the surface were then projected onto the theoretical map of SFG signal intensity and χ ratios to delineate the anticipated experimental quantities for comparison with the measurements.

3.1.3 Results and Discussion

3.1.3.1 SFG Characterization of Alkyne Terminated SAM and Maleimide Terminated SAM Surfaces

Background SFG spectra were first collected from the SAM surfaces in the absence of immobilized proteins. The supporting substrate used in this study for SAM deposition is a CaF_2 right-angle prism with a layer of 100 nm SiO_2 coating (to facilitate silane chemistry). SFG spectra were collected in the amide I frequency region (1500 cm^{-1}-1800 cm^{-1}) from clean CaF_2 prism with the SiO_2 coating, alkyne terminated SAM on the prism, as well as the alkyne terminated SAM reacted with the maleimide linker. As shown in Figure 3.2a, no noticeable SFG signals were generated from the clean prism before the SAM deposition in the amide I frequency range. Once the alkyne-silane SAM was immobilized onto the CaF_2 prism, a small peak at ~1710 cm^{-1}, originated from the C=O stretching in the alkyne silane molecule, was observed in the ppp SFG spectrum (Figure 3.2b).

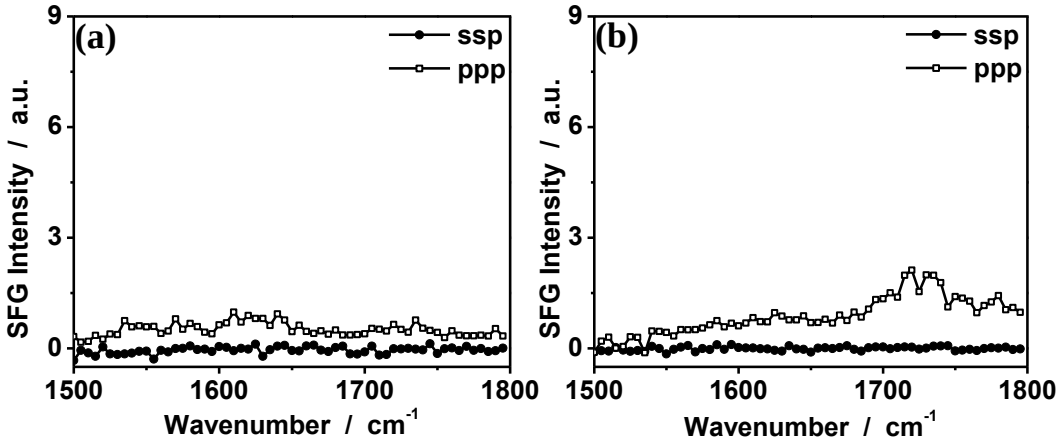

Figure 3.2 SFG ssp and ppp spectra collected from (a) clean CaF_2 prism with a layer of 100 nm SiO_2 coating and (b) alkyne silane functionalized prism surface in contact with phosphate buffer.

After the characterization of the alkyne-terminated SAM surface, a maleimide terminated surface after coupling the maleimide linker to the alkyne terminated SAM was also examined using SFG. The azido-PEG_3-maleimide linker (Figure 3.1) was attached to the alkyne derivatized surface by "click" chemistry. The SFG spectra were collected from the maleimide terminated SAM surface in phosphate buffer (Figure 3.3). As seen in Figure 3.3, a peak at ~1710 cm^{-1} was observed from the maleimide-terminated SAM surface in both the ssp and ppp spectra. The measured intensity of this peak in the ppp spectrum was higher than that detected from the alkyne-terminated SAM surface (before the linker coupling, Figure 3.2b). This is likely due to the increase of the number of C=O bonds in the system from the azido-PEG_3-maleimide linkers. This result was also confirmed by angular-resolved XPS, shown in Figure 3.4, which will be discussed below. After fitting the SFG spectra shown in Figure 3.3 (fitting parameters shown in Table 3.1), the peak center was measured to be 1711 cm^{-1}. We also studied the mixed SAM surface (1:10 maleimide to hydroxyl group terminated SAMs prepared by coupling the maleimide and

hydroxyl linkers with a ratio of 1:10) using SFG (data not shown). The results are similar to that from the pure maleimide terminated SAM surface. Nevertheless, no SFG signal was detected from all the above background surfaces between 1600 and 1700 cm^{-1}, where the protein amide I signal would be detected.

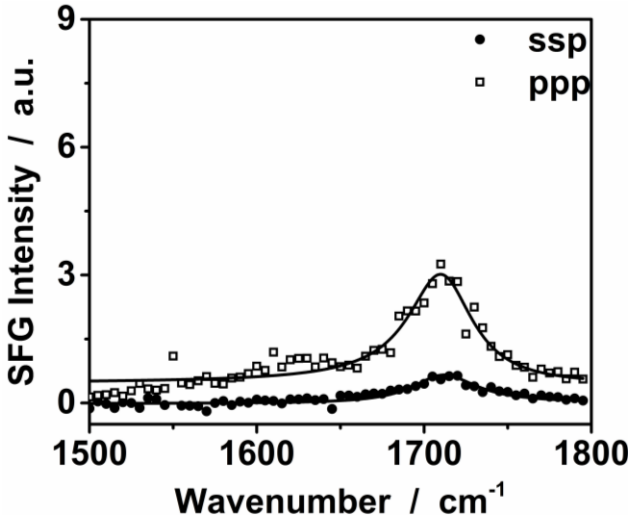

Figure 3.3 SFG ssp and ppp spectra collected from maleimide functionalized surface in phosphate buffer.

Table 3.1 Fitting parameters for SFG spectrum shown in Figure 3.3

	χ_{NR}	A	ω (cm^{-1})	Γ (cm^{-1})
ppp	0.45	37.6 (0.8)	1711	23.5
ssp	-0.01	19.2 (0.8)	1711	23.5

With angular-resolved XPS, more accurate results could be collected from thin SAM surfaces, minimizing the signal contribution from silicon wafer substrates. However, the ratio calculation of different chemical bonds based on the XPS intensity is still not reliable due to the thinness of the SAM.

XPS results were shown below in Figure 3.4. Spectra were collected from many surfaces, including silicon wafer substrate used for SAM construction, which contained air contaminants on the wafer surface, as well as wafers functionalized using an alkyne terminated SAM. Signals of C-C/C-H, C-O, and C=O increased and those bonds can all be found in alkyne silane molecular structure, shown in Figure 3.1a. Then the surface was functionalized either with pure maleimide terminated SAM, or a mixture of maleimide and hydroxyl groups, and XPS spectra were collected, shown in Figure 3.4c and d. In both cases, a large increase of C-O signals was observed. As seen in Figure 3.1b and 3.1c, large amounts of C-O bonds were present in azido-PEG_3-maleimide and azido-PEG_3-alcohol linkers.

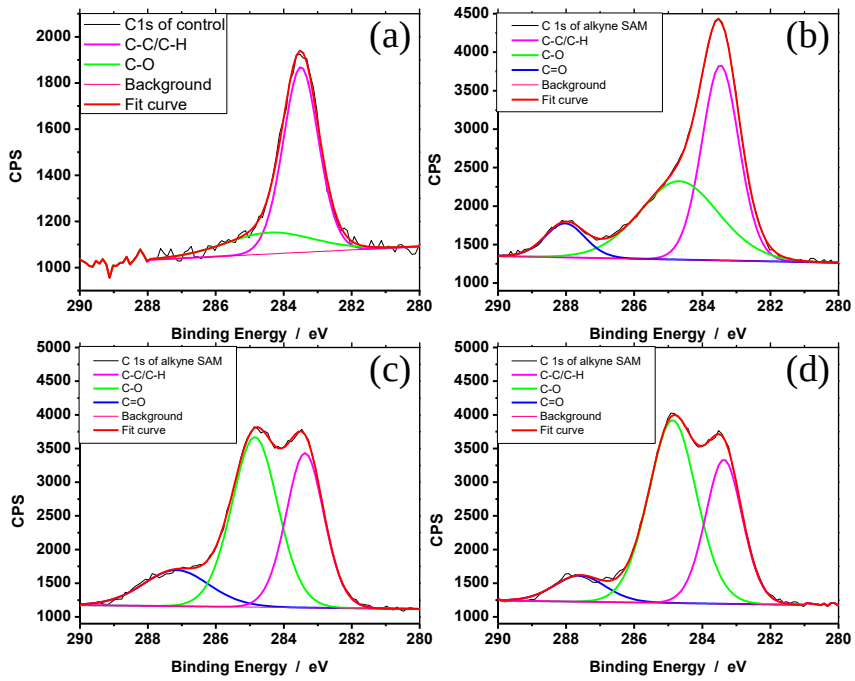

Figure 3.4 Angular-resolved XPS spectra collected from (a) silicon wafer with 100 nm silica (control); (b) alkyne terminated SAM; (c) maleimide terminated SAM; (d) 1:10 (maleimide : hydroxyl) terminated mixed SAM.

3.1.3.2 Surface Immobilization of β-gal-D308C and β-gal-E227C on Pure Maleimide Surfaces

SFG spectra were collected from the maleimide terminated SAM interface with buffer and no signal was detected between 1600 and 1700 cm^{-1}. The β-gal-D308C enzyme was then chemically coupled to the maleimide terminated SAM surface and examined by SFG. The reaction of enzyme with the surface was followed by monitoring the SFG signal at amide I frequency of 1650 cm^{-1} as a function of time.[68, 69] Figure 3.5a shows an increase followed by a decrease of the SFG amide I signal before it finally reaches equilibrium. We hypothesize that this dynamic behavior was due to a two-step immobilization process: firstly, β-gal molecules are rapidly non-covalently adsorbed to the maleimide surface, indicated by the SFG signal increase. The adsorption process was then followed by the chemical attachment of β-gal-D308C (possibly with a protein reorientation) onto the surface. At the same time, some non-covalently attached protein molecules left the surface. Both the immobilized protein reorientation and protein desorption could cause the SFG signal to decrease.

In order to remove any remaining nonspecifically bound protein molecules on the maleimide SAM surface, the prism was then washed with 5% Tween 20 after the SFG amide I signal reached equilibrium. Following the detergent wash, several additional phosphate buffer washes were performed in order to remove the residual loosely adsorbed protein molecules, TCEP, and detergent on the surface.

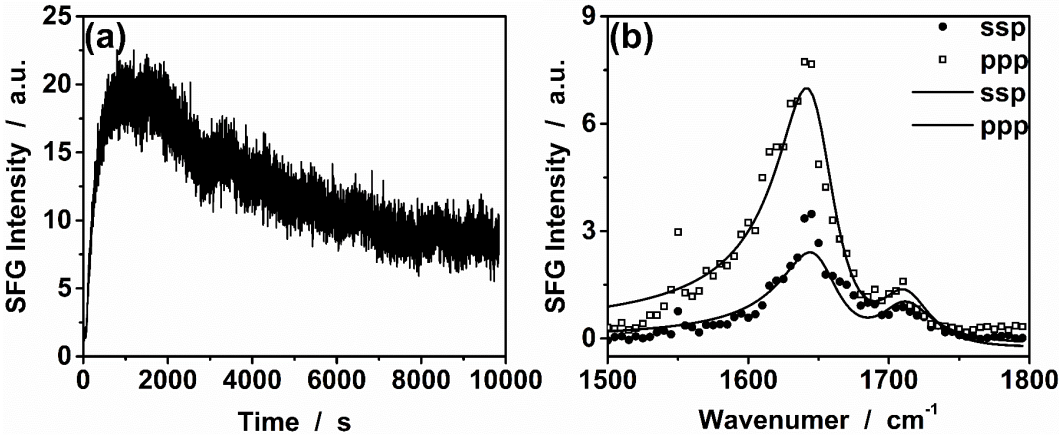

Figure 3.5 (a) SFG time dependent signal collected from the maleimide surface in contact with the phosphate buffer with β-gal-D308C mutant added at time 0 s; (b) SFG ssp and ppp spectra collected from the surface immobilized β-gal-D308C in phosphate buffer.

SFG ssp and ppp spectra were collected from the immobilized proteins at the SAM/phosphate buffer interface (Figure 3.5b). Both the spectra contain a dominant peak at 1650 cm^{-1}, mainly originating from the predominant alpha-helical secondary structure in β-gal. Another peak at 1711 cm^{-1}, found in Figure 3.3, originated from the carbonyl group in alkyne SAM and maleimide linker. After fitting the SFG spectra (fitting parameters shown in Table 3.2), the χ_{zzz}/χ_{yyz} ratio was determined to be 1.90. This ratio can be used to deduce the possible orientation of the β-gal-D308C after surface immobilization, which will be discussed later.

Table 3.2 Fitting parameters for SFG spectra shown in Figure 3.5

	χ_{NR}	A	ω (cm^{-1})	Γ (cm^{-1})
ppp	-0.57	58.4 (1.5)	1648	25
		21.8 (2.9)	1711	23.5

ssp	-0.25	33.4 (0.6)	1650	25
		20.3 (1.9)	1711	23.5

β-gal-E227C, immobilized under the same conditions as β-gal-D308C, was also studied by SFG. The SFG signal at 1650 cm^{-1} was monitored as a function of time (Figure 3.6a) to follow the enzyme immobilization to the surface. After the SFG signal reached equilibrium, the prism surface was washed to remove non-specifically bound enzyme and SFG ssp- and ppp-polarized spectra were collected from the immobilized enzyme molecules at the SAM/buffer interface, as shown in Figure 3.6b. By fitting the spectra (fitting parameters shown in Table 3.3), the χ_{zzz}/χ_{yyz} ratio for β-gal-E227C on surface was determined to be 1.86.

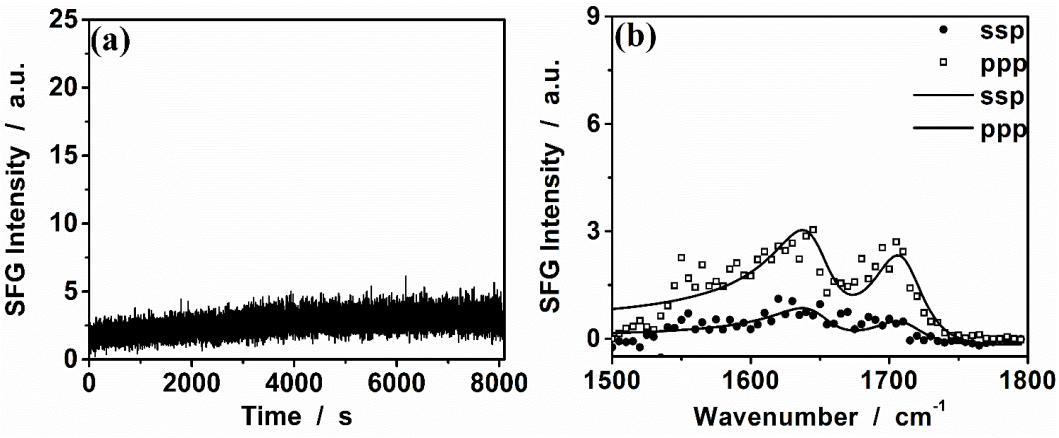

Figure 3.6 (a) SFG time-dependent signal collected from the maleimide terminated SAM surface in contact with the phosphate buffer with β-gal-E227C mutant added at time 0 s; (b) SFG ssp and ppp spectra collected from the surface immobilized β-gal-E227C in phosphate buffer.

Table 3.3 Fitting parameters for SFG spectra shown in Figure 3.6b

	χ_{NR}	A	ω (cm^{-1})	Γ (cm^{-1})
ppp	-0.68	26.9 (0.8)	1648	25
		32.3 (1.7)	1711	23.5
ssp	-0.39	15.7 (1.9)	1648	25
		16.0 (1.7)	1711	23.5

β-gal-D308C and β-gal-E227C were engineered to contain the single cysteinyl residue near the active site (Figure 3.1). Therefore, we expected that the immobilized β-gal-D308C and β-gal-E227C enzymes should be similarly oriented. This expectation is supported by fact that the χ_{zzz}/χ_{yyz} ratios, which are 1.90 and 1.86 for immobilized β-gal-D308C and β-gal-E227C respectively, are very similar. However, we would also expect that the two immobilized enzymes should have a similar SFG intensity as well (if the surface coverage is similar), which, comparing the spectra shown in Figures 3.5b and 3.6b is clearly not the case.

The surface concentrations of immobilized β-gal-D308C and β-gal-E227C were measured using the bicinchoninic acid method.[26] The surface concentrations for the two immobilized enzyme variants were the same within error (Figure 3.7a). The specific activity of the immobilized enzymes was determined using the fluorogenic substrate, resorufin β-D-galactopyranoside. Both immobilized enzymes were similarly active in the assay, but, interestingly, were significantly less active than the previously characterized β-gal-V152C[24] variant immobilized on maleimide-terminated SAM. The β-gal-V152C

construct oriented the active site towards the bulk solution, rather than towards the immobilization surface, as is the case for β-gal-D308C and β-gal-E227C. This suggests that substrate access to the enzyme active site may affect the activity of immobilized β-gal.

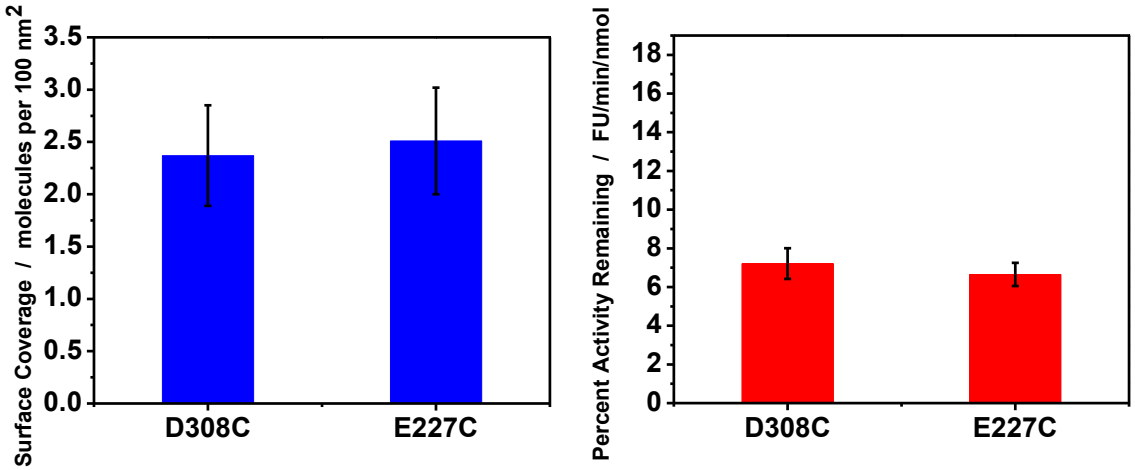

Figure 3.7 (a) Surface coverage of immobilized β-gal-D308C and β-gal-E227C measured using bicinchoninic acid assay; (b) Enzymatic activity of surface immobilized β-gal-D308C and β-gal-E227C measured using resorufin β-D-galactopyranoside. Error bars represent standard error of five measurements.

3.1.3.2 Molecular Dynamics Simulations

To more accurately determine the immobilized β-gal orientation and further interpret the SFG data, we performed molecular dynamics simulations using a coarse-grained protein model. The orientations of the surface immobilized β-gal-D308C and β-gal-E227C obtained from the MD simulations were plotted on the orientation dependent SFG signal strength χ_{zzz} map (Figure 3.8a) and on the orientation dependent SFG χ_{zzz}/χ_{xxz} ratio map. These maps were calculated using previously published methods described in previous publications [23, 26] with the crystal structure of β-gal as the model.

Figure 3.8a shows that although the orientations of the two surface immobilized enzymes are similar, the measured SFG signal strengths change substantially with small changes in enzyme orientation in this region of the orientation map. This simulation result is well correlated to the SFG data presented above.

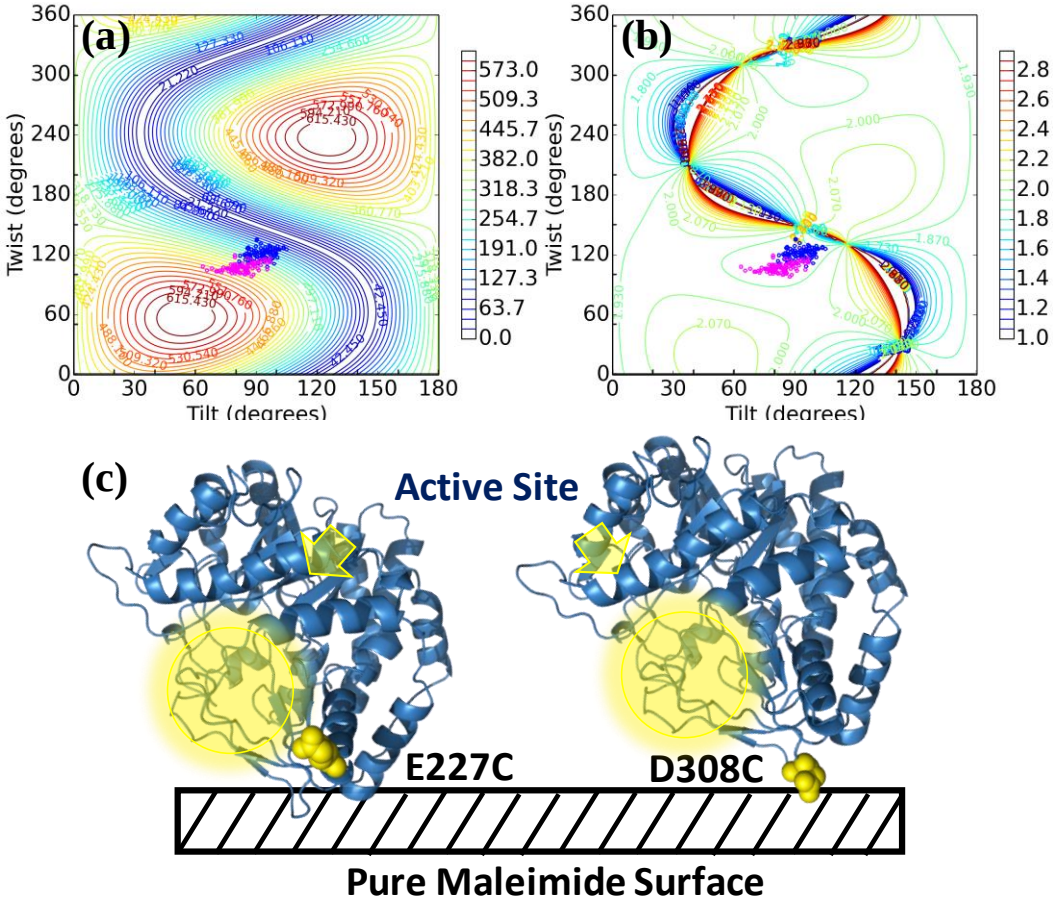

Figure 3.8 The calculated orientation dependent maps of (a) SFG χ_{zzz} and (b) SFG χ_{zzz}/χ_{xxz}. Protein orientation is defined by a tilt angle and a twist angle. The orientation angle regions of β-gal-D308C and β-gal-E227C from our MD simulations are denoted by the dots in the maps. The blue dots indicate the orientation of β-gal-E227C and the magenta dots indicate the orientation of β-gal-D308C. (c) Schematic showing the orientations of surface immobilized β-gal-E227C and β-gal-D308C.

From the simulated orientation data for the two enzymes and the calculated orientation dependent SFG ppp-polarized signal plots, we find the ratio of $\chi_{zzz,D308C}/\chi_{zzz,E227C}$ to be 2.3, which is very similar to the experimentally derived value of 2.2. Also, from Figure 3.8b, we see that the simulated χ_{zzz}/χ_{xxz} ratios for the two cases are around 2.0, which is close to the experimentally measured value of ~1.9 for both cases. Thus, our molecular dynamics simulations on SFG intensity and ppp/ssp ratio provide a molecular level interpretation of the protein orientation for surface-tethered β-gal-D308C and β-gal-E227C. Table 3.4 summaries the possible orientation angle regions of surface immobilized β-gal-D308C and β-gal-E227C as determined from our molecular dynamics simulations. In both cases, with either tethering site, β-gal is found from the simulations to maintain its folded structure on the surface with no substantial conformational changes. A representative orientation of the surface immobilized β-gal-D308C or β-gal-E227C is shown in Figure 3.8c

Table 3.4 Possible Orientation Angle Ranges Obtained by MD Coarse Grained Simulation

Mutants	Tilt Angle Range	Twist Angle Range
β-gal-D308C	(63.5, 97.1)	(98.0, 119.0)
β-gal-E227C	(81.6, 105.3)	(108.4, 135.2)

3.1.3.3 Immobilization of β-gal on Mixed SAM Surfaces

To explore the effects of altering the hydrophobicity of the SAM surface on the structure and activity of the immobilized enzymes, a mixed SAM surface was prepared comprising 9% maleimide- and 91% hydroxyl-terminated PEG linkers. For this study, β-

gal-D308C was chosen because when immobilized this enzyme generates a much larger SFG signal than β-gal-E227C. The enzymatic activity of β-gal-D308C on this surface was significantly higher than that on the pure maleimide-terminated SAM surface, as shown in Figure 3.9b. This may be due to surface crowding effects and the different orientations of β-gal-D308C after surface immobilization on the two SAM surfaces, which will be discussed in more detail below.

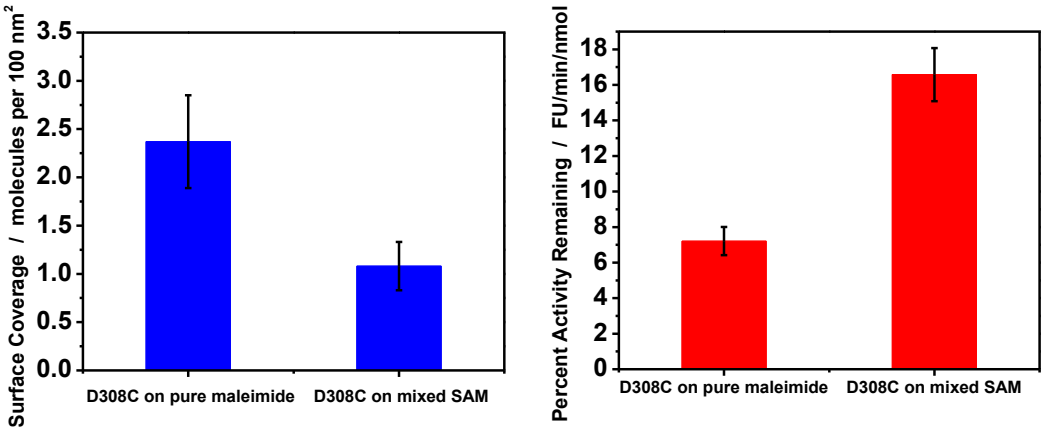

Figure 3.9 (a) Measured surface coverages of β-gal-D308C immobilized on the maleimide SAM surface and a maleimide/OH mixed surface; (b) Measured activities of β-gal-D308C on the maleimide SAM surface and maleimide/OH mixed surface. Error bars were generated from five measurements.

The surface coverage of β-gal-D308C immobilized onto the maleimide : hydroxyl mixed SAM surface decreased (Figure 3.9a), possibly due to the lower concentration of maleimide groups on the mixed SAM surface. Therefore, the increase in specific activity when β-gal-D308C was immobilized on the maleimide : hydroxyl mixed surface might be due to an increase in freedom of motion of the immobilized enzyme, which could reduce potential unfavorable interactions between the enzyme active site and the surface. To study how the change in SAM composition affected the orientation of immobilized β-gal-D308C,

SFG spectra were collected from the immobilized protein at the SAM/phosphate buffer interface. In this case much weaker SFG signals were detected in amide I range, as shown in Figure 3.10. The weaker SFG signals are unlikely due to just the lower surface concentration of enzyme. They may reflect a more disordered enzyme structure (e.g., a larger orientation distribution).

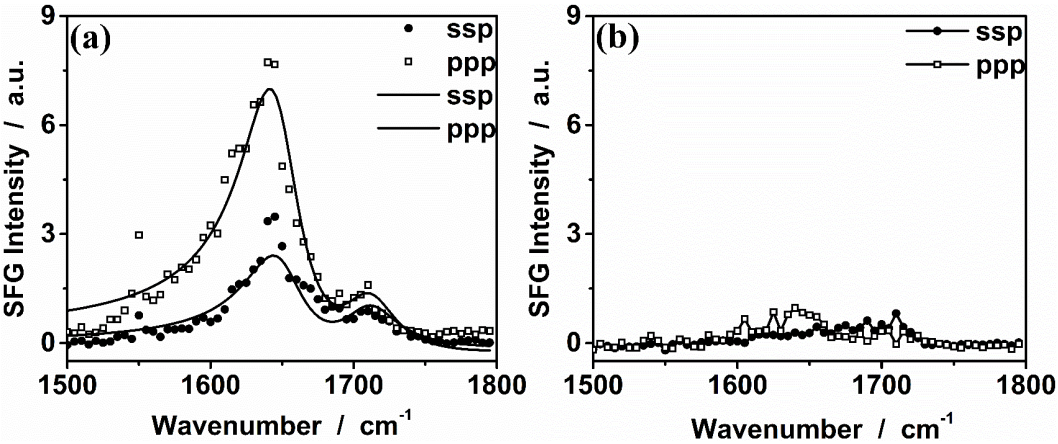

Figure 3.10 SFG ssp and ppp spectra collected from surface immobilized β-gal-D308C on (a) pure maleimide SAM surface and (b) mixed SAM surface in contact with phosphate buffer.

We also performed molecular dynamics simulations to examine the orientation of β-gal-D308C immobilized on mixed SAM surface. The most probable orientations identified by the simulations are shown in Figure 3.11 as magenta dots. For comparison, the most probable orientations of immobilized β-gal-D308C on pure maleimide SAM surface are replotted in Figure 3.11 as cyan dots. The possible distribution of orientations found in these simulations was much larger for β-gal-D308C immobilized on the mixed SAM surface than that on the pure maleimide surface.

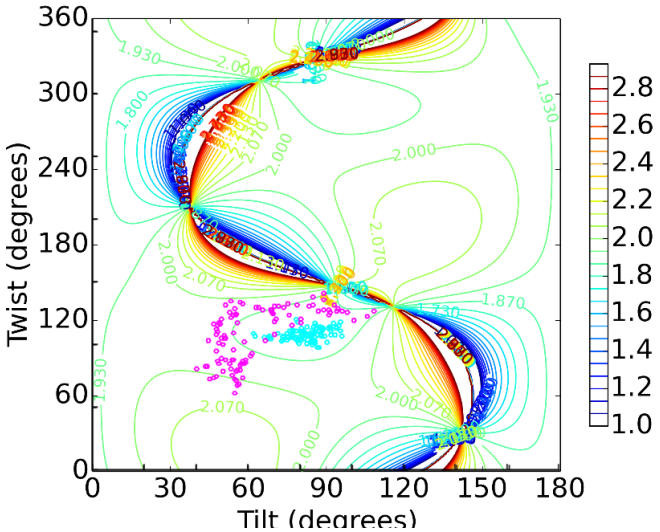

Figure 3.11 Dependence of the SFG χ_{zzz}/χ_{xxz} ratio on the tilt and twist angles of immobilized β-gal.[23, 26] Magenta dots indicate the orientations of β-gal-D308C on the 1:10 maleimide/OH surface and the cyan dots indicate the orientation of β-gal-D308C on a pure maleimide surface.

3.1.3.4 Comparison to β-gal-V152C Mutant

In order to have a deeper understanding of the effect of orientation and surface property on enzymatic activity, we compare what was studied in this section to a previously published β-gal mutant V152C, in which its mutation site is at the opposite side of the active site.[24] Surface coverage and activity of β-gal-V152C immobilized on pure maleimide and mixed SAM surface were measured and plotted in the same figure with other mutants (Figure 3.12).

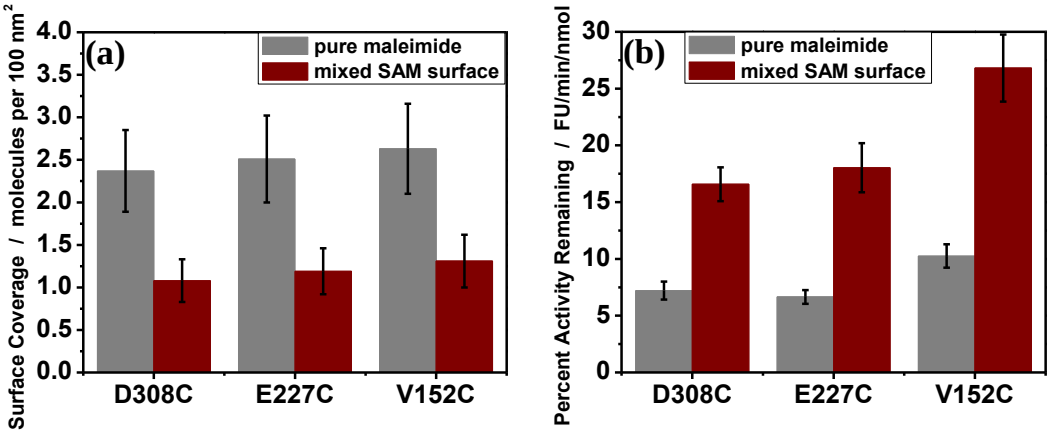

Figure 3.12 (a) Surface coverage and (b) activity of surface immobilized β-gal-D308C, E227C, and V152C.

Figure 3.12 shows both the surface coverage and enzymatic activity of D308C, E227C, and V152C immobilized on maleimide and mixed SAM surfaces. Similar to the mutants D308C and E227C discussed above, the surface coverage of V152C is lower after immobilization on the mixed SAM surface compared to that on the pure maleimide SAM surface. Moreover, the enzymatic activity of V152C was found to increase when the enzyme was immobilized on a mixed SAM surface. With a more preferred orientation with the active site farther away from the surface, surface immobilized mutant V152C exhibits a higher activity compared to mutants D308C and E227C.

3.1.4. Conclusion

We have characterized β-gal immobilized on both pure maleimide-functionalized SAM and on a more hydrophilic mixed SAM surface. Despite having very different SFG spectral intensities, molecular dynamics simulations indicate that β-gal immobilized at

either position 308 or 227, which are located at nearby positions on the enzyme surface close in space, adopt similar orientations. β-gal-D308C and β-gal-E227C also possess similar activities, consistent with their similar surface orientations. Moreover, the immobilized β-gal-D308C and β-gal-E227C enzymes exhibit lower activity compared to previously studied β-gal-V152C in which the immobilization site is far from the active site. This suggests that enzyme orientation influences the enzyme activity after surface immobilization.

β-gal-D308C exhibited significantly higher activity when immobilized on a mixed maleimide : hydroxyl-terminated SAM surface than on a pure maleimide-terminated SAM. Molecular dynamics simulations show that β-gal-D308C is much more mobile on the more hydrophilic mixed SAM surface, which was supported by SFG measurements. Therefore we believe that for immobilized enzymes with active sites close to a substrate surface, the interaction between the active sites and a hydrophilic surface could be decreased, leading to higher activity. This can be used as a design rule for enzyme immobilization.

More generally, this Section demonstrates the combined SFG measurements and molecular dynamics simulations could provide important structural insights on surface immobilized enzymes. The understanding gained by such studies helps the rational design of surface-immobilized enzyme catalysts with optimal activity and stability.

3.2 CHARACTERIZATION OF SURFACE IMMOBILIZED HALOALKANE DEHALOGENASE (HLD)

3.2.1 Introduction

As introduced in Chapter 1, the development of methods in maintaining the function and activity of biomolecules in harsh conditions (e. g. low humidity, or even dry

condition) is very interesting and important. As a model protein to be able to catalyze reactions in low humidity, haloalkane dehalogenase (HLD, PDB ID: 1D07) was selected which catalyzes the hydrolysis of a wide range of alkyl halides and is of interest for the sensing and bioremediation of haloalkane pollutants.[70] The high volatility of its haloalkane substrates makes this enzyme attractive for optimization as a solvent-free biocatalyst.[71]

Our recent research demonstrated the feasibility to improve the HLD activity in air by 40 times through surface immobilized with hydromimetic functionalities.[28] Before the structure of enzyme was examined in low humidity conditions, we applied SFG and ATR-FTIR to study the surface immobilized HLD in aqueous buffer solution. In this Section, three engineered HLD mutants, each with a single cysteine residue, A141C, A196C, and N262C, were investigated after surface immobilization in aqueous buffer solutions.

3.2.2 Materials and Methods

3.2.2.1 HLD Expression, Purification and Mutagenesis

The codon-optimized wild-type gene encoding haloalkane dehalogenase from *Sphingomonas paucimobilis* UT26 (linB)[72, 73] cloned in pET23a was a generous gift from Dr. J. Damborsky (University of Masaryk). Mutagenesis of selected surface residues of HLD to Cysteine was performed using a QuikChange Lightning Site-Directed Mutagenesis Kit (Agilent) according to the manufacturer's protocol.

The expression vectors encoding wild-type and engineered HLD variants were transformed to *E. coli* BL21(DE3). The proteins were expressed and purified by standard methods as described previously,[74] and performed by Prof. Neil Marsh's group at the University of Michigan. Prior to surface immobilization, HLD proteins were dialyzed at

4 °C for 24 h against “buffer A” containing 50 mM HEPES-SO_4 buffer, pH 8.0 with 5% Glycerol, 1 mM EDTA and 1 mM TCEP (tris(2-carboxyethyl)phosphine) to insure cysteine residues were reduced. Typical purifications yielded 50-65 mg of purified HLD per liter of culture with a purity of >95% as judged by SDS-PAGE.

3.2.2.2 Surface Functionalization and HLD Immobilization

SiO_2 coated CaF_2 prisms were immobilized with a maleimide terminated SAM using the method presented in Section 3.1.2.1. Then a 5 μM solution of enzyme in PBS, pH 7.4, was incubated with freshly prepared functionalized prisms for 16 h at 4 °C in the presence of 5 μM TCEP to break the disulfide bonds. The surfaces were then vigorously washed twice with PBS buffer, followed by 5% Tween 20, and PBS buffer again to remove non-chemically bound protein.

3.2.2.3 SFG Measurement

Same SFG measurement and data analysis methods were used in this Section as those described in Section 3.1.

3.2.2.4 ATR-FTIR Measurements

Trapezoidal germanium attenuated total reflectance crystal surfaces (CRYSTRAN, U. K.) were functionalized with a maleimide-terminated SAMs as described above. A background spectrum was collected from SAM functionalized ATR crystal surfaces before immobilization of HLD variants on the surface as described above. The p- and s-polarized ATR-FTIR spectra of the surface immobilized protein in deuterated buffer solution were measured using a Nicolet Magna IR 550 spectrometer.

3.2.3 Results and Discussion

Maleimide-terminated SAM surfaces were characterized by SFG (shown in Chapter 3.1) and ATR-FTIR (data not shown) in aqueous buffer solution and they do not generate background SFG or ATR-FTIR signals in the amide I range.

After the enzyme surface immobilization, SFG and ATR-FTIR spectra were collected from the immobilized HLD A141C, A196C, or N262C in aqueous solution (Figure 3.13). All SFG spectra contain a dominant peak at 1650 cm^{-1}, originating from the alpha-helical secondary structure in the enzymes. Similar to the case in Section 3.1 of β-gal, the weak peak at 1711 cm^{-1} observed in the SFG spectra originated from the carbonyl group in alkyne terminated SAM and maleimide linker (with molecular structures shown in Figure 3.1). After fitting SFG spectra (fitting parameters shown in Table 3.5), the χ_{zzz}/χ_{yyz} ratios were determined to be 2.15, 1.92, and 1.87, respectively. P- and S-polarized ATR-FTIR spectra of the A141C (fitting parameters shown in Table 3.6), A196C, and N262C were fitted to determine a dichroic ratio of R^{ATR} of 1.72, 1.83, and 1.89, respectively, for the peak centered at 1655 cm^{-1} in each spectrum.

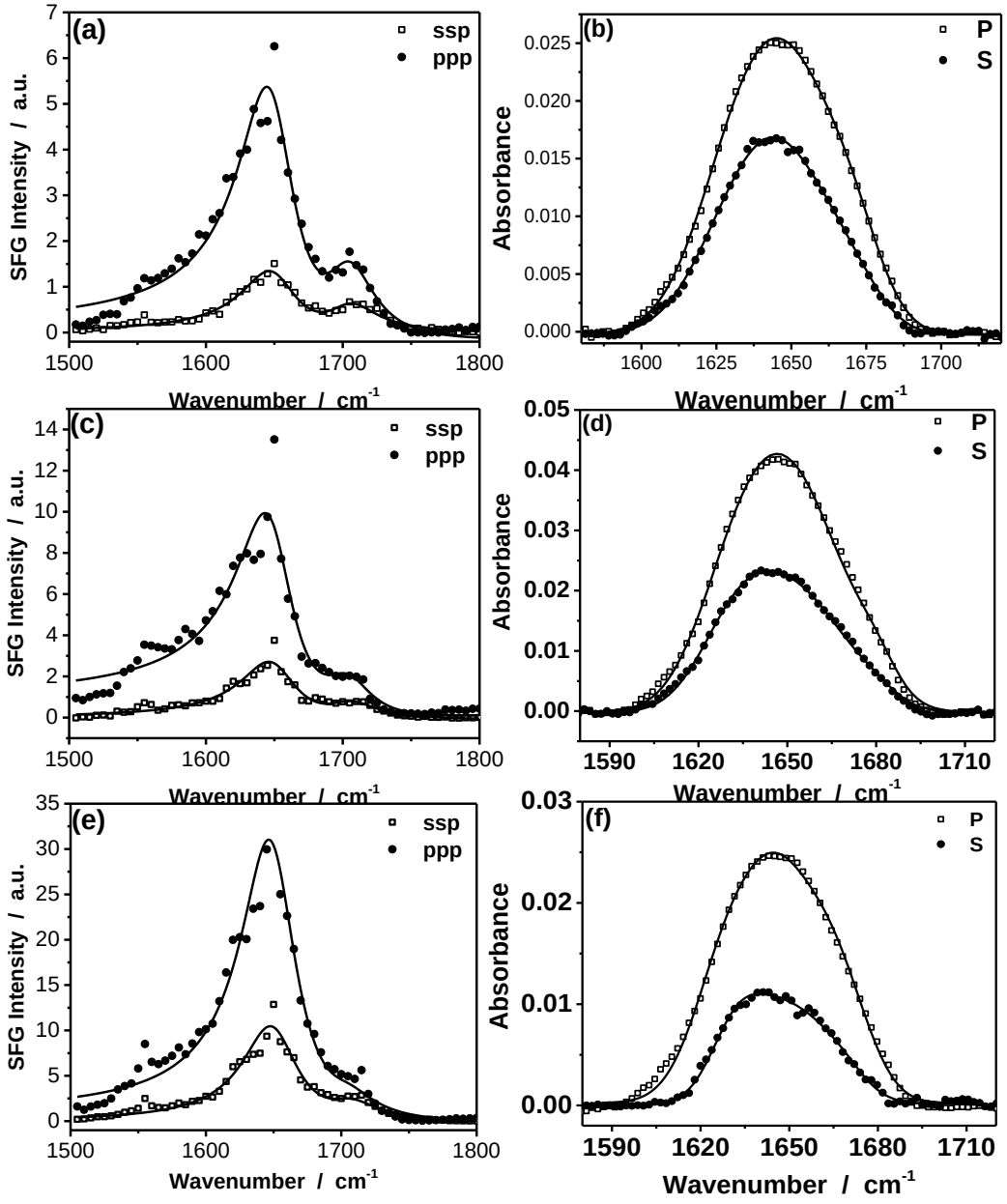

Figure 3.13 SFG amide I signals collected from surface immobilized HLD (a) A141C, (c) A196C, and (e) N262C in phosphate buffer. ATR-FTIR amide I signals collected from surface immobilized HLD (b) A141C, (d) A196C, and (f) N262C in phosphate buffer.

Table 3.5 Fitting parameters for SFG spectra shown in Figure 3.13a, c, and e.

HLD	Polarizations	χ_{NR}	A	ω (cm^{-1})	Γ (cm^{-1})
A141C	**ppp**	-0.39	51.5 (1.0)	1650	25.0
	ssp	-0.08	26.0 (0.4)	1650	25.0
A196C	**ppp**	-0.76	67.4 (2.3)	1650	25.0
	ssp	-0.18	38.1 (0.9)	1650	25.0
N262C	**ppp**	-0.69	133.8 (1.5)	1650	25.0
	ssp	-0.18	77.8 (1.4)	1650	25.0

Table 3.6 ATR-FTIR fitting parameters for the spectra shown in Figure 3.13b, d, f.

HLD	Polarization	Peak center (cm^{-1})	Peak width (cm^{-1})	Peak Strength	Assignment
A141C	P	1635	10.9	0.0171	β-sheet
		1645	8.9	0.0010	Random coil /disorder
		1655	9.9	0.0136	α-helix
		1671	7.1	0.0053	β-turn
	S	1635	10.9	0.0112	β-sheet
		1645	8.9	0.0017	Random coil /disorder
		1655	9.9	0.0079	α-helix
		1671	7.1	0.0024	β-turn
A196C	P	1633	9.6	0.0204	β-sheet
		1645	7	0.0020	Random coil /disorder
		1655	11.3	0.0327	α-helix

		1680	5	0.0039	β-turn
	S	1633	9	0.0133	β-sheet
		1645	7	0.0003	Random coil /disorder
		1655	11.3	0.0179	α-helix
		1680	5	0.0013	β-turn
N262C	P	1632	8.7	0.0172	β-sheet
		1645	6.3	0.0072	Random coil /disorder
		1657	7.7	0.0137	α-helix
		1670	7.0	0.0064	β-turn
	S	1632	6.2	0.0075	β-sheet
		1645	6.3	0.0044	Random coil /disorder
		1658	8.2	0.0068	α-helix
		1670	4.8	0.0006	β-turn

We first deduced the likely orientations of the surface immobilized HLD A141C by comparing the experimentally measured χ_{zzz}/χ_{yyz} ratio and the calculated SFG result as a function of protein orientation, using the crystal structure of the HLD in a standard pose as (0,0,0) position. We then performed a similar operation with the measured dichroic ratio and calculated orientation dependent ATR-FTIR data. Figure 3.14a shows that the orientation angle ranges of surface immobilized HLD that can satisfy both SFG and ATR-FTIR measurements. Figure 3.15a depicts a representative likely orientation with a twist angle of 180° and a tile angle of 45°. In this pose, the engineered site, in this case A141C,

was facing the maleimide surface, indicated by a blue parallelogram. This shows that the deduced orientation of surface immobilized HLD A141C using SFG and ATR-FTIR is reasonable. Similar operations were performed to deduce the orientations of the other two variants: V196C, and N262C after surface immobilization. Heat maps that satisfy both SFG and ATR-FTIR results were shown in Figures 3.14b and c, and deduced possible orientations were depicted in Figures 3.15b and c, respectively. The results for these two mutants are also reasonable because with the deduced orientations, the immobilization sites are next to the surface.

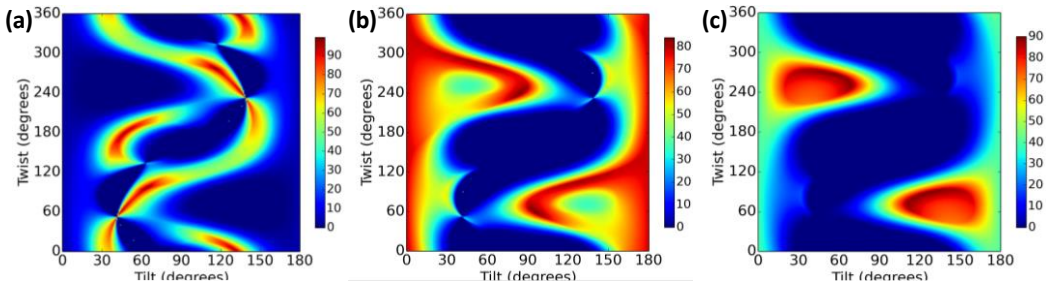

Figure 3.14 Possible orientations of surface immobilized HLD. (a) Possible orientation of A141C deduced using a combination of SFG ($\chi^{(2)}_{ZZZ}/\chi^{(2)}_{XXZ} = 2.15$) and ATR-FTIR (dichroic ratio $R^{ATR} = 1.72$). (b) The possible orientation of A196C deduced using a combination of SFG ($\chi^{(2)}_{ZZZ}/\chi^{(2)}_{XXZ} = 1.92$) and ATR-FTIR (dichroic ratio $R^{ATR} = 1.83$); (c) The possible orientation of N262C deduced using a combination of SFG ($\chi^{(2)}_{ZZZ}/\chi^{(2)}_{XXZ} = 1.87$) and ATR-FTIR (dichroic ratio $R^{ATR} = 1.89$).

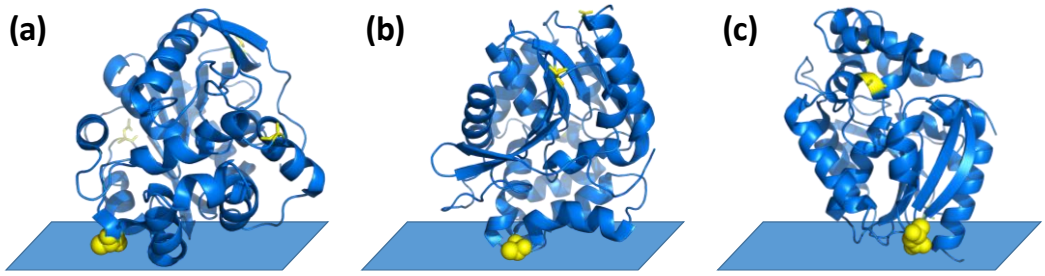

Figure 3.15 Deduced possible orientation of HLD (a) A141C (twist=180°, tilt=45°), (b) A196C (twist=110°, tilt=130°), and (c) N262C (twist=80°, tilt=130°) as determined from our experimental measurements. The immobilization site is colored with yellow in spheres, and other mutation residues are colored in yellow in stick. The plane of the surface relative to the protein is shown as a blue parallelogram.

3.2.4 Conclusion

In summary, this research again demonstrated that we could control the enzyme orientation by selecting the surface immobilization site on the enzyme for surface immobilization. HLD mutants with a unique cysteine residue were successfully immobilized on maleimide terminated SAM surfaces. The orientations of surface immobilized HLD molecules were determined by a combination of SFG and ATR-FTIR. Moreover, this study on the surface immobilized HLD in buffer provides structural information of such enzymes, laying a good foundation for surface immobilized enzymes in harsh conditions (e.g., in the absence of bulk water), which will be discussed in Chapter 4.

3.3 REFERENCES

1. Q. Yu, Y. Zhang, H. Wang, J. Brash and H. Chen, *Acta biomaterialia*, 2011, **7**, 1550-1557.
2. I. Banerjee, R. C. Pangule and R. S. Kane, *Advanced Materials*, 2011, **23**, 690-718.

3. A. Liese and L. Hilterhaus, *Chemical Society Reviews*, 2013, **42**, 6236-6249.

4. Z. Liu, S. Tabakman, K. Welsher and H. Dai, *Nano research*, 2009, **2**, 85-120.

5. F. Rusmini, Z. Zhong and J. Feijen, *Biomacromolecules*, 2007, **8**, 1775-1789.

6. J. N. Talbert and J. M. Goddard, *Colloids and Surfaces B: Biointerfaces*, 2012, **93**, 8-19.

7. S. D. Minteer, B. Y. Liaw and M. J. Cooney, *Current opinion in biotechnology*, 2007, **18**, 228-234.

8. C. Mateo, J. M. Palomo, G. Fernandez-Lorente, J. M. Guisan and R. Fernandez-Lafuente, *Enzyme and Microbial Technology*, 2007, **40**, 1451-1463.

9. K. Hernandez and R. Fernandez-Lafuente, *Enzyme and microbial technology*, 2011, **48**, 107-122.

10. T. L. Ogorzalek, S. Wei, Y. Liu, Q. Wang, C. L. Brooks, Z. Chen and E. N. G. Marsh, *Langmuir*, 2015.

11. R. C. Rodrigues, C. Ortiz, Á. Berenguer-Murcia, R. Torres and R. Fernández-Lafuente, *Chemical Society Reviews*, 2013, **42**, 6290-6307.

12. R. J. Chen, Y. Zhang, D. Wang and H. Dai, *Journal of the American Chemical Society*, 2001, **123**, 3838-3839.

13. K. Jiang, L. S. Schadler, R. W. Siegel, X. Zhang, H. Zhang and M. Terrones, *Journal of Materials Chemistry*, 2004, **14**, 37-39.

14. X.-L. Sun, C. L. Stabler, C. S. Cazalis and E. L. Chaikof, *Bioconjugate Chemistry*, 2006, **17**, 52-57.

15. Z. Zhang, S. Chen and S. Jiang, *Biomacromolecules*, 2006, **7**, 3311-3315.

16. L. S. Wong, F. Khan and J. Micklefield, *Chemical Reviews*, 2009, **109**, 4025-4053.

17. M. B. Soellner, K. A. Dickson, B. L. Nilsson and R. T. Raines, *Journal of the American Chemical Society*, 2003, **125**, 11790-11791.

18. S. V. Rao, K. W. Anderson and L. G. Bachas, *Microchimica Acta*, 1998, **128**, 127-143.

19. B. Lu, M. R. Smyth and R. O'Kennedy, *Analyst*, 1996, **121**, 29R-32R.

20. L. L. Chang, D. Shepherd, J. Sun, D. Ouellette, K. L. Grant, X. C. Tang and M. J. Pikal, *Journal of pharmaceutical sciences*, 2005, **94**, 1427-1444.

21. W. Norde and T. Zoungrana, *Biotechnology and Applied Biochemistry*, 1998, **28**, 133-143.

22. L. Shen, M. Schroeder, T. L. Ogorzalek, P. Yang, F.-G. Wu, E. N. G. Marsh and Z. Chen, *Langmuir*, 2014, **30**, 5930-5938.

23. P. Yang, A. Boughton, K. T. Homan, J. J. Tesmer and Z. Chen, *Journal of the American Chemical Society*, 2013, **135**, 5044-5051.

24. Y. Liu, T. L. Ogorzalek, P. Yang, M. M. Schroeder, E. N. G. Marsh and Z. Chen, *Journal of the American Chemical Society*, 2013, **135**, 12660-12669.

25. P. Yang, A. Glukhova, J. J. Tesmer and Z. Chen, *PloS One*, 2013, **8**, e82072.

26. A. P. Boughton, P. Yang, V. M. Tesmer, B. Ding, J. J. Tesmer and Z. Chen, *Proceedings of the National Academy of Sciences*, 2011, **108**, E667-E673.

27. B. Ding, J. Jasensky, Y. Li and Z. Chen, *Accounts of Chemical Research*, 2016, **49**, 1149-1157.

28. S. Badieyan, Q. Wang, X. Zou, Y. Li, M. Herron, N. L. Abbott, Z. Chen and E. N. G. Marsh, *Journal of the American Chemical Society*, 2017.

29. Y. Shen, *Nature*, 1989, **337**, 519-525.

30. X. Zhuang, P. Miranda, D. Kim and Y. Shen, *Physical Review B*, 1999, **59**, 12632.

31. Z. Chen, Y. Shen and G. A. Somorjai, *Annual review of physical chemistry*, 2002, **53**, 437-465.

32. S. Roy, P. A. Covert, W. R. FitzGerald and D. K. Hore, *Chemical Reviews*, 2014, **114**, 8388-8415.

33. G. Richmond, *Chemical reviews*, 2002, **102**, 2693-2724.

34. Y. Su, H.-L. Han, Q. Cai, Q. Wu, M. Xie, D. Chen, B. Geng, Y. Zhang, F. Wang and Y. Shen, *Nano Letters*, 2015, **15**, 6501-6505.

35. X. Chen, T. Yang, S. Kataoka and P. S. Cremer, *Journal of the American Chemical Society*, 2007, **129**, 12272-12279.

36. S. C. Flores, J. Kherb and P. S. Cremer, *The Journal of Physical Chemistry C*, 2012, **116**, 14408-14413.

37. X. Chen, L. B. Sagle and P. S. Cremer, *Journal of the American Chemical Society*, 2007, **129**, 15104-15105.

38. Y. Horowitz, H.-L. Han, P. N. Ross and G. A. Somorjai, *Journal of the American Chemical Society*, 2016, **138**, 726-729.

39. C.-S. Hsieh, R. K. Campen, A. C. V. Verde, P. Bolhuis, H.-K. Nienhuys and M. Bonn, *Physical review letters*, 2011, **107**, 116102.

40. T. Weidner and D. G. Castner, *Physical Chemistry Chemical Physics*, 2013, **15**, 12516-12524.

41. K. A. Lovering, A. K. Bertram and K. C. Chou, *The Journal of Physical Chemistry C*, 2016, **120**, 18099-18104.

42. P. A. Covert and D. K. Hore, *The Journal of Physical Chemistry C*, 2014, **119**, 271-276.

43. S. Ye, Y. Tong, A. Ge, L. Qiao and P. B. Davies, *The Chemical Record*, 2014, **14**, 791-805.

44. J. Huang, K. Tian, S. Ye and Y. Luo, *The Journal of Physical Chemistry C*, 2016, **120**, 15322-15328.

45. L. M. Haupert and G. J. Simpson, *Annual Review of Physical Chemistry*, 2009, **60**, 345-365.

46. M. Xiao, X. Zhang, Z. J. Bryan, J. Jasensky, A. J. McNeil and Z. Chen, *Langmuir*, 2015, **31**, 5050-5056.

47. X. Zhang, Y. Li, J. M. Hankett and Z. Chen, *Physical Chemistry Chemical Physics*, 2015, **17**, 4472-4482.

48. J. Wang, C. Chen, S. M. Buck and Z. Chen, *The Journal of Physical Chemistry B*, 2001, **105**, 12118-12125.

49. J. Wang, Z. Paszti, M. A. Even and Z. Chen, *Journal of the American Chemical Society*, 2002, **124**, 7016-7023.

50. P. Hu, X. Zhang, C. Zhang and Z. Chen, *Physical Chemistry Chemical Physics*, 2015, **17**, 9873-9884.

51. J. A. Mondal, S. Nihonyanagi, S. Yamaguchi and T. Tahara, *Journal of the American Chemical Society*, 2010, **132**, 10656-10657.

52. J. M. Troiano, L. L. Olenick, T. R. Kuech, E. S. Melby, D. Hu, S. E. Lohse, A. C. Mensch, M. Dogangun, A. M. Vartanian and M. D. Torelli, *The Journal of Physical Chemistry C*, 2014, **119**, 534-546.

53. P. Yang, K. T. Homan, Y. Li, O. Cruz-Rodríguez, J. J. Tesmer and Z. Chen, *Biochemistry*, 2016, **55**, 2841-2848.

54. L. Fu, J. Liu and E. C. Yan, *Journal of the American Chemical Society*, 2011, **133**, 8094-8097.

55. P. Yang, A. Ramamoorthy and Z. Chen, *Langmuir*, 2011, **27**, 7760-7767.

56. S. Ye, H. Li, F. Wei, J. Jasensky, A. P. Boughton, P. Yang and Z. Chen, *Journal of the American Chemical Society*, 2012, **134**, 6237-6243.

57. J. Kim and G. A. Somorjai, *Journal of the American Chemical Society*, 2003, **125**, 3150-3158.

58. Y. Li, X. Zhang, J. Myers, N. L. Abbott and Z. Chen, *Chemical Communications*, 2015, **51**, 11015-11018.

59. S. Wei, X. Zou, K. Cheng, J. Jasensky, Q. Wang, Y. Li, J. Lahann, C. L. Brooks and Z. Chen, *The Journal of Physical Chemistry C*, 2016.

60. B. Ding, J. Jasensky, Y. Li and Z. Chen, *Accounts of Chemical Research*, 2016.

61. N. K. Chaki and K. Vijayamohanan, *Biosensors and Bioelectronics*, 2002, **17**, 1-12.

62. S. Wei and T. A. Knotts IV, *The Journal of Chemical Physics*, 2013, **139**, 095102.

63. J. Karanicolas and C. L. Brooks, *Protein Science*, 2002, **11**, 2351-2361.

64. J. Karanicolas and C. L. Brooks, *Proceedings of the National Academy of Sciences*, 2003, **100**, 3954-3959.

65. J. Karanicolas and C. L. Brooks III, *Proc Natl Acad Sci U S A*, 2003, **100**, 3954-3959.

66. J. Karanicolas and C. L. Brooks, *Proceedings of the National Academy of Sciences of the United States of America*, 2004, **101**, 3432-3437.

67. T. L. Ogorzalek, S. Wei, Y. Liu, Q. Wang, C. L. Brooks III, Z. Chen and E. N. G. Marsh, *Langmuir*, 2015, **31**, 6145-6153.

68. J. Bandekar, *Biochimica et Biophysica Acta (BBA)-Protein Structure and Molecular Enzymology*, 1992, **1120**, 123-143.

69. J. Wang, M. A. Even, X. Chen, A. H. Schmaier, J. H. Waite and Z. Chen, *Journal of the American Chemical Society*, 2003, **125**, 9914-9915.

70. T. Koudelakova, S. Bidmanova, P. Dvorak, A. Pavelka, R. Chaloupkova, Z. Prokop and J. Damborsky, *Biotechnology journal*, 2013, **8**, 32-45.

71. B. C. Dravis, K. E. LeJeune, A. D. Hetro and A. J. Russell, *Biotechnology and Bioengineering*, 2000, **69**, 235-241.

72. A. J. Oakley, M. Klvaňa, M. Otyepka, Y. Nagata, M. C. Wilce and J. Damborský, *Biochemistry*, 2004, **43**, 870-878.

73. J. Marek, J. Vévodová, I. K. Smatanová, Y. Nagata, L. A. Svensson, J. Newman, M. Takagi and J. Damborský, *Biochemistry*, 2000, **39**, 14082-14086.

74. V. Liskova, D. Bednar, T. Prudnikova, P. Rezacova, T. Koudelakova, E. Sebestova, I. K. Smatanova, J. Brezovsky, R. Chaloupkova and J. Damborsky, *ChemCatChem*, 2015, **7**, 648-659.

CHAPTER 4 Strategies of Structure and Orientation Protection of Biomolecules in Water-Free Environment

The contents in Section 4.3 have been adapted with permission from the following publication: **Li Y**, Zhang X, Myers J, Abbott NL, Chen Z. Room Temperature Freezing and Orientation Control of Surface Immobilized Peptide in Air. *Chem. Comm.* **2015**, 51:11015-11018.

4.1 INTRODUCTION

Water is typically required to maintain both the structure and activity of biological molecules such as proteins and peptides.[1] Removal of water often destroys the native conformation of a protein or peptide, especially at ambient (room temperature or RT) or high temperatures. Therefore, maintaining the structure and function of proteins and peptides under harsh conditions, e.g., in the absence of bulk water, is very challenging, but is very important for some applications such as biosensors and biofuel cells.[2-4] Previous studies have shown that many solvent additives, e.g. sugars and poly alcohols, can retain the function of biomolecules and reduce the extent of denaturation during or after drying processes.[5-9] Sugar stabilization of proteins in solution has been well established for more than twenty years.[10-12] However, most studies describing sugar stabilization of proteins have been performed in bulk and they largely focused on the variation of the protein storage conditions modified with sugar additives. Few studies have investigated surface-immobilized proteins and protein/sugar interactions at the molecular level in air.

An in-depth understanding of the structure, e.g., conformation and orientation of molecules at interfaces is very important in many fields, including antimicrobial coatings,[13] electronic materials,[14] sensors and biosensors,[15] catalysis,[16] and energy storage/production.[17] The conformation and orientation of biological molecules at interfaces have been controlled and maintained by various methods.[18-22] However, such methods have not been able to maintain the structure and orientation of proteins in a dry condition. We hypothesized that surrounding sugar molecules may be able to retain the conformation and orientation of surface immobilized biomolecules in air, similar to what they could do for biomolecules in the bulk environment.

Since the structure of a protein is complex, probing the effects of sugars on protein structure in detail can be challenging. Moreover, during protein drying processes, low temperatures, such as -45 °C, are commonly required.[23-25] A method that is capable of operating under RT and maintaining the structure/function of peptide/protein during/after a drying process would be more broadly applicable. Herein, we present a simple method to control the orientation of a peptide immobilized on a surface by simply spin coating sugars on the immobilized peptide at RT. In addition, we also developed a method for a chemically attached sugar coating to retain peptide structure and activity in harsh conditions.

In this chapter, we have investigated the molecular structure of such a peptide first in dry conditions at RT using SFG, with the help of circular dichroic spectroscopy CD. As we discussed above, SFG has been widely used to study molecular structures of surfaces and interfaces, including peptides and proteins.[26-40] Here we used peptides with well-

defined secondary structures, discussed in Section 2.1, as models to investigate the interactions between sugar molecules and proteins in dry conditions. The method developed is general and was applied to more complicated molecules such as HLD (will be discussed in Section 4.4), which are widely used for many applications such as biosensors, biochips, and biofuel cells. We then chemically tethered sugar molecules on peptides. It was found that chemically attached sugars help retain peptide structure longer after the surface was exposed to air. Moreover, tethered sugar molecules help increase the antimicrobial activity of surface immobilized AMPs.

4.2 EXPERIMENTAL SECTION

4.2.1 Materials

All chemicals and solvents were purchased from Sigma-Aldrich (St. Louis, MO, USA) and used without further purification unless otherwise stated.

In Section 4.3, azide terminated MSI-78 (N-terminus MSI-78: nMSI-78), with the amino acid sequence: KGIGKFLKKAKKFGKAFVKILKK-NH_2 was the same peptide material as that used in Section 2.1. Surface immobilization of nMSI-78 was done identically as that discussed in Section 2.1. Surfaces for SFG experiments were prepared on SiO_2 coated CaF_2 prisms, and substrates for CD experiments were quartz slides prepared using the same method as presented above in Section 2.1.2.

In Section 4.4, enzyme HLD was used and surface immobilized on maleimide-terminated SAM with the same method discussed in Section 3.2.

In Section 4.5, both azido-terminated MSI-78 and hybrid peptide were prepared using the same method used in Section 2.1.

4.2.2 Sugar Coating Preparation

All sucrose solutions were prepared in water. The sucrose solution concentrations were varied, as discussed later.

Spin Coating: several drops of sucrose solution were placed on top of the surface immobilized peptides and spin coated at 2000 rpm for 40 s. Then the surface was dried under a nitrogen stream for several minutes to remove the residual water left from the spin coating process.

Solvent Casting Fast Drying: several drops of sucrose solution were added to the surface with immobilized peptides and after 30 s, the surface was blown under a nitrogen stream for fast drying.

Solvent Casting Slow Drying: several drops of the sucrose solution were placed on the surface with immobilized nMSI-78. After 30s, the solution in contact with the surface was removed and the surface dried slowly in air (without blowing using N_2 stream).

Spin coating sucrose, as mentioned above, was also prepared on immobilized enzyme surfaces. The sucrose solution concentration used is 200 mM.

4.2.3 Chemically Attachment of Sugars onto Peptide

Maltodextrin (dextrose equivalent, 4.0-7.0) was used to attached to the primary amine-containing lysine residues. Peptide functionalized prisms were placed in the 70%DMSO/30% acetic acid solution containing 58.4 μmol/ml maltodextrin, 318 μmol/ml

sodium cyanoborohydride, incubated at 37 ºC for two days. The functionalized prisms were then cleaned using water.

4.2.4 Antimicrobial Tests in Dry Conditions

The antimicrobial test described below was developed by Prof. Nicholas Abbott lab, University of Wisconsin, Madison. 40 μL of a bacterial inoculum of *Pseudomonas aeruginosa* (~ 3×10^7 colony forming units (CFU)) was pipetted over a tryptic soy agar dish (1.5 wt.% agar, d = 85 mm and thickness of 5 mm). Next, bacteria were spread uniformly across the surface of agar using a spreader that has been sterilized, and then let the bacteria on the agar surface dry for about 1 min. This surface-contaminated agar was placed against peptide-decorated surfaces, and the remaining CFU counts of bacteria on the agar surface was then subsequently counted, following the contact of the contaminated agar with the peptide-decorated surfaces.

The peptide immobilized wafer surfaces (12.5 × 12.5 mm) were placed over the agar dish such that the peptide-decorated side was in contact with the surface of contaminated agar. The peptide was in contact with bacteria for 2 h at room temperature. Then the CFU of bacteria remaining on the agar following the contact with the peptide surface was quantified. To do this, the peptide immobilized wafers were removed from agar surface. The agar disk was then punched out that has been in contact with the peptide surface using an 8-mm punch (i.e. using the larger-diameter-end of 1mL pipette tip). The punched agar dish was then placed in 1 mL PBS for 15 mins. The mashed agar mixtures were then placed onto blood agar plates at appropriate dilutions (10^{-1} to 10^{-4}). After overnight incubation at 37 °C, bacterial colonies were counted. The remaining bacteria

were also counted from the contacted peptide immobilized wafer surfaces. The total bacteria left after treatment is the sum of bacteria counted from agar, and bacteria left on peptide immobilized surfaces.

4.2.5 SFG Measurement

SFG spectra were collected from prism surface immobilized peptide or protein/phosphate buffer (PB) or sugar film interface, shown in Figure 4.1, at both ppp and ssp polarization combinations. By fitting and analyzing SFG spectra, peptide orientation was deduced. In this chapter, SFG spectra were collected from several different interfaces: (1) solid (immobilized peptide)/liquid (buffer, or sucrose solution) interface, (2) solid (immobilized peptide)/solid (spin-coated sucrose coating) interface, and (3) solid (immobilized peptide)/air (without buffer or sucrose solution or sucrose coating) interface. The refractive indices of the medium in contact with the peptide decorated prism surface (medium such as buffer, sucrose solution, sucrose coating, or air) affect the effective second order nonlinear susceptibility, which then affect SFG intensities.

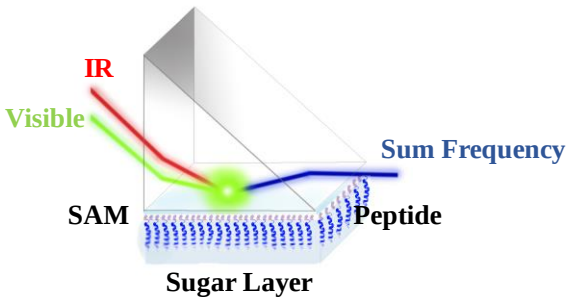

Figure 4.1 SFG experimental geometry (near-total-reflection geometry) to study immobilized peptide on a right angle CaF_2 prism under a sugar layer. Different components in the figure were not drawn to scale.

4.2.6 CD Measurement

For surface immobilized peptide: CD measurements were performed on a J-815 CD spectrometer (Jasco Inc., Japan) using a continuous scanning mode at room temperature. Scans were made from 190 nm to 240 nm at a 0.5 nm resolution and 20 nm min^{-1} scan rate. Each spectrum was averaged by five successive scans for the same sample.

For surface immobilized protein: CD measurements were collected on a J-1500 CD spectrometer (Jasco Inc., Japan) using a continuous scanning mode at room temperature. All the spectra were scanned between 190 nm and 240 nm at a 1 nm resolution, 20 nm min^{-1} scan rate and averaged by five successive scans for every sample.

4.2.7 Ellipsometry Measurement

Sucrose solutions with different concentrations were used to spin coat sucrose on silicon wafer (100 nm silica coating) with immobilized peptide. Sugar film thickness was measured with a multi-wavelength imaging null-ellipsometry instrument (EP3 Nanofilm, Germany). The measured delta and psi values were used to determine the film thickness.

4.3 ORIENTATION CONTROL OF SURFACE-IMMOBILIZED PEPTIDES IN AIR

4.3.1 Protection of Structure of Immobilized Peptide Using Sucrose

Results from Section 2.1 demonstrated that the surface immobilized N-terminus azido mutated MSI-78 (nMSI-78) peptide adopts an alpha helical conformation when in contact with aqueous phosphate buffer and is oriented with a small tilt angle relative to the surface normal (standing up) on an alkyne-terminated SAM surface.[41] This nMSI-78

peptide was used as a model in the research reported in this Section. As shown in Figure 4.2a, a peak centered near 1650 cm^{-1} was detected in the SFG ppp (p-polarized SFG, p-polarized visible beam, and p-polarized IR beam) spectrum collected from the immobilized peptide/PB interface, which is assigned to the amide I vibrational mode of the alpha-helical structure. This peak disappears when the immobilized peptide was removed from the PB and exposed to air (Figure 4.2b and 4.2c). The disappearance of the peak indicates that the alpha helical structure of the peptide either transformed into a random coiled structure, or that the alpha-helical peptide lay down with a large tilt angle at the surface.

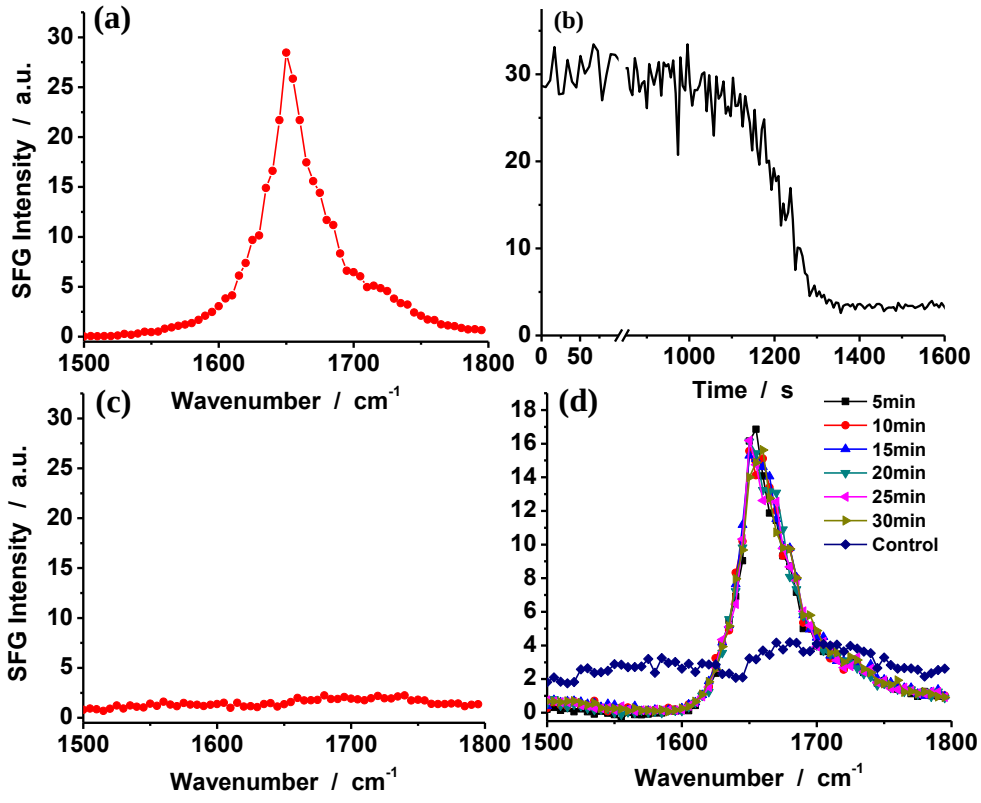

Figure 4.2 (a) SFG spectrum of surface immobilized nMSI-78 in phosphate buffer with ppp polarization combination; (b) time-dependent SFG signals (at 1650 cm^{-1}) detected from the immobilized peptide after removal from the phosphate buffer and exposure to air; (c) SFG spectrum of surface immobilized nMSI-78 in air; (d) SFG spectra of surface immobilized nMSI-78 with spin-coated sucrose (200 mM sucrose solution) in air with ppp polarization combination

detected as a function of time. (The control spectrum in (d) is same as the one in (c)). The slight difference of the spectral features in (d) compared to (a) is caused by the sugar non-resonance background.

CD spectra collected from the immobilized peptides exposed to buffer and air are similar (Figure 4.3), both showing helical structures. Therefore, the absence of SFG amide I signal from the surface immobilized nMSI-78 in air is mainly due to a parallel orientation of the alpha helical peptide on the surface.

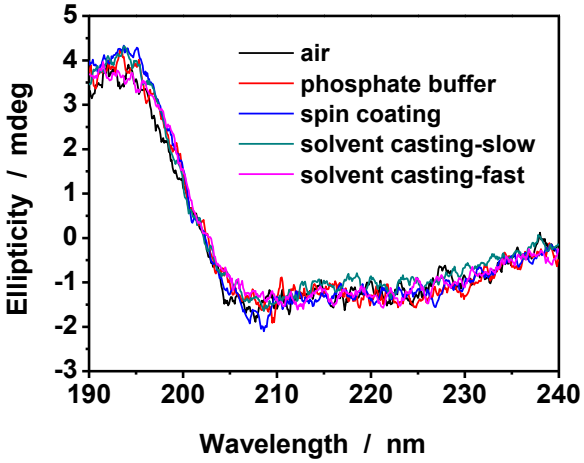

Figure 4.3 CD spectra of surface immobilized nMSI-78 in air, in phosphate buffer, with sucrose layer on top prepared using spin coating, solvent casting with the slow drying method, and solvent casting with the fast drying method.

To retain the SFG signals detected from the immobilized peptides in air, a layer of sugar was applied to the immobilized peptides. Sucrose, which has been widely used to stabilize proteins,[6] was chosen as the sugar coating. When a spin-coated sucrose layer using 200 mM sucrose solution was deposited over the peptide, the secondary structure of the surface immobilized nMSI-78 was similar to that measured in PB, as demonstrated by the

detection of an SFG signal centered at 1650 cm^{-1} in the SFG ppp spectrum (Figure 4.2d). The SFG intensity decrease observed in Figure 4.2d (compared to that in Figure 4.2a) is due to the refractive index difference between PB and sugar (Table 4.1), and/or the orientation change of the immobilized peptides. The time-dependent SFG signal detected at 1650 cm^{-1} exhibited no noticeable change within 40 min of surface preparation (Figure 4.2d) which indicates that the spin-coated sucrose layer is stable at RT and that the molecular structure of the peptides was retained in the dry condition due to the interactions with the overlying protective sugar layer. CD spectroscopic data further showed that the immobilized nMSI-78 with a sugar coating on top adopts an alpha-helical structure (Figure 4.3).

Table 4.1 Refractive indices of PB and sugar layer, which were measured using ellipsometry.

	PB	Sugar Layer
VIS (532 nm)	1.335	1.501
IR (1064 um)	1.297	1.494
SFG (489 nm)	1.337	1.503

4.3.2 Effect of Sucrose Concentration on Surface Immobilized Peptide

We further investigated the effect of the sugar concentration in the spin-coated solution on the peptide orientation in air. Sucrose solutions with concentrations ranging from 25 to 325 mM were spin coated on a surface presenting the immobilized peptide, and then SFG ssp and ppp spectra were collected from the immobilized peptides (Figure 4.4).

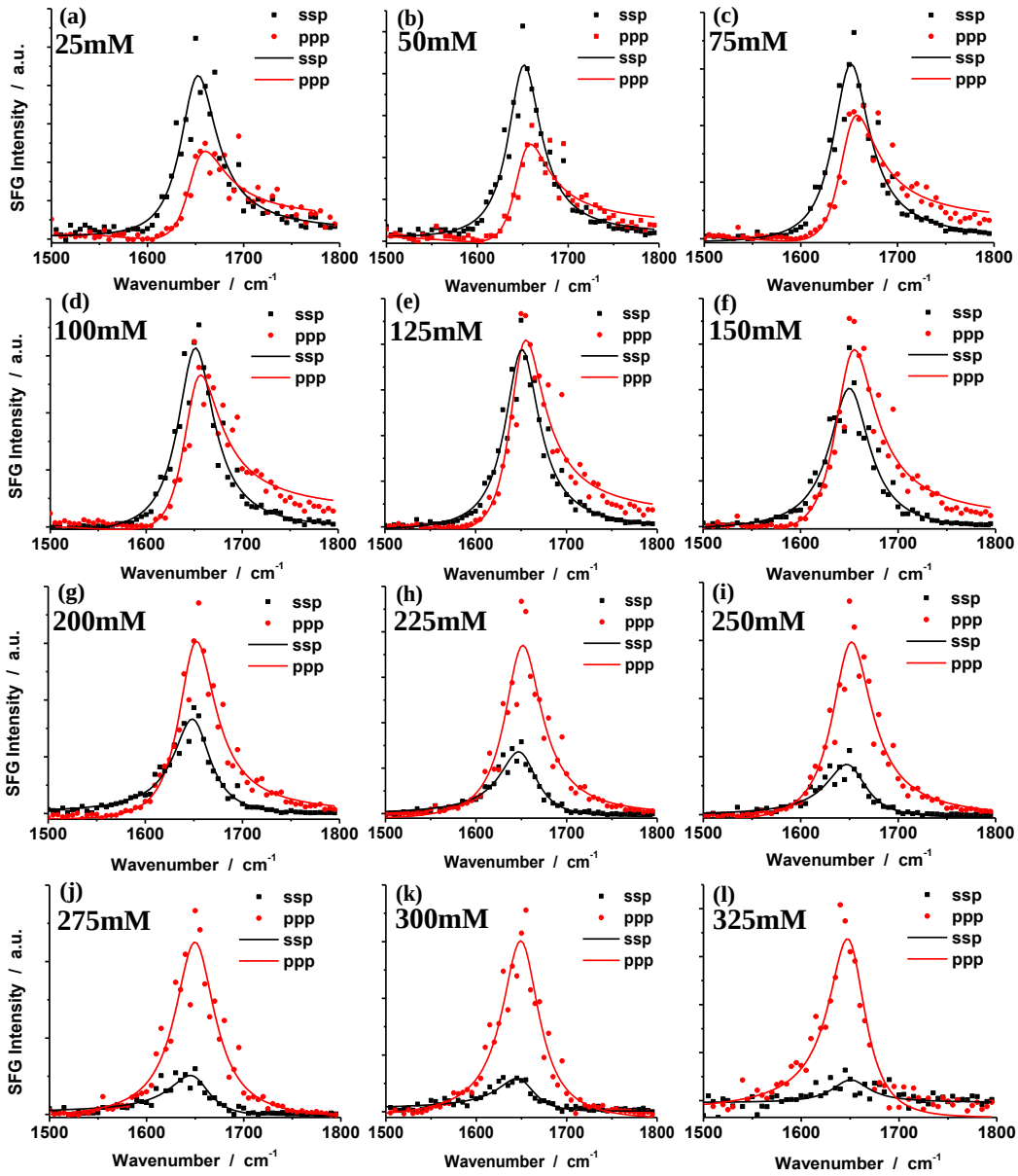

Figure 4.4 SFG ssp (■, black line) and ppp (●, red line) spectra collected from nMSI-78 immobilized on SAM surface with spin coated sucrose using sugar solutions with different concentrations: a) 25.0 mM; b) 50.0 mM; c) 75.0 mM; d) 100.0 mM; e) 125.0 mM; f) 150.0 mM; g) 200.0 mM; h) 225.0 mM; i) 250.0 mM; j) 275.0 mM; k) 300.0 mM; l) 325.0 mM.

An amide I peak centered at 1650 cm^{-1} was observed in each SFG spectrum, indicating that the immobilized peptide adopted an alpha helical structure with sucrose

coating, regardless of the sucrose solution concentration. The SFG spectra collected using different polarization combinations (ssp and ppp) were then used to deduce the orientation of the peptide. SFG orientation analysis of the alpha helical structure has been discussed in detail in Chapter 1 and previous papers.[42, 43] The orientation of an alpha helical peptide on a surface can be defined by a tilt angle θ, the angle between the axis of peptide relative to the surface normal. The relationship between the measured χ_{ppp}/χ_{ssp} ratio and the tilt angle θ can be plotted using the discussed method by assuming the orientation angle θ adopts a δ-distribution (meaning that all peptides adopt an identical orientation). Detailed descriptions of the orientation analysis can be found in Chapter 1 and previous publications and will not be repeated here.[42, 43] Experimentally measured χ_{ppp}/χ_{ssp} ratios of the sugar-coated, immobilized peptides in air (prepared using different sugar solution concentrations) are summarized in Table 4.2 and are plotted in Figure 4.5. For comparison purposes, the measured χ_{ppp}/χ_{ssp} ratios of immobilized peptides exposed to sugar solutions (peptide/sugar solution interface) are also shown in Figure 4.5a.

Table 4.2 Fitted amide I χ_{ppp}/χ_{ssp} ratio values of the immobilized peptide in air with a sugar coating prepared with sugar solutions with different concentrations and when exposed to sugar solutions with different sugar concentrations.

Sucrose Concentration (mM)	Measured χ_{ppp}/χ_{ssp} Ratio in air (with a spin-coated sucrose layer)	Measured χ_{ppp}/χ_{ssp} Ratio (exposed to sucrose solution)
25	0.62	1.79
50	0.65	1.75
75	0.74	1.84
100	0.84	1.84
125	0.98	1.81
150	1.08	1.81
200	1.35	1.86
225	1.65	1.80

250	1.85	1.84
275	2.20	1.75
300	2.45	1.75
325	2.77	1.80

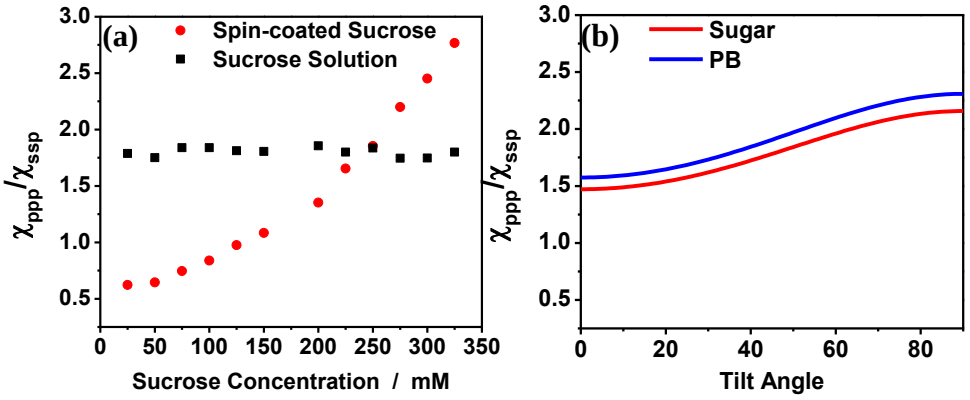

Figure 4.5 (a) Experimentally measured χ_{ppp}/χ_{ssp} ratios of immobilized peptides in air with sugar coating prepared using different sugar solution concentrations (red dots) and experimentally measured χ_{ppp}/χ_{ssp} ratios of immobilized peptides exposed to sucrose solutions with different concentrations (black squares); (b) Relations between χ_{ppp}/χ_{ssp} ratio and peptide orientation (assuming a delta orientation angle distribution) for immobilized peptides with sugar coating in air (red curve) and for immobilized peptides exposed to PB (blue curve).

Figure 4.5b shows that as the χ_{ppp}/χ_{ssp} ratio increases, the immobilized peptide tilt angle also increases, demonstrating that peptides tend to lie down on surfaces at a high χ_{ppp}/χ_{ssp} ratio within the range 1.5 to 2.2. A χ_{ppp}/χ_{ssp} ratio lower than 1.5 is consistent with peptides exhibiting multiple orientations rather than one specific orientation.[44] Figure 4.5a shows that when the sucrose concentration used for spin-coating was between 25 and 225 mM, the measured χ_{ppp}/χ_{ssp} ratio was smaller than 1.5. This shows that the immobilized peptides may adopt a multiple orientation distribution, e.g., they may have contributions from at least two different tilt angles. At a concentration of 225 mM, the tilt angle

calculated was close to zero, indicating that the peptide was oriented along the surface normal. As the concentration increased from 225 to 275 mM, the peptides, which likely adopted a single orientation, increasingly tilted away from the surface normal. The peptides lay down when 275 mM sucrose was used for spin coating. Therefore, the tilt angle of the immobilized nMSI-78 peptide could be controlled by simply adjusting the sucrose solution concentration used for sugar spin coating.

As described above, the different concentrations of the sugar solutions used for spin coating lead to different immobilized peptide orientations. Such orientation differences may be due to the different interactions between the immobilized peptides with sugar solutions with different concentrations. To study such possible differences, SFG spectra were collected from the surface immobilized peptides when exposed to sucrose solutions with different concentrations (Figure 4.6). Regardless of the sugar concentration, the SFG spectra are dominated by a signal centered at ~1650 cm^{-1}, indicating the alpha-helical structure of immobilized peptides. Also, for all sugar solution concentrations, the measured χ_{ppp}/χ_{ssp} ratio was around 1.70 (Figure 4.5a), which suggests that the immobilized nMSI-78 was standing up on the surface with a tilt angle of around 25°. This suggests that the different orientations of immobilized peptides with sugar layer coated with different concentrations of the sugar solution in air are not due to the different interactions between peptides and sugar solutions with different concentrations. Such a difference must be induced in the spin coating process or the sugar solution drying process.

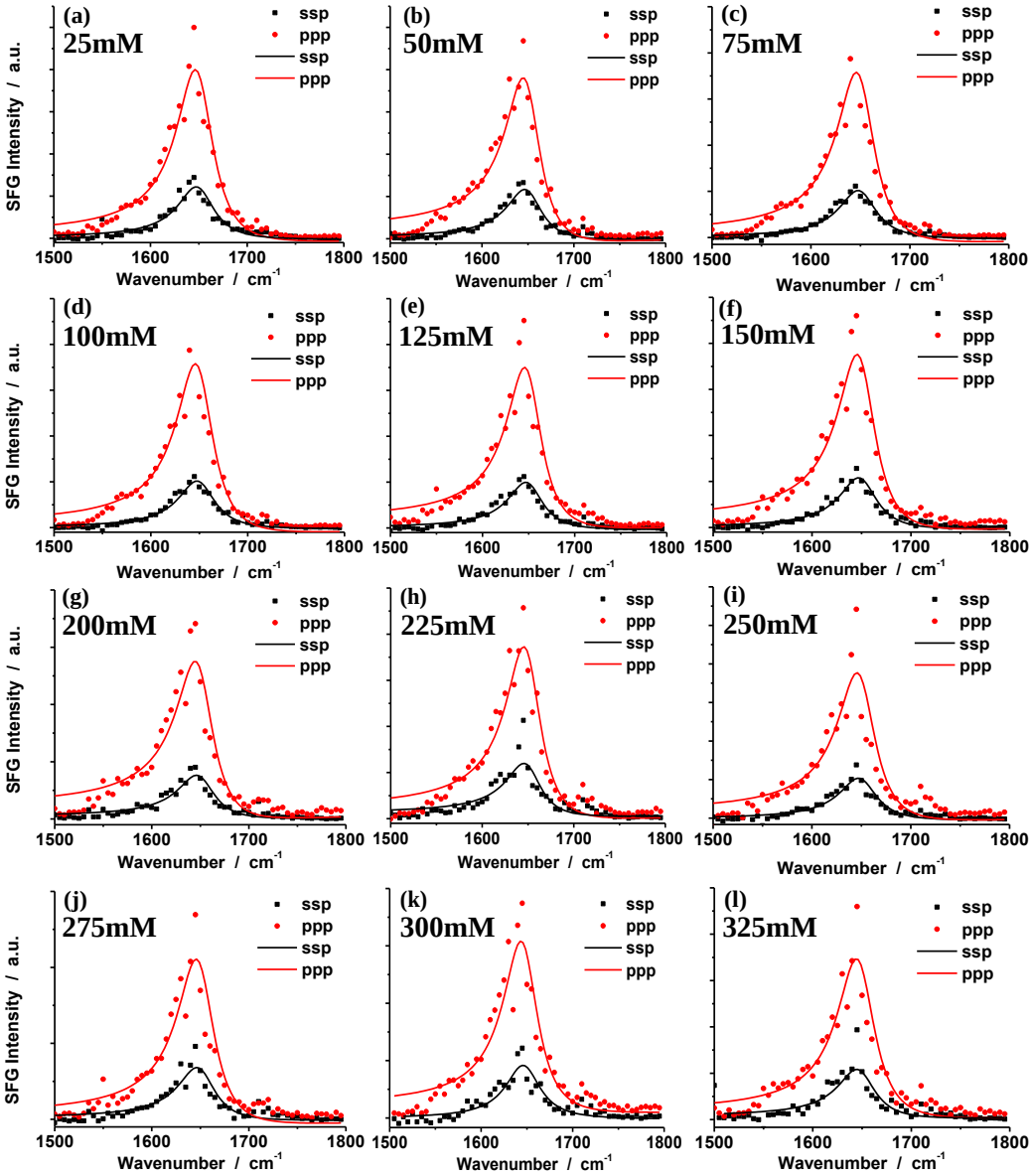

Figure 4.6 SFG ssp (■, black line) and ppp (●, red line) spectra collected from nMSI-78 immobilized on SAM surface exposed to sucrose solutions at different concentrations a) 25.0 mM; b) 50.0 mM; c) 75.0 mM; d) 100.0 mM; e) 125.0 mM; f) 150.0 mM; g) 200.0 mM; h) 225.0 mM; i) 250.0 mM; j) 275.0 mM; k) 300.0 mM; l) 325.0 mM.

4.3.3 Investigation of the Mechanism of Sugar Protection

To further understand how the spin coating process or drying process affects the structure of the surface immobilized peptide, three different sugar "film-forming" methods were used to coat the sugar layer on peptide immobilized surfaces in air: spin coating, solvent casting with fast drying, and solvent casting with slow drying. SFG spectra were then collected from the surface immobilized peptides with sucrose coating prepared using the above three methods. The results obtained from these three methods (details of the procedures of the three methods can be found in Section 4.2.2) are not the same, as shown in Figure 4.7.

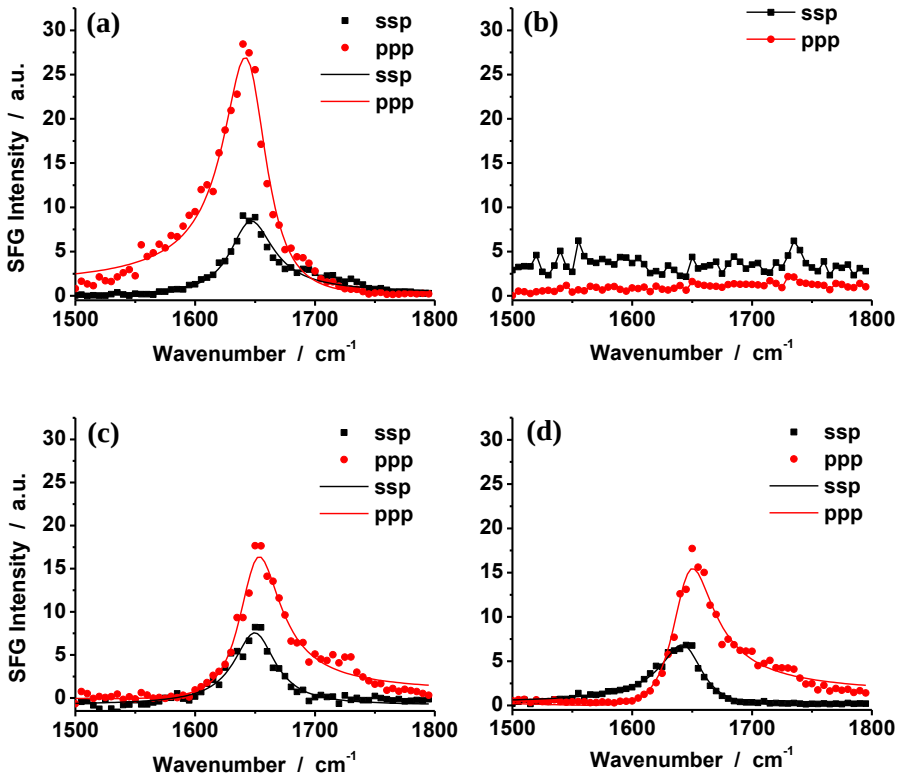

Figure 4.7 SFG ssp ((■, black line) and ppp (●, red line) spectra collected from nMSI-78 immobilized on SAM surface (a) in phosphate buffer; (b) with solvent casting slow dried sucrose; (c) with spin coated sucrose (χ_{ppp}/χ_{ssp} =1.35); (d) with solvent casting quickly dried sucrose (χ_{ppp}/χ_{ssp}=1.44).

As Figure 4.2d showed previously, on the sucrose spin coated surface, peptides were ordered and generated strong SFG signal at 1650 cm^{-1}. Similar to the spin coating, when the solvent casting fast drying method was used to prepare the sugar layer, the alpha helical structure of the immobilized peptides was stabilized with a specific orientation (Figure 4.7d). In contrast, after coating a sucrose layer on the surface immobilized peptides using the solvent casting slow drying method, SFG amide I signal was not detected from the surface immobilized nMSI-78 in air (Figure 4.7b). During both the spin coating and solvent casting with fast drying processes, the surfaces were dried quickly – while the drying process was slow during the solvent casting with slow drying process. Both the "fast-drying" methods were able to retain the conformation and orientation of the immobilized peptides underneath. However, solvent casting with the slow drying method could not. Moreover, the sugar layers from both "fast-drying" methods clearly have different interactions with immobilized peptides from those from "slow-drying" method, shown in Figure 4.7b, which indicates that spin coating itself does not induce the orientation difference. Thicknesses of the sugar film prepared by spin coating with different sugar solution concentrations were measured (Figure 4.8). As the sugar solution concentration increases, the resulting sugar film thickness increases. We therefore believe that the sugar film thickness may influence the drying rate, which influences the peptide orientation. Likely, the sugar may form different amorphous/crystalline phases when drying at different speeds. We performed X-ray diffraction analysis on the sugar coating layer on immobilized peptides prepared with the above three different methods. No X-ray diffraction pattern was observed from any of the three sucrose coatings (data not shown

here). Therefore, the possible role of different sugar amorphous/crystalline phases is still speculative. Another possible reason for the differences might be due to the formation of a glassy state with the retention of a small amount of water within the sugar layer during the drying process. The different drying rates may lead to different bound water amounts and different sugar-water-peptide interactions. Moreover, sucrose molecules contain large amounts of hydroxyl groups, and such groups can mimic the interactions between water and biological molecules, resulting in the protection effects. More details of the effect of sugar coating preparation methods on the immobilized peptide conformation/orientation are being studied.

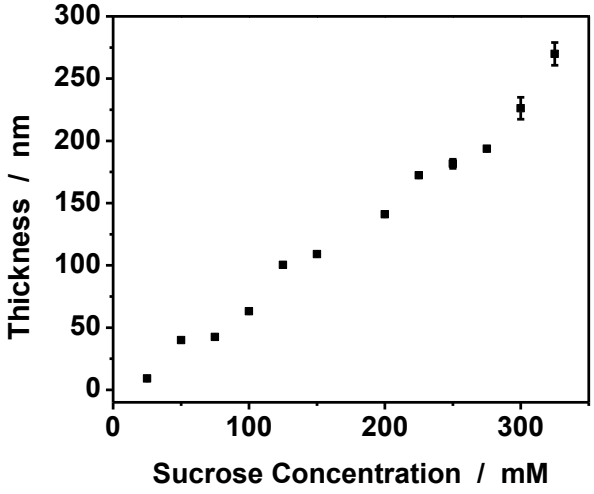

Figure 4.8 Measured sucrose thickness of the spin coated sugar layer as a function of the sucrose solution concentration used for spin coating.

4.4 ORIENTATION CONTROL OF SURFACE-IMMOBILIZED PROTEINS IN AIR

After the development of the spin coating method of sucrose on surface immobilized peptides, we then applied this method to surface immobilized protein, HLD,

which was studied and discussed in Section 3.2. HLD-A141C was immobilized on maleimide terminated SAM surface using the same method discussed in Section 3.2. SFG spectra of surface immobilized HLD-A141C was shown in Figure 4.9a. The immobilized protein exhibited alpha helical structures, which will be discussed below. After exposing the surface immobilized HLD-A141C to air, no SFG signal could be observed (not shown). A 200 mM sucrose buffer solution was used to spin coat sucrose onto the surface immobilized HLD-A141C surface. SFG spectra were then collected from immobilized HLD-A141C with sugar coating in air, as shown in Figure 4.9b. Similar to the case of surface immobilized peptides presented above, here SFG signals could be detected from HLD-A141C with a sugar coating. SFG intensities decreased as compared to those in buffer solution. It is likely because of the refractive index change of the media (phosphate buffer vs. sugar). A peak centered at 1650 cm^{-1} was observed for both ppp and ssp spectra, indicating that the secondary structures of surface immobilized protein were protected by the sugar coating in air. It was also confirmed by CD results, shown in Figure 4.10a.

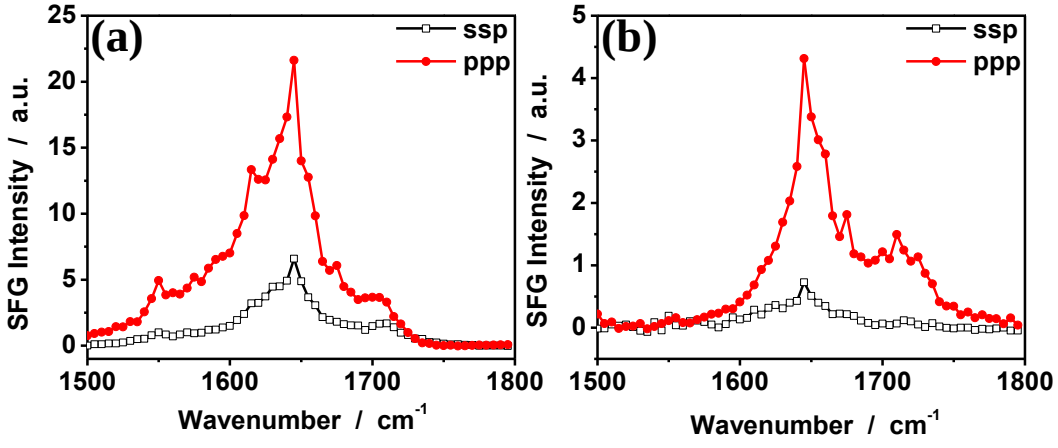

Figure 4.9 SFG spectra collected from surface immobilized HLD-A141C (a) in buffer solution; (b) in air with spin coated sucrose coating (prepared with a 200 mM sucrose solution).

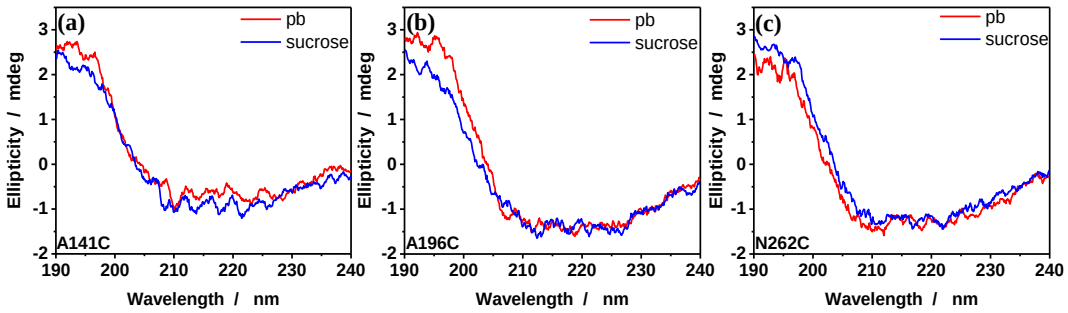

Figure 4.10 CD spectra collected from surface immobilized HLD- (a) A141C; (b) A196C; (c) N262C in buffer solution and in air.

The same method was applied to other two mutants of HLD: A196C and N262C. Similar effects were found: the secondary structures of protein could also be protected and retained in air by spin-coated sucrose, evidenced by CD spectra. As shown in Figures 4.10b and c, after spin coating sucrose on surface immobilized HLD, HLD secondary structure is similar in air and phosphate buffer, meaning that the conformation of HLD was retained by sucrose coatings in air.

SFG spectra were also collected from surface immobilized HLD A196C and N262C (Figures 4.11 and 4.12). Figures 4.11a and 4.12a show the SFG spectra of immobilized proteins in phosphate buffer (Section 3.2). SFG spectra were shown in Figure 4.11b and 4.12b were collected from surface immobilized proteins with freshly spin coated sucrose in air. The alpha-helical secondary structure is still present as indicated by the peak at 1650 cm^{-1}. The protein conformations can be retained under sucrose coating in air for at least two weeks. Within these two weeks, SFG spectra were collected in air and shown in

Figures 4.11b, c, d, e and Figures 4.12b, c, d, e. After fitting the spectra, it was found that orientation of immobilized protein can also be retained, indicated by similar χ_{ppp}/χ_{ssp} ratios. For examples, with a freshly prepared sucrose coating on immobilized HLD-A196C, the χ_{ppp}/χ_{ssp} ratio is deduced to be 2.12. Then on the 4th, 7th, 13th day, the χ_{ppp}/χ_{ssp} ratios are 2.08, 2.20, and 2.10. With a longer storage time at room temperature, the χ_{ppp}/χ_{ssp} ratio decreased, as seen in Figure 4.11f. χ_{ppp}/χ_{ssp} ratio was decreased to 1.84 from immobilized HLD-A196C with sucrose coating after 14 days, meaning that sucrose coating may lose its ability to retain protein conformation. Similar effect was also found in Figure 4.12 for surface immobilized HLD-N262C.

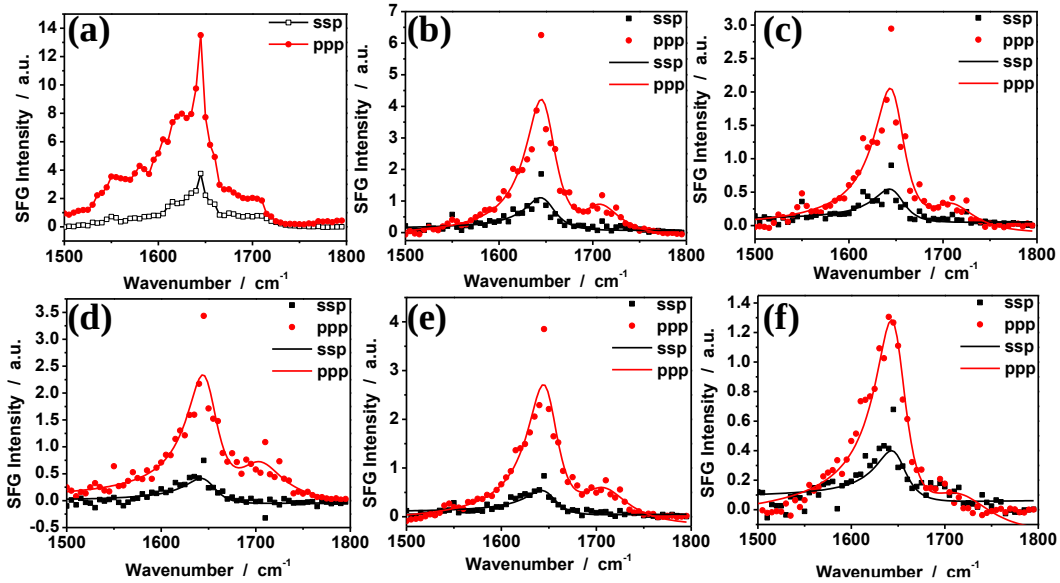

Figure 4.11 SFG spectra collected from surface immobilized HLD-A196C in (a) buffer solution; (b) with freshly prepared sucrose coating in air, and on (c) 4th (d) 7th (e)13th (f)15th day after the sucrose coating was prepared. χ_{ppp}/χ_{ssp} ratios are 2.12, 2.08, 2.20, 2.10, and 1.84 for (b)(c)(d)(e)(f).

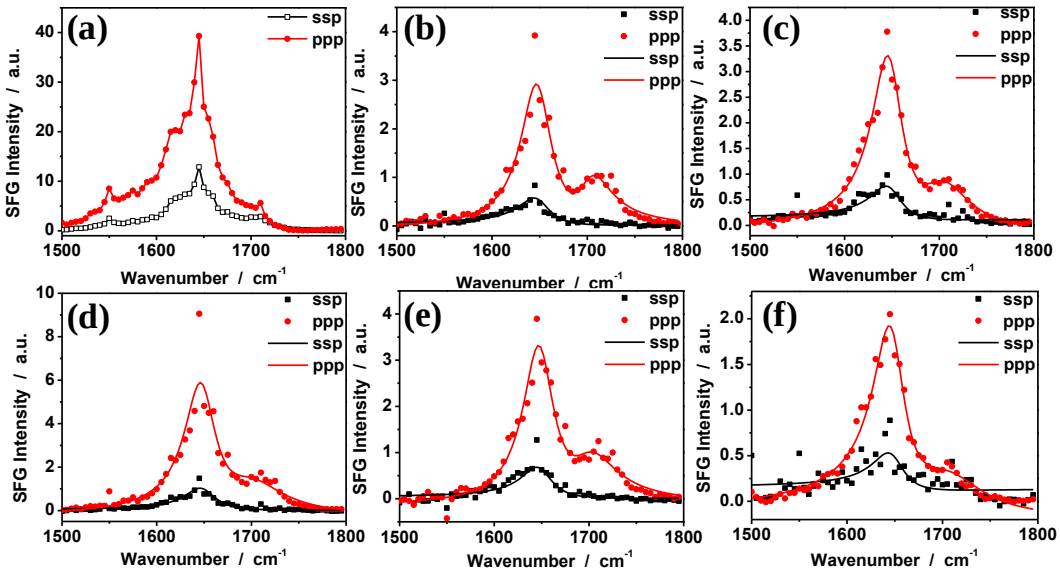

Figure 4.12 SFG spectra collected from surface immobilized HLD-N262C in (a) buffer solution; (b) with freshly prepared sucrose coating in air, and on (c) 4th (d)7th (e)13th (f)15th day after the sucrose coating was prepared. χ_{ppp}/χ_{ssp} **ratios are 2.33, 2.25, 2.20, 2.30, and 2.0 for (b)(c)(d)(e)(f).**

After two weeks, SFG signals of immobilized protein with sucrose coatings in air disappeared, as shown in Figure 4.13. We believe that it is because water from the sucrose coating evaporated after two weeks in storage. Sucrose crystals were then left on surfaces, which do not protect the protein structures and orientations. We believed that such protein structure and orientation change is due to the sugar form change (amorphous to crystalline). Therefore, there is a different interaction between sucrose and protein. When the surface with sucrose coating was stored for two weeks, the small amount of water trapped in the sugar coating evaporated, resulting in a change to the sugar form and consequently, its protein interaction.

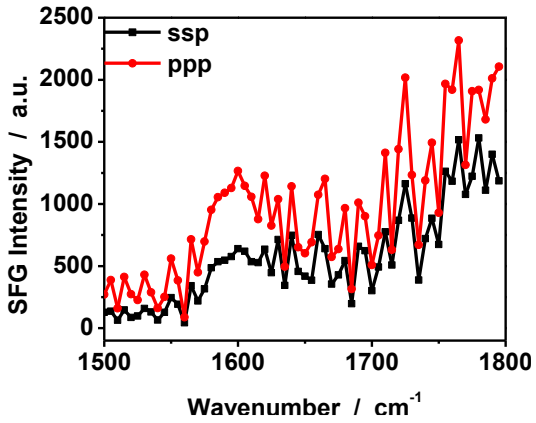

Figure 4.13 SFG spectrum collected from surface immobilized HLD-A196C in sucrose coatings after two weeks.

Similar effects have been found and studied with protein using freeze drying. Thermodynamic studies have found that with sugars in solvent, unfolding of a protein becomes thermodynamically less favorable.[11] Other studies showed that sugars, rich in hydroxyl functional groups, form strong hydrogen bonds with proteins, stabilizing the protein structure.[24, 45] In addition, sugars can modify the hydration layer of a protein in aqueous buffer which eventually can reduce the flexibility of the protein, making it more rigid and stable.[46]

4.5 IMPROVING ANTIMICROBIAL ACTIVITY OF SURFACE IMMOBILIZED PEPTIDE IN AIR, WITH CHEMICALLY TETHERED SUGARS

As discussed above, physically attached sucrose molecules can protect both secondary structures and orientations of surface immobilized peptides. However, physically attached sugar coatings can be washed away very easily. Moreover, such physically attached sugars may block the active site of biomolecules, and reduce their

activity. In this section, we developed a method to chemically attach sugar molecules onto surface immobilized peptides instead of spin-coating. Here we are studying MSI-78 and a hybrid peptide (Cecropin A(1-8)-Melittin (1-18)).

Azido mutated MSI-78 and hybrid peptide molecules were immobilized on an alkyne-terminated SAM surface and SFG spectra were collected from such immobilized peptides in buffer, shown in Figure 4.14. The peptides generated alpha helical signals, indicated by the single peak at 1650 cm^{-1} in each spectrum.

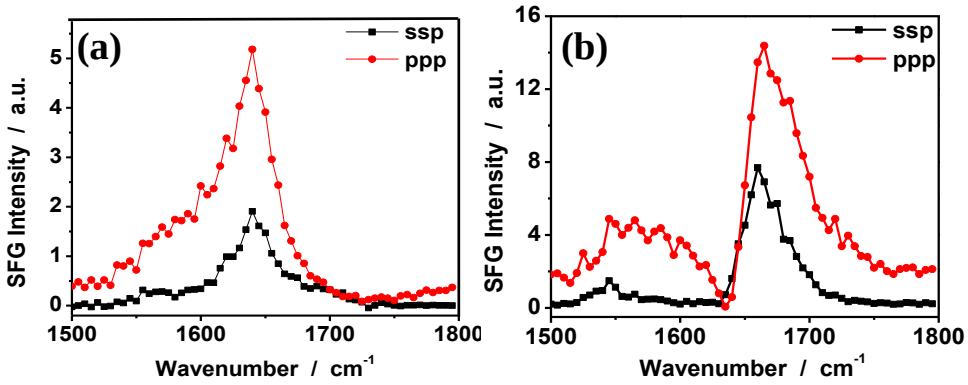

Figure 4.14 SFG spectra collected from surface immobilized (a) MSI-78; and (b) hybrid peptide in phosphate buffer.

When the surface was removed from phosphate buffer and exposed to air, SFG time-dependent signal under ppp polarization was monitored as a function of time (Figure 4.15) from surface immobilized MSI-78. It took about 20 mins for the surface to dry completely, as indicated by the disappearance of the amide I SFG signal. The disappearance of SFG signals indicates that peptide has either lost its secondary structure or changed orientation in air. CD results indicate that the SFG signal disappearance in air

was due to lying down of the peptide on surface (Figure 4.3). Surface immobilized hybrid peptide have shown similar results.

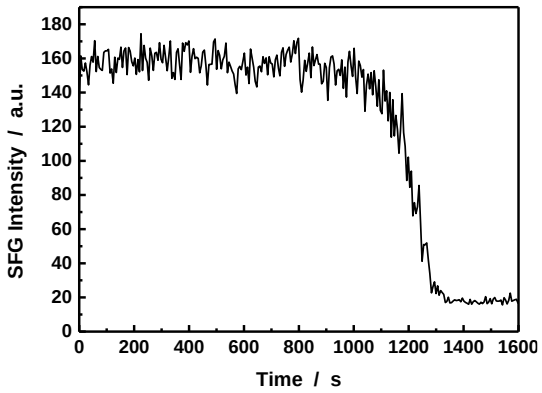

Figure 4.15 SFG time-dependent signal at ppp polarization collected from surface immobilized MSI-78 removed from phosphate buffer and exposed to air at time 0s.

In order to maintain orientation and functions of surface immobilized peptide, maltodextrin was chemically reacted to the amine groups on the side chains of peptides. Then the surface with immobilized peptides (with sugar chemically attached) was exposed to air and SFG signals at 1650 cm^{-1} were monitored from the surface as a function of time (Figure 4.16). Compared to the surface with immobilized peptides without sugar attached, it took a much longer time for the surface to dry and for the immobilized peptides to loose their orientation ordering completely. For example, it took more than two hours for the SFG signal from the hybrid/sugar surface to disappear. It took more than one hour for the signal to disappear from surface immobilized MSI-78 with sugar tethered. We believe that sugar molecules attached to the peptides could help hold more water and retain the peptide

orientation for a longer time in air. This may impact the antimicrobial activity of the surface immobilized peptides in air, which will be discussed in detail below.

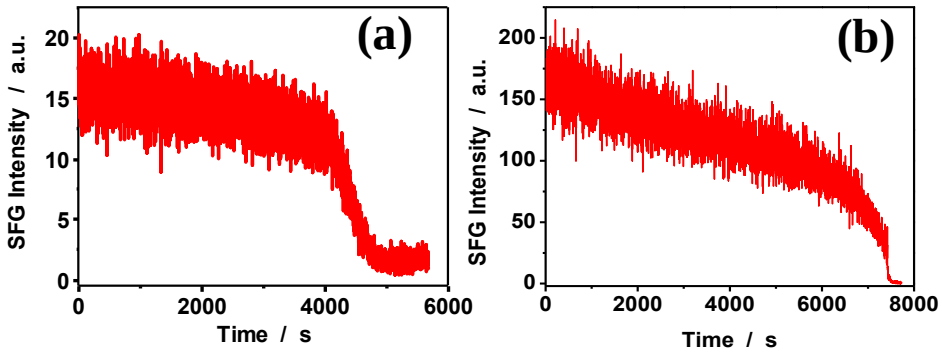

Figure 4.16 SFG ppp time-dependent signal collected from the surface immobilized (a) MSI-78 and (b) hybrid peptides with sugar molecule chemically tethered exposed to air starting at time 0 s.

Antimicrobial tests of surface immobilized peptides towards bacteria were performed on agar plate with no bulk water. As seen in Figure 4.17, silicon wafer, SAM, SAM+sugar were used for the activity tests as controls. No activity was observed from such control samples. With peptides immobilized on surfaces with or without sugar attached, the surfaces showed activity, indicated by the smaller percentage of the visible bacteria left on agar and sample surfaces. With sugar molecules chemically attached, the surface immobilized peptides showed better activity.

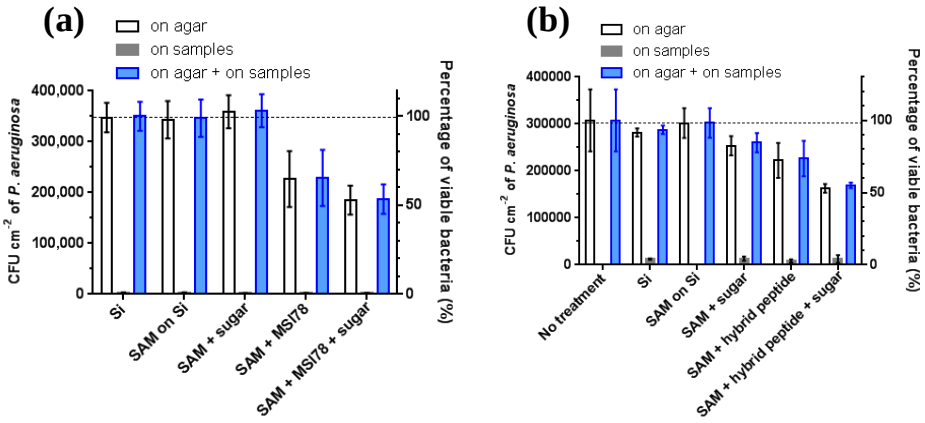

Figure 4.17 Antimicrobial activity of silicon wafer surface, alkyne terminated SAM surface, alkyne terminate SAM surface after immersed in sugar reaction solution, surface with immobilized peptide: (a) MSI-78 and (b) hybrid peptide, and surface immobilized peptides with sugar chemically tethered.

We believe that this enhancement in the antibacterial activity is due to the interaction between chemically tethered sugar molecules and surface immobilized peptides. Their interaction may affect the structure and orientation of peptide when it is in contact with bacterial cells. The detailed mechanism of such effect is still under current investigation.

4.6 CONCLUSION

In this chapter we studied how sugar coating is able to affect the secondary structure and orientation of surface immobilized biomolecules at RT in dry conditions. First, we observed that spin coated sugar on top of the surface immobilized nMSI-78 at RT could support and orient the alpha-helical secondary structures of immobilized peptides. The effect of sucrose was observed to be very stable at even higher temperatures (Figure 4.18).

Then, we studied the effect of the concentration of sugar solution used for spin-coating on immobilized peptide structure. It was found that immobilized peptide orientation could be varied by varying the concentration of the sugar solutions used for spin-coating. Therefore, changing the sugar solution concentration allows us to easily control the orientation of surface immobilized peptides, which builds a foundation for the control of conformation and orientation of more complex biomolecules such as enzymes in air for optimized sensing response. This method of controlling immobilized peptide orientation using spin-coating was also found to be reversible (Figure 4.19). We discovered that in order to retain the standing-up alpha-helical structure of immobilized MSI-78 on the surface, it is necessary to quickly dry the sugar molecules on the peptides to "freeze" the secondary structure of the peptide with a specific orientation. More details about the drying process and the effect of different drying rates are under the current investigation. Interestingly, it was found that spin coated sugars of different types, e.g., sucrose, trehalose, and mannitol have different influences on the conformation and orientation of immobilized peptides underneath, which will be examined in detail in the future.

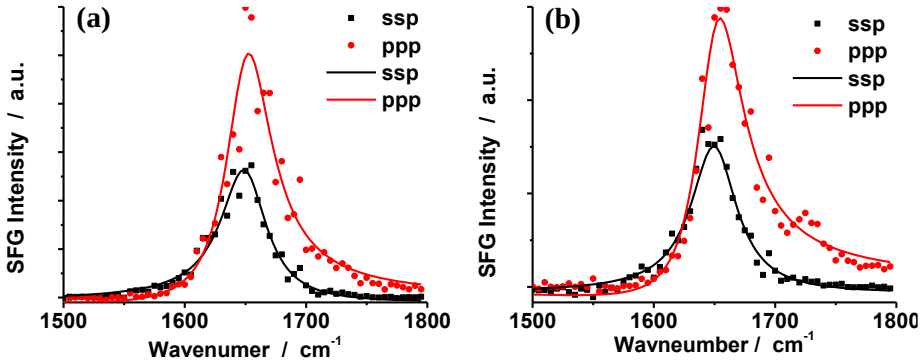

Figure 4.18 SFG ssp and ppp spectra collected from nMSI-78 immobilized on a SAM surface with sucrose spin coated: (a) freshly prepared; (b) stored at 75 ºC for two hours and tested at RT.

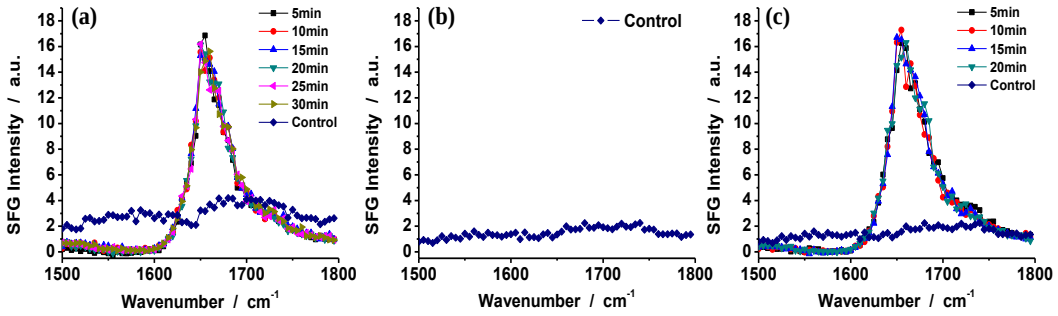

Figure 4.19 SFG ppp spectra collected from same nMSI-78 immobilized on SAM surface (a) with spin-coated sucrose layer on top in air; (b) in air with sugar coating washed away; (c) with sucrose spin coated again on top of this immobilized peptide surface in air.

This method was also successfully applied to protein systems. It was found that spin-coated sucrose can retain the secondary structures and orientations of immobilized HLD for at least two weeks.

Other than sugar coatings that are applied by physical adsorption, we also chemically tethered sugar molecules onto the side chains of surface immobilized peptides. We found that tethered sugar molecules can help retain the orientation of immobilized peptide longer. Moreover, a better antimicrobial activity was observed from the surface immobilized peptide with sugar tethered. We believed that sugar molecules may affect the structure and orientation of immobilized peptide when in contact with bacteria cell membranes.

In this chapter, hydro-mimetic strategies were developed to retain both structure and orientation of surface immobilized biomolecules. The interaction between the sugar molecule and biomolecule (peptide and protein) plays an important role. Chemically attached sugar molecules help to increase the antibacterial activity of immobilized AMPs. The detailed mechanism will be studied in the future. We believe that this will provide

more fundamental information and guidance of preserving the functions of biological interfaces in harsh conditions.

4.7 REFERENCES

1. P. Ball, *Chemical Reviews*, 2008, **108**, 74-108.
2. J. Kim, H. Jia and P. Wang, *Biotechnology advances*, 2006, **24**, 296-308.
3. S. D. Minteer, B. Y. Liaw and M. J. Cooney, *Current Opinion in Biotechnology*, 2007, **18**, 228-234.
4. S. Fujita, S. Yamanoi, K. Murata, H. Mita, T. Samukawa, T. Nakagawa, H. Sakai and Y. Tokita, *Scientific reports*, 2014, **4**, 1-8.
5. J. H. Crowe, L. M. Crowe, J. F. Carpenter and C. A. Wistrom, *Biochemical Journal*, 1987, **242**, 1-10.
6. S. B. Leslie, E. Israeli, B. Lighthart, J. H. Crowe and L. M. Crowe, *Applied and environmental microbiology*, 1995, **61**, 3592-3597.
7. W. Q. Sun, A. C. Leopold, L. M. Crowe and J. H. Crowe, *Biophysical Journal*, 1996, **70**, 1769-1776.
8. M. A. Usmani, *Thermochimica Acta*, 2014, **575**, 331-335.
9. M. Goel, E. N. G. Marsh, Z. Chen and N. L. Abbott, *Langmuir*, 2014, **30**, 7143-7151.
10. J. F. Back, D. Oakenfull and M. B. Smith, *Biochemistry*, 1979, **18**, 5191-5196.
11. J. C. Lee and S. N. Timasheff, *Journal of Biological Chemistry*, 1981, **256**, 7193-7201.
12. T. Arakawa and S. N. Timasheff, *Biochemistry*, 1982, **21**, 6536-6544.
13. G. Cheng, H. Xue, G. Li and S. Jiang, *Langmuir*, 2010, **26**, 10425-10428.
14. S. Braun, W. R. Salaneck and M. Fahlman, *Advanced Materials*, 2009, **21**, 1450-1472.
15. K. A. Marx, *Biomacromolecules*, 2003, **4**, 1099-1120.
16. G. A. Somorjai, A. M. Contreras, M. Montano and R. M. Rioux, *Proceedings of the National Academy of Sciences*, 2006, **103**, 10577-10583.
17. D. R. Rolison, J. W. Long, J. C. Lytle, A. E. Fischer, C. P. Rhodes, T. M. McEvoy, M. E. Bourg and A. M. Lubers, *Chemical Society Reviews*, 2009, **38**, 226-252.

18. C. D. Hodneland, Y.-S. Lee, D.-H. Min and M. Mrksich, *Proceedings of the National Academy of Sciences*, 2002, **99**, 5048-5052.

19. X.-L. Sun, C. L. Stabler, C. S. Cazalis and E. L. Chaikof, *Bioconjugate Chemistry*, 2006, **17**, 52-57.

20. F. Rusmini, Z. Zhong and J. Feijen, *Biomacromolecules*, 2007, **8**, 1775-1789.

21. T. Cha, A. Guo and X. Y. Zhu, *Proteomics*, 2005, **5**, 416-419.

22. Y. Liu, T. L. Ogorzalek, P. Yang, M. M. Schroeder, E. N. G. Marsh and Z. Chen, *Journal of the American Chemical Society*, 2013, **135**, 12660-12669.

23. J. F. Carpenter and J. H. Crowe, *Biochemistry*, 1989, **28**, 3916-3922.

24. S. J. Prestrelski, N. Tedeschi, T. Arakawa and J. F. Carpenter, *Biophysical Journal*, 1993, **65**, 661-671.

25. J. H. Crowe, L. M. Crowe and S. A. Jackson, *Archives of Biochemistry and Biophysics*, 1983, **220**, 477-484.

26. Y. Shen, *Nature*, 1989, **337**, 519-525.

27. Z. Chen, Y. Shen and G. A. Somorjai, *Annual review of physical chemistry*, 2002, **53**, 437-465.

28. L. Fu, J. Liu and E. C. Yan, *Journal of the American Chemical Society*, 2011, **133**, 8094-8097.

29. J. Kim and P. S. Cremer, *ChemPhysChem*, 2001, **2**, 543-546.

30. S. Roy, P. A. Covert, W. R. FitzGerald and D. K. Hore, *Chemical Reviews*, 2014, **114**, 8388-8415.

31. J. Kim and G. A. Somorjai, *Journal of the American Chemical Society*, 2003, **125**, 3150-3158.

32. K. McCrea, J. S. Parker, P. Chen and G. Somorjai, *Surface Science*, 2001, **494**, 238-250.

33. S. Ye, K. T. Nguyen, A. P. Boughton, C. M. Mello and Z. Chen, *Langmuir*, 2009, **26**, 6471-6477.

34. J. Wang, M. A. Even, X. Chen, A. H. Schmaier, J. H. Waite and Z. Chen, *Journal of the American Chemical Society*, 2003, **125**, 9914-9915.

35. X. Chen, J. Wang, J. J. Sniadecki, M. A. Even and Z. Chen, *Langmuir*, 2005, **21**, 2662-2664.

36. B. Ding and Z. Chen, *The Journal of Physical Chemistry B*, 2012, **116**, 2545-2552.

37. S. Roeters, C. van Dijk, A. Torres-Knoop, E. H. Backus, R. Campen, M. Bonn and S. Woutersen, *The Journal of Physical Chemistry A*, 2013, **117**, 6311-6322.

38. T. Weidner, N. F. Breen, K. Li, G. P. Drobny and D. G. Castner, *Proceedings of the National Academy of Sciences*, 2010, **107**, 13288-13293.

39. D. Hu and K. C. Chou, *Journal of the American Chemical Society*, 2014, **136**, 15114-15117.

40. D. Hu, Z. Yang and K. C. Chou, *The Journal of Physical Chemistry C*, 2013, **117**, 15698-15703.

41. Y. Li, S. Wei, J. Wu, J. Jasensky, C. Xi, H. Li, Y. Xu, Q. Wang, E. N. G. Marsh, C. L. Brooks and Z. Chen, *The Journal of Physical Chemistry C*, 2015, **119**, 7146-7155.

42. K. T. Nguyen, S. V. Le Clair, S. Ye and Z. Chen, *The Journal of Physical Chemistry B*, 2009, **113**, 12358-12363.

43. K. T. Nguyen, S. V. Le Clair, S. Ye and Z. Chen, *The Journal of Physical Chemistry B*, 2009, **113**, 12169-12180.

44. X. Chen, J. Wang, A. P. Boughton, C. B. Kristalyn and Z. Chen, *Journal of the American Chemical Society*, 2007, **129**, 1420-1427.

45. S. D. Allison, B. Chang, T. W. Randolph and J. F. Carpenter, *Archives of Biochemistry and Biophysics*, 1999, **365**, 289-298.

46. M. Sola-Penna and J. R. Meyer-Fernandes, *Archives of Biochemistry and Biophysics*, 1998, **360**, 10-14.

CHAPTER 5 Antimicrobial Peptide Immobilization on Polymer Surfaces Prepared by Chemical Vapor Deposition (CVD)

5.1 INTRODUCTION

Antimicrobial peptides (AMPs) have been extensively studied for their ability to efficiently kill bacteria.[1-7] They are potential attractive alternatives for current antibiotics and can be developed into new anti-bacterial surfaces and coatings. Moreover, they have broad-spectrum antimicrobial activity, high structural stability, low toxicity for healthy mammalian cells, and low susceptibility to bacterial resistance compared to conventional antibiotics and other antibacterial agents including quaternary ammonium salts, silver, and titanium compounds.[1-3, 8, 9] However, most studies about AMPs are mainly focused on their properties in bulk solutions.[10, 11] Here in this chapter, we will focus on the surface attachment of such peptides to polymer materials. As we presented in the previous chapters, surface immobilized biomolecules including peptides and proteins are widely used in many different fields, including biosensors, biochips, anti-fouling surfaces, anti-bacteria surfaces, and biofuel cells. When immobilized onto a surface, the activity and function of the biomolecules are normally influenced, possibly resulted from the structural change of the biomolecules due to their interactions with the surface, which are not fully understood yet.

Chapter 2 showed that MSI-78, an AMP, can be successfully immobilized on an alkyne terminated self-assembled monolayer (SAM) surface through an azido-mutated

lysine group engineered at either the N- or C- terminus.[12, 13] Our previous studies have also shown that a self-assembled monolayer (SAM) can provide an ordered surface with well-defined functional groups terminated, that enables surface immobilization of biomolecules through different chemical reactions. Unfortunately, SAM surfaces cannot be prepared on a wide range of solid surfaces, which largely limited their applications. Compared to SAMs, polymer surfaces are more practical and versatile and can have a myriad of different functional groups. Chemical vapor deposition (CVD) polymerization has been proven to be a versatile coating method that can effectively functionalize surfaces with various surface chemistry.[14, 15] Moreover, reactive polymer thin film coatings prepared by CVD can be deposited on a broad range of substrates and materials, which largely broaden their applications. These polymer coatings presenting reactive functional groups allow for surface attachment of peptides and proteins. CVD polymer coatings can also be designed to bear multiple reactive functional groups. For example, atom-transfer radical-polymerization (ATRP) initiators can be attached to CVD coating surfaces, which can allow for polymer brush growth through these initiators. As we discussed in Chapter 1, developing a method that can keep biomolecule structures in harsh conditions (e.g., in the absence of bulk water) is very important. With such CVD coating surfaces designed, we will be able to co-immobilize both biomolecules and polymer brush molecules on the same surface and study how co-immobilized polymer brush molecules with different properties affect the structure of biomolecules on the surface.

In this chapter, we studied MSI-78 (both N- and C-terminus azido-lysine engineered) surface immobilization on a CVD prepared polymer surface with alkyne group

functionalized through "click" chemistry. As compared to the SAM surface immobilization presented in previous chapters, we found that peptide molecules exhibit different orientations on a CVD polymer surface. Moreover, we also co-immobilized both peptides and polymer brushes on a CVD polymer coating surface functionalized with both alkyne and ATRP initiators. It was found that polymer brushes help increase the antimicrobial activity of the co-immobilized peptides. Results of this chapter provide an important fundamental understanding on how to optimize the performance of immobilized peptides on polymer surfaces in harsh conditions by using different co-immobilized polymer brushes. This knowledge may also lead to more practical applications of CVD polymer coating surfaces for antimicrobial coatings and biosensing.

5.2 EXPERIMENTAL SECTION

5.2.1 CVD Coatings and Characterization

CVD coatings were prepared by Prof. Joerg Lahann's group at the University of Michigan. The synthesis of the precursors, 4-ethynyl[2,2]paracyclophane (precursor 1) and [2,2]paracyclophane-4-methyl 2-bromoisobutyrate (precursor 2) has been described in previous publication.[16] CVD polymerization was performed using a custom-built CVD system previously developed.[17] For alkyne-functionalized polymer coatings, the CVD process was carried out at 0.1 mbar, with 20 sccm argon as carrier gas. The precursor 1 was sublimed at 90-110 ºC in vacuum and converted into corresponding diradical by pyrolysis (660 ºC). The diradicals spontaneously polymerized into poly[(p-xylylene-4-ethynyl)-co-(p-xylylene)] on cooled (15 ºC) substrates placed on top of a rotating stage.

For polymer coatings containing both alkyne and ATRP initiator groups, precursors 1 and 2 were introduced simultaneously into the CVD system. The sublimation, pyrolysis and stage temperatures were fixed at 100 ºC, 540 ºC and 15 ºC, respectively, and the pressure was set at 0.1 mbar. The chemical structures of CVD polymers were shown in Figure 5.1.

Sorbitol methacrylate (0.4 g/ml), ME6TREN (0.11 mg/ml), and Cu(II)Cl_2 (0.24 mg/ml) was stirred in a Schlenk flask at room temperature. The homogeneous solution was degassed using three freeze-pump-thaw cycles. Next, Cu(I)Cl (3.56 mg/ml) was added under nitrogen purge to the frozen solution. The mixture was warmed up to room temperature and was stirred until a homogeneous dark brown solution was formed. The solution was then transferred into a nitrogen-purged glove bag, and split into several 20 mL scintillation vials containing one CVD-coated substrate per vial. The polymerizations proceeded at room temperature for a set reaction time.

FTIR spectroscopy (Nicolet 6700 spectrometer with the grazing angle accessory at a grazing angle of 85 º) was used to characterize the CVD polymers. The FTIR spectrum in Figure 5.2 clearly shows the stretching bands at 2100 cm^{-1}, which are characteristic of the terminal alkyne groups. Figure 5.2b characterized the alkyne-ATRP polymer surfaces. The carbonyl stretching band at 1723 cm^{-1} and C-O stretching bank at 1219 cm^{-1} indicate the presence of the ester bonds.

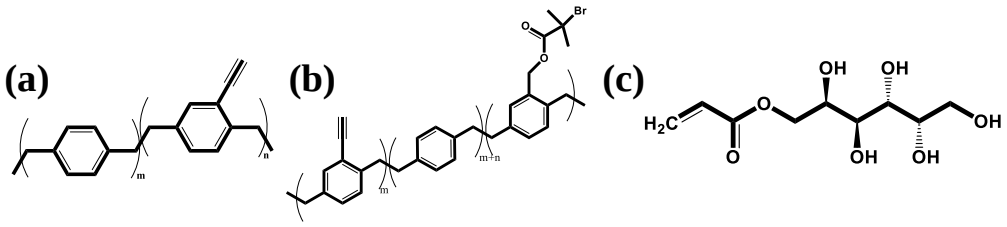

Figure 5.1 Molecular formulas of (a) alkyne functionalized CVD polymer; (b) alkyne and ATRP initiator functionalized CVD polymer; (c) sorbitol acrylate.

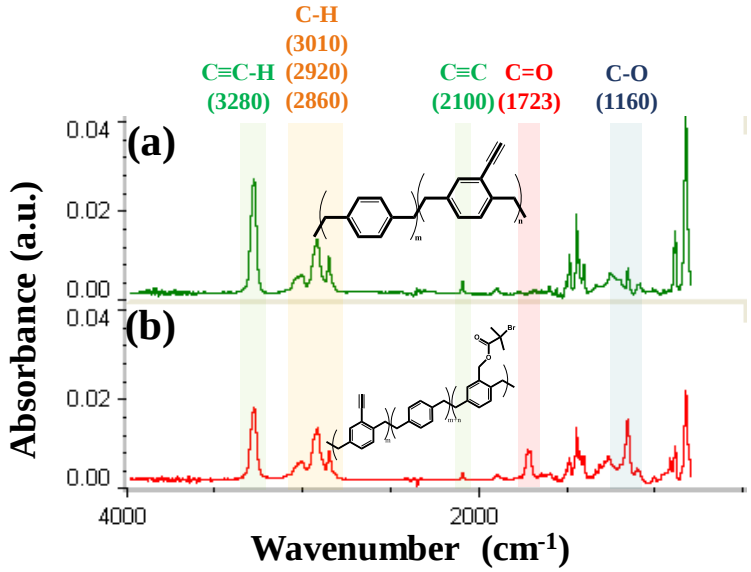

Figure 5.2 FTIR spectra of (a) alkyne functionalized CVD polymer film; (b) alkyne-ATRP initiator functionalized polymer film.

5.2.2 Surface Immobilization of Peptide

Azido-modified MSI-78 at the N- (nMSI-78) or C-terminus (MSI-78n) was immobilized onto alkyne terminated CVD polymer surfaces using methods discussed in Chapter 2.

5.2.3 Antimicrobial Activity Test

Surfaces used for antimicrobial activity test were prepared on 100-nm silica coated silicon wafer surfaces. The anti-bacteria test was performed using the same method discussed in Chapter 4.

5.3 RESULTS AND DISCUSSIONS

5.3.1 Immobilization of Peptides on Alkyne-CVD Surface

As shown in Section 5.2, CVD polymer coatings with alkyne groups were deposited onto CaF_2 prisms, presenting alkyne groups on the surface. Evidence of these reactive alkyne groups has been demonstrated via fluorescence.[14, 16]

After polymer deposition, peptide molecules were immobilized on the alkyne-CVD polymer surface through "click" chemistry using conditions presented in Chapter 2. SFG ssp and ppp spectra in the amide I frequency region were collected from the immobilized MSI-78 (nMSI-78 or MSI-78n) molecules at the polymer/buffer solution interface, shown in Figure 5.3. Figure 5.3a shows the SFG spectra collected from surface immobilized nMSI-78 in phosphate buffer solution. Both ssp and ppp contain a peak indicative of alpha-helical structure of the peptides, centered at about 1650 cm^{-1}. Different from nMSI-78, after surface immobilization of MSI-78n, peak at 1650 cm^{-1} was only observed at ssp polarization. At ppp polarization in Figure 5.3b, no alpha helical structure SFG signal was observed. However, a peak at 1610 cm^{-1} was observed, mainly coming from the phenyl ring of the CVD polymer backbone.

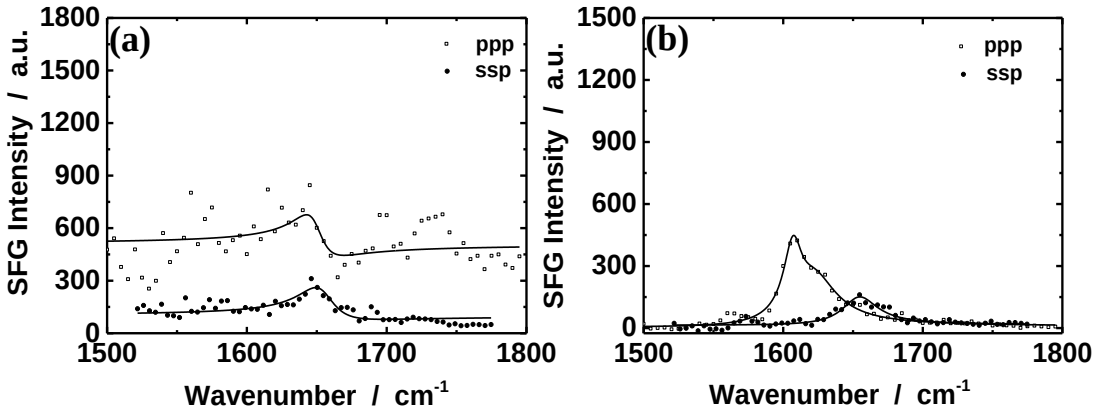

Figure 5.3 SFG spectra collected from (a) alkyne-CVD surface immobilized nMSI-78; (b) alkyne-CVD surface immobilized MSI-78n in buffer.

After fitting SFG spectra, both fitted χ_{ppp}/χ_{ssp} ratios from nMSI-78 and MSI-78n were out of the calculated curve assuming a delta orientation distribution, in Figure 2.4. This indicates that the delta orientation distribution assumption for MSI-78 immobilization on the CVD polymer coating is not valid anymore. Compared to a SAM surface, a CVD polymer surface can be more disordered. Therefore, after surface immobilization, the peptide molecules may adopt the same orientation. The above results demonstrated that MSI-78 can be immobilized on to a CVD polymer coating, but both the immobilized nMSI-78 and MSI-78n adopted multiple orientations.

5.3.2 Co-Immobilization of Peptide and Polymer Brush

Since nMSI-78 molecules generated stronger SFG signals when immobilized on an alkyne-CVD surface, we then selected nMSI-78 to study the co-immobilization of peptide and polymer brush.

CVD polymer surfaces bearing alkyne groups and ATRP-initiators were prepared and characterized using FTIR (Figure 5.2). As discussed above, the alkyne groups are used to immobilize peptides, and ATRP initiators are for polymer brush growth. SFG spectra were collected from a CVD polymer surface with both alkyne functionality and ATRP initiator in air and in phosphate buffer solution. One peak centered at about 1720 cm^{-1} was observed in both spectra (Figure 5.4). This comes from the carboxyl groups on alkyne-ATRP initiator bearing CVD surfaces. When the surface was in contact with a phosphate buffer solution, a new peak centered at 1610 cm^{-1} was also observed. This peak was also observed from alkyne functionalized CVD polymer surfaces, originating from the phenyl

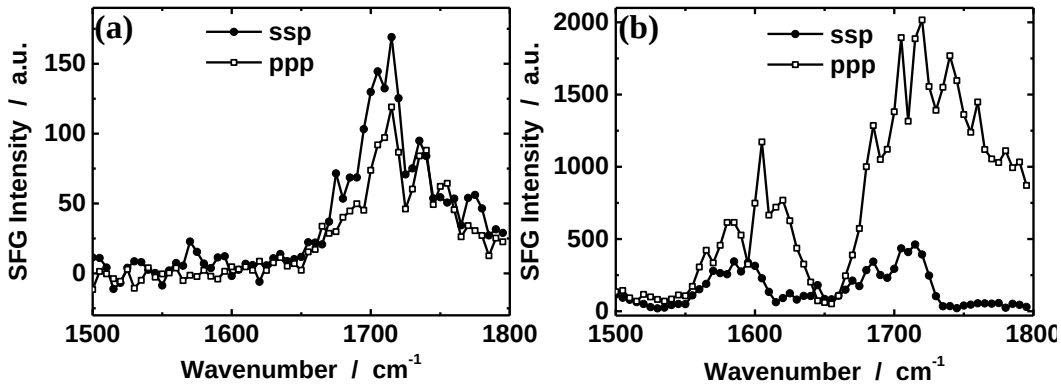

Figure 5.4 SFG spectra collected from a CVD polymer coating surface with alkyne functionality and ATRP initiator (a) in air and (b) in phosphate buffer solution.

ring of the CVD polymer backbones. Polymer surfaces generate some background SFG signals, however, no peak at 1650 cm^{-1} (which should be the peptide signal) was observed. We therefore believe that such surfaces can be used to immobilize peptides and characterized by SFG.

We then co-immobilized peptide molecules and polymer brushes on to a CVD polymer surface presenting alkyne groups and ATRP initiators. We firstly studied the effect of the immobilization order: Peptide molecules were immobilized to alkyne groups on the CVD coating first, then polymer brushes were grown later, or vice versa. We found that MSI-78 peptide can be immobilized successfully using both ways. Therefore, here peptides were immobilized after the polymer brushes because due to ease of preparation.

It has been shown in Chapter 4 that sugar molecules can improve the antimicrobial activity of surface immobilized hybrid peptides. Here, polymer brushes used in this study were a poly-sugar: a poly-sorbitol brush (with monomer molecular structure shown in Figure 5.1c) prepared using ATRP polymerization. After the CVD polymer surface was immobilized with poly sorbitol polymer brush, nMSI-78 molecules were then immobilized. Such a surface with both peptides and polymer brushes was then characterized by SFG. Figure 5.5a shows SFG spectra of surface co-immobilized peptides and poly sorbitol brushes in a phosphate buffer solution. With polymer brush and peptide co-immobilized, the orientation of the phenyl rings from the CVD polymer backbones is random, indicated by the disappearance of the original SFG peak at 1610 cm^{-1} before immobilization. Strong SFG amide I signals were detected from peptides, showing the successful immobilization of the peptides. Fitted χ_{ppp}/χ_{ssp} ratio is 1.82, indicating that the surface co-immobilized peptide with polymer brushes exhibit an orientation of 38 º relative to the surface normal. Therefore, with polymer brush co-immobilized, it can help retain the peptide orientations after immobilization on CVD polymer surfaces.

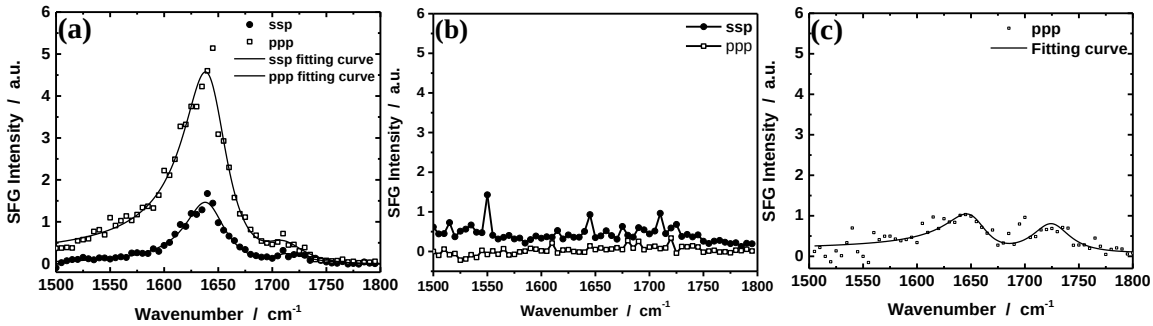

Figure 5.5 SFG spectra collected from a CVD polymer surface with co-immobilized peptides and polymer brushes (a) in phosphate buffer; (b) in air; (c) in air at 75% relative humidity condition.

When the surface was removed from the buffer and exposed to air, no SFG amide I signal was detected from the surface immobilized peptides. This means that immobilized peptides became randomly distributed in air. Poly sorbitol, in this case, unfortunately could not have a similar effect as the spin coated sucrose as discussed in Chapter 4. Interestingly, when the surface was exposed to air with 75% relative humidity, an SFG peak at 1650 cm^{-1} was observed from the surface, seen in Figure 5.5c. With a higher humidity, surface co-immobilized poly sorbitol slightly affect the orientation of the immobilized peptides. Without the co-immobilized poly sorbitol, no SFG amide I signal could be detected from surface immobilized MSI-78 peptides on alkyne functionalized CVD polymer coating in air, regardless of the humidity (not shown).

In order to test if poly sorbitol exhibits similar activity enhancement as maltodextrin discussed in Section 4.5, the antimicrobial activity was tested on surface co-immobilized peptide and poly sorbitol brush. As seen in Figure 5.6, a CVD polymer coating surface and a CVD polymer surface with only poly sorbitol brushes, as control samples, did not exhibit any observable anti-bacterial activity. The CVD polymer immobilized with MSI-78

peptides only indeed exhibited antimicrobial activity. More importantly, the surface with co-immobilized peptides and poly sorbitol brushes (either peptides or polymer brushes immobilized first) showed higher antimicrobial activities (16-19% ± 8% more killing) than the surface with peptides but without poly sorbitol brushes. Therefore, co-immobilized poly sorbitol brushes showed similar activity enhancement effect as the chemically tethered maltodextrin discussed in Chapter 4. We believed that this is due to the fact that the surface immobilized peptides adopt a better structure (e.g., a better orientation orientation) by surrounding co-immobilized poly sorbitol brushes, leading to better bacterial killing.

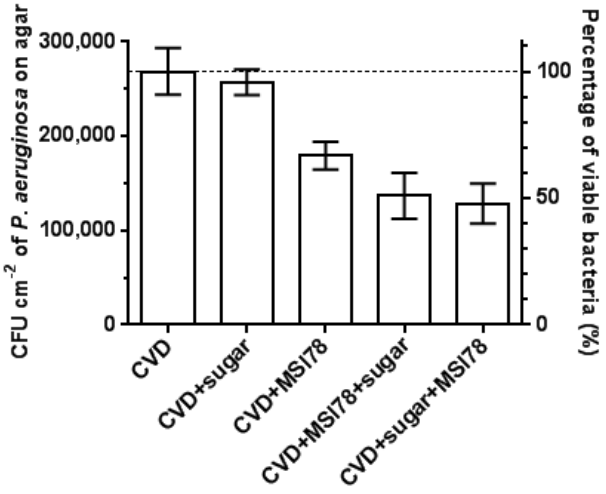

Figure 5.6 Viable colony forming units (CFU) of *P. aeruginosa* on agar surface remaining following contact of the agar with nMSI-78 peptides that were co-immobilized with poly sorbitol on a CVD polymer surface. Error bars show standard of errors (n>3).

5.4 CONCLUISON

In this chapter, we have shown that peptide molecules can be successfully immobilized on alkyne functionalized CVD polymer surfaces through "click" chemistry. Due to a more disordered polymer surface compared to a SAM surface, we found that the immobilized peptides adopt multiple orientations (not a delta orientation distribution).

Nevertheless, surface immobilized peptides on a CVD polymer coating can kill bacteria, showing that we are able to use CVD polymer coatings to immobilize peptides for antimicrobial purposes. Since CVD polymer coatings have much less limitations to construct compared to SAM formation, they have more practical applications.

Furthermore, we demonstrated the successful co-immobilization of peptides and poly sorbitol brushes on CVD polymer surfaces. The co-immobilized poly sorbitol brushes could retain the peptide structure in humid air, leading to improved antimicrobial activity. This result further validated our hypothesis that surface immobilized hydro-mimetics may enhance the activity of surface immobilized biological molecules in the absence of bulk water. Our recent research on surface immobilized enzymes showed that co-immobilized poly sorbitol molecules with enzyme could enhance the enzymatic activity by 6 times compared to the case without the poly sorbitol co-immobilization in air at 50% humidity.[18] Structural characterization data indicated that the co-immobilized poly sorbitol could retain the native structure of the enzyme, enhancing the activity. In that case, the enzyme activity enhancement was not caused by more adsorbed water molecules with the co-immobilized sugar, because with and without the co-immobilized poly sorbitol, the adsorbed water amount is similar on the surface.[18] Here, we believe that the co-immobilized poly sorbitol has a similar effect to better retain the peptide native structure, leading to better activity of the surface immobilized peptides.

5.5 REFERENCES

1. R. E. Hancock and H.-G. Sahl, *Nature biotechnology*, 2006, **24**, 1551-1557.

2. M. R. Yeaman and N. Y. Yount, *Pharmacological reviews*, 2003, **55**, 27-55.

3. R. E. Hancock and R. Lehrer, *Trends in biotechnology*, 1998, **16**, 82-88.

4. H. Jenssen, P. Hamill and R. E. Hancock, *Clinical microbiology reviews*, 2006, **19**, 491-511.

5. J. R. Uzarski, A. Tannous, J. R. Morris and C. M. Mello, *Colloids and Surfaces B: Biointerfaces*, 2008, **67**, 157-165.

6. T. Ganz, *Nature Reviews Immunology*, 2003, **3**, 710-720.

7. M. Zasloff, *nature*, 2002, **415**, 389-395.

8. D. E. Schlamadinger, Y. Wang, J. A. McCammon and J. E. Kim, *The Journal of Physical Chemistry B*, 2012, **116**, 10600-10608.

9. D. Andreu, J. Ubach, A. Boman, B. Wåhlin, D. Wade, R. Merrifield and H. G. Boman, *FEBS letters*, 1992, **296**, 190-194.

10. A. Ramamoorthy, S. Thennarasu, D.-K. Lee, A. Tan and L. Maloy, *Biophysical journal*, 2006, **91**, 206-216.

11. B. C. Buer, J. Chugh, H. M. Al-Hashimi and E. N. G. Marsh, *Biochemistry*, 2010, **49**, 5760-5765.

12. Y. Li, S. Wei, J. Wu, J. Jasensky, C. Xi, H. Li, Y. Xu, Q. Wang, E. N. G. Marsh, C. L. Brooks III and Z. Chen, *The Journal of Physical Chemistry C*, 2015, **119**, 7146-7155.

13. Y. Li, X. Zhang, J. Myers, N. L. Abbott and Z. Chen, *Chemical Communications*, 2015, **51**, 11015-11018.

14. X. Deng, C. Friedmann and J. Lahann, *Angewandte Chemie International Edition*, 2011, **50**, 6522-6526.

15. L. Shen, K. C. K. Cheng, M. Schroeder, P. Yang, E. N. G. Marsh, J. Lahann and Z. Chen, *Surface Science*, 2016, **648**, 53-59.

16. H. Nandivada, H. Y. Chen, L. Bondarenko and J. Lahann, *Angewandte Chemie International Edition*, 2006, **45**, 3360-3363.

17. H.-Y. Chen and J. Lahann, *Langmuir*, 2010, **27**, 34-48.

18. S. Badieyan, Q. Wang, X. Zou, Y. Li, M. Herron, N. L. Abbott, Z. Chen and E. N. G. Marsh, *Journal of the American Chemical Society*, 2017, **139**, 2872-2875.

CHAPTER 6 Understanding Protein-Interface Interactions of a Fusion Protein at Silicone Oil-Water Interface Probed by Sum Frequency Generation Vibrational Spectroscopy

The contents in this chapter will be included in the following publication: **Li Y**, Pan D, Nashine V, Deshmukh S, Chen Z. Understanding protein-interface interactions of a fusion protein at silicone oil-water interface probed by sum frequency generation vibrational spectroscopy.

6.1 INTRODUCTION

In modern pharmaceuticals, protein therapeutics have shown significance in clinical therapy, where these large biomolecules have proven to be biocompatible with limited inherent side effects.[1, 2] However, protein function is directly dependent on protein structure, which is highly sensitive to surrounding environments and can easily be denatured or misfolded. Proteins in aqueous solutions are generally surface-hydrophilic, core-hydrophobic and highly surface-active. This often results in strong adsorption of proteins onto surfaces/interfaces, and leads to protein aggregation, structural denaturation, and eventual loss of protein activity.[3-6] Such a loss in function through agitation, surface distortion, surface-induced adsorption and aggregation often happens during formulation, purification, and transportation of therapeutic proteins, especially in the presence of silicone oil, which is commonly used as a lubricant on the inner faces of storage and delivery devices.[7-9]

Silicone oil is a necessary component in pharmaceutical devices as it facilitates efficient delivery and dosage. However, it simultaneously creates a hydrophobic surface/interface to which proteins tend to be deactivated by exposure of their hydrophobic core, resulting in activity loss and shortened shelf life. Nonionic surfactants, e.g. polysorbate 20 (PS20) or polysorbatae 80 (PS80), are often used to minimize or prevent the structural denaturation of protein and interfacial-induced damage of protein drugs.[2, 10-13]

Protein adsorption and aggregation in the presence of silicone, and the effect of nonionic surfactants on the stabilization and protection of protein structure/function at silicone oil surfaces have been studied previously.[2, 10-13] Different mechanisms, including formation of surfactant and protein complexes, and competitive adsorption of nonionic surfactants and protein on silicone oil surfaces were reported. Such results were obtained by studies using various analytical techniques such as differential scanning calorimetry, circular dichroism, total internal reflection fluorescence, ellipsometry, and quartz crystal microbalance.[11-14] However, detailed structural information of protein molecules at the silicone oil surface/interface, in the absence or presence of surfactants *in situ* is not known, due to the lack of appropriate methods to probe such surfaces/interfaces.

In this chapter, we investigated the interfacial structures of fusion proteins at silicone oil/water interfaces with or without nonionic surfactants *in situ* by sum frequency generation vibrational spectroscopy (SFG), a surface/interface sensitive technique.[15] We found that at the silicone oil/water interface, the fusion protein contains both alpha helical and beta sheet secondary domains. We also studied the behaviors of proteins at the silicone

oil/water interface in the presence of surfactants PS20 or PS80. Our SFG results showed that PS20 and PS80 had similar effects on the interfacial protein structure. Three different methods were used to introduce the surfactants to the system. It was found that in the presence of surfactants, SFG signals from protein molecules were greatly reduced, showing that surfactants could minimize protein adsorption to the silicone oil/solution interface.

6.2 MATERIALS AND METHODS

6.2.1 Materials

Protein sample used in this study was an Fc-fusion protein provided by Bristol-Myers Squibb (NY), in stock concentration of 50 mg/ml, dissolved in pH = 7.0, 25 mM phosphate buffer (150 mM trehalose) solution. Silicone oil was also provided by Bristol-Myers Squibb (NY). All other chemicals including polysorbate 20, polysorbate 80, toluene, methanol were obtained from Sigma-Aldrich (St. Louis, MO, USA) and used as received.

6.2.2 Surface Preparation

Right-angle CaF_2 prisms were soaked in toluene for 24 h and in 1 % Contrex AP solution (Decon Laboratories, King of Prussia, PA, USA) for 10 mins for cleaning. The prisms were then thoroughly rinsed with deionized water (18.2 MΩ cm) and dried under gaseous nitrogen. The clean prisms were treated with O_2 plasma (Glen 1000P) for 30 s immediately before being coated with silica (100 nm thick). Detailed coating parameters have been reported previously.[16] Silicone oil was dissolved in a mixture solvent of toluene and methanol, and then spun-coated onto silica-coated CaF_2 prism surfaces at 1500 rpm for the first 10 seconds, and then 3000 rpm for another 20 seconds. Since silicone oil is

very viscous, the coated oil film is still too thick. In order to partially remove silicone oil and create a thinner oil layer, a lint-free wipe was used to wipe away most of the silicone oil after spin-coating.

6.2.3 SFG Measurement

The details of its setup, measurements, and theories have been reported in Chapter 1 and previous publications.[17-22] SFG is a second order nonlinear optical vibrational spectroscopy and is intrinsically surface/interface sensitive. The SFG experimental data collection sample geometry used in this study is shown in Figure 6.1. As seen in Figure 6.1, two laser beams, one 532 nm visible laser beam and one frequency-tunable IR beam, overlap spatially and temporally at the silicone oil film (on bottom surface of a silica coated CaF_2 prism) surface. The protein sample solution was placed in contact with the silicone oil surface. SFG signal was then collected from the silicone oil/protein solution interface. SFG spectra were collected with polarization combinations of ssp (s-polarized output SFG signal, s-polarized input visible beam, and p-polarized input IR beam) and psp using the near total internal reflection geometry. For protein structures, the amide I SFG signal contributed by alpha helical structure is centered at about 1650 cm^{-1}, and the signal generated by beta sheet conformation is centered at about 1630 cm^{-1}.[20-22] Time-dependent SFG signals were monitored at a specific wavenumber 1650 cm^{-1}.

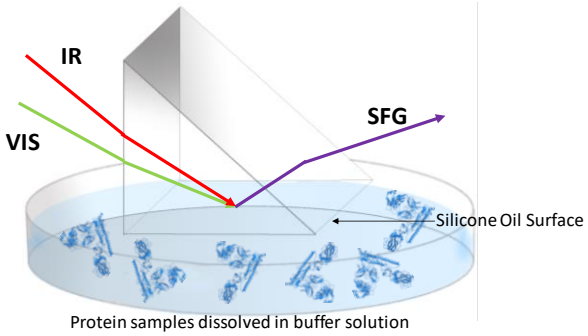

Figure 6.1 SFG geometry used in Chapter 6.

6.3 RESULTS AND DISCUSSION

6.3.1 Silicone Oil Film Coated on Substrate Surface

In order to determine whether any SFG background signal could be generated from the silicone oil interface in the absence of proteins or surfactants, SFG spectra were collected from the silicone oil surface/interface only. Figure 6.2 shows the SFG spectra collected from the silicone oil/air interface and the silicone oil/buffer solution interface in the protein amide I frequency range (1500-1800 cm^{-1}). No SFG signals were detected from these two silicone interfaces, showing that both interfaces are background free.

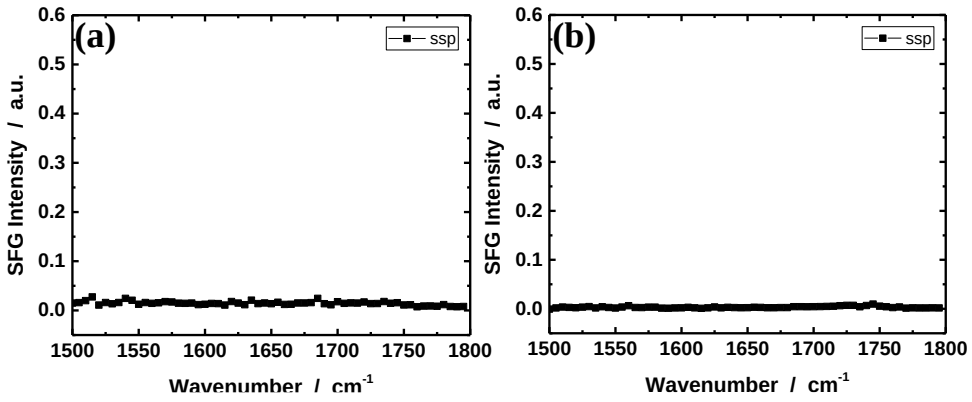

Figure 6.2 SFG spectra collected from (a) silicone oil/air interface and (b) silicone oil/buffer solution interface.

6.3.2 Behaviors of Protein at the Silicone Oil/Buffer Interface

Extensive results from previous studies have demonstrated that protein molecules tend to aggregate to the silicone oil/buffer solution interface.[11-14] However, the structures of proteins at such an interface are unknown. In this study, for the first time, SFG was used to monitor the secondary structures of protein molecules at the silicone oil/buffer solution interface *in situ*. SFG spectra collected with different polarization combinations of the input/output beams can be used to study different protein secondary structures. Here we collected both regular or non-chiral (ssp) and chiral (psp) SFG spectra to examine interfacial alpha helical and beta sheet secondary structures.[20]

After creating a thin layer of silicone oil on the substrate surface, a protein solution (1.0 mg/ml) was placed in contact with the silicone oil surface and SFG amide I signal of interfacial protein molecules was monitored in real time. After the silicone oil surface was in contact with the protein solution, SFG amide I signal of the alpha helical structure at 1650 cm^{-1} increased gradually and finally reached an equilibrium. Both regular (ssp) and chiral (psp) SFG spectra were collected from the silicone oil/protein solution interface when the SFG signal reached a plateau, as shown in Figure 6.3. In Figure 6.3a, a single peak centered at 1650 cm^{-1} was observed, which is contributed by the alpha helical secondary structural domains of the protein at this interface. A single peak centered at about 1630 cm^{-1} was also observed in the psp SFG spectrum (Figure 6.3b), indicating the beta-sheet secondary structure. This indicates that both the alpha helical and beta sheet secondary structural domains are present and ordered in protein molecules adsorbed at the silicone oil/protein solution interface.

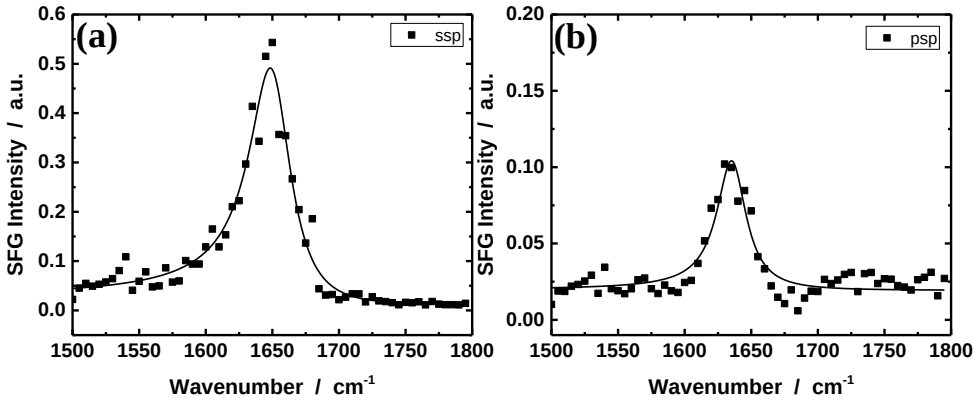

Figure 6.3 SFG spectra collected from silicone oil/protein solution (1.0 mg/ml) interface using (a) ssp and (b) psp polarization combinations.

In order to test the stability of the protein molecules adsorbed at the silicone surface, we washed the silicone surface with buffer solutions. To do so, we replaced the protein solution with a buffer solution to contact the silicone oil surface, and then replaced the buffer with new buffer solutions twice (we refer this process to "washing the surface for three times"). SFG spectra were then collected from the silicone oil/new buffer solution interface, as shown in Figure 6.4. SFG spectra did not exhibit any substantial change, and signals from both alpha helical and beta-sheet secondary structures were still observed, indicating that protein adsorption at the silicone oil/protein solution or buffer solution interface is very stable. Mild buffer washes do not remove proteins from the interface or induce noticeable protein structural changes. Previous research showed that no substantial amount decrease of the proteins adsorbed at the silicone oil interface by buffer washing,[2] but this is the first time to show that the adsorbed protein structure exhibits no change at the silicone oil interface after buffer washing.

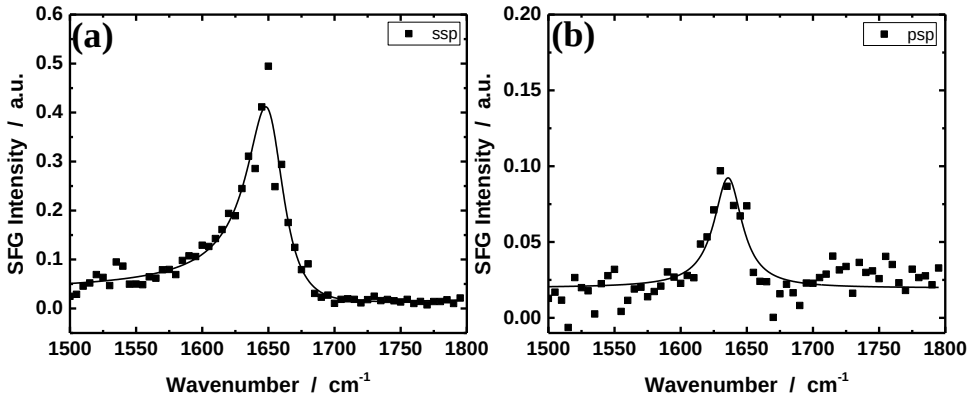

Figure 6.4 SFG spectra collected from the silicone oil/buffer solution interface after three buffer washes on the silicone oil/protein solution interface using (a) ssp and (b) psp polarization combinations.

6.3.3 Effects of Surfactants on Interfacial Proteins

In pharmaceutical industry, surfactants are widely used in protein formulations to reduce or minimize protein aggregation during storage. However, the molecular structures of proteins at silicone oil interface in the presence of different surfactants have not been previously reported. Here we applied SFG to investigate protein structures at the silicone oil interface in the presence of polysorbate 20 (PS20) or polysorbate 80 (PS80), commonly used nonionic surfactants (molecular structure shown in Figure 6.5).

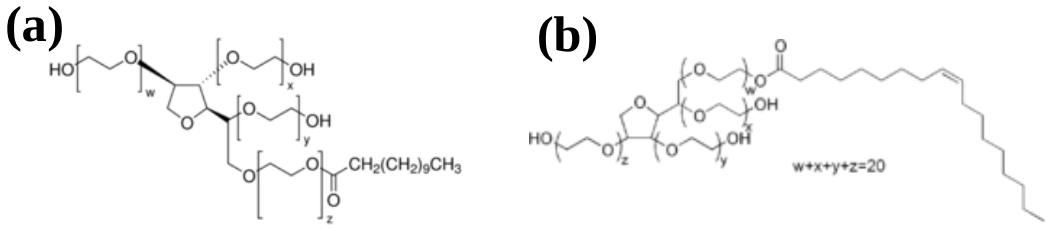

Figure 6.5 Molecular structures of (a) polysorbate 20 and (b) polysorbate 80.

6.3.3.1 Protein Adsorption Followed by Surfactant Solution Contact

As discussed in the previous section, both alpha helical and beta-sheet secondary structures of the adsorbed proteins at the silicone oil/protein solution interface are present and ordered. The structures of the interfacial proteins are also very stable, with no visible change in SFG signals collected from the interfacial proteins after three buffer washes. To investigate the effect of surfactant on interfacial proteins at the silicon oil interface, a buffer solution containing 0.2 % PS20 or PS80 was used to replace the buffer solution in contact with the silicone oil surface (after washing the silicone oil/protein solution interfaces with buffer for three times). The time-dependent change in SFG signal was monitored after the replacement (Figure 6.6). This is different from the case where the protein solution was replaced with a "pure" buffer solution leading to no SFG signal change as discussed above. Here, after contacting the silicone oil surface (with adsorbed proteins) to the buffer solution containing small amounts of surfactants, the regular ssp SFG protein amide I signal (Figure 6.6) decreased and eventually reduced to almost 0. SFG signal decrease may be due to two possible reasons: (1) Adsorbed proteins at the silicone oil surface were washed away by the surfactant buffer solution; (2) Proteins may stay on the silicone oil surface with different orientations (e.g., a random orientation distribution). According to previous QCM studies,[12] surfactant (PS20) was not able to displace the protein molecules aggregated at the silicone oil/buffer interface under the similar experimental conditions but with much lower surfactant concentration. However, in our study, no change in protein amount at the interface could not interpret the large decrease in SFG amide I signal (see more discussions

below). Therefore, we believe that SFG signal decease here likely should be due to the removal of proteins from the interface by surfactants (More details below).

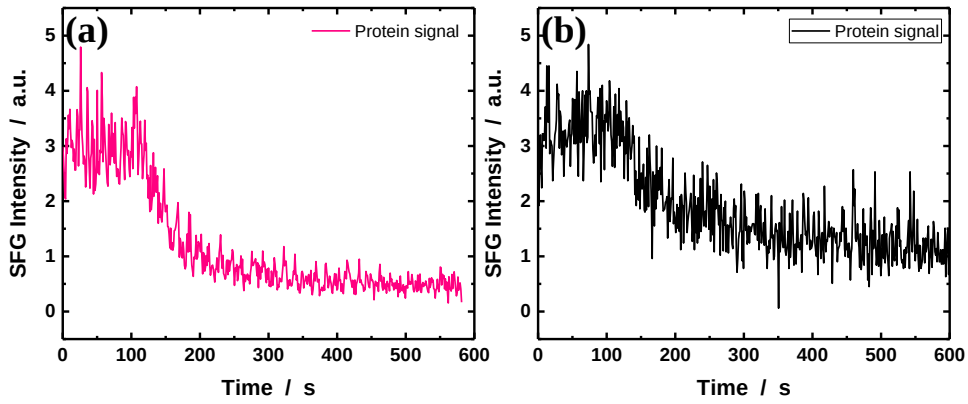

Figure 6.6 SFG time-dependent signals monitored at 1650 cm^{-1} after replacing the buffer solution in contact with silicone oil with a buffer solution containing (a) 0.2% PS20 or (b) 0.2% PS80.

After the SFG signal stabilized, SFG spectra were collected from the silicone oil/buffer (with 0.2% surfactant) solution interface. As seen in Figure 6.7, at the silicone oil/buffer solution containing 0.2% PS20 interface, neither alpha helix nor beta sheet signal was observed. However, it is very interesting to notice that at the silicone oil/buffer solution containing 0.2% PS80 interface, very weak regular or non-chiral SFG signal was observed (Figure 6.7c), but no chiral signal was detected. Since the regular SFG signal is several times stronger than the chiral signal (see results presented above), here the absence of detection of chiral signal from the silicone oil/buffer solution containing 0.2% PS80 interface may be because the chiral signal is too weak to be observed. Nevertheless, it seems that the PS 20 has stronger effect to influence the protein molecules at the silicone oil interface than PS80.

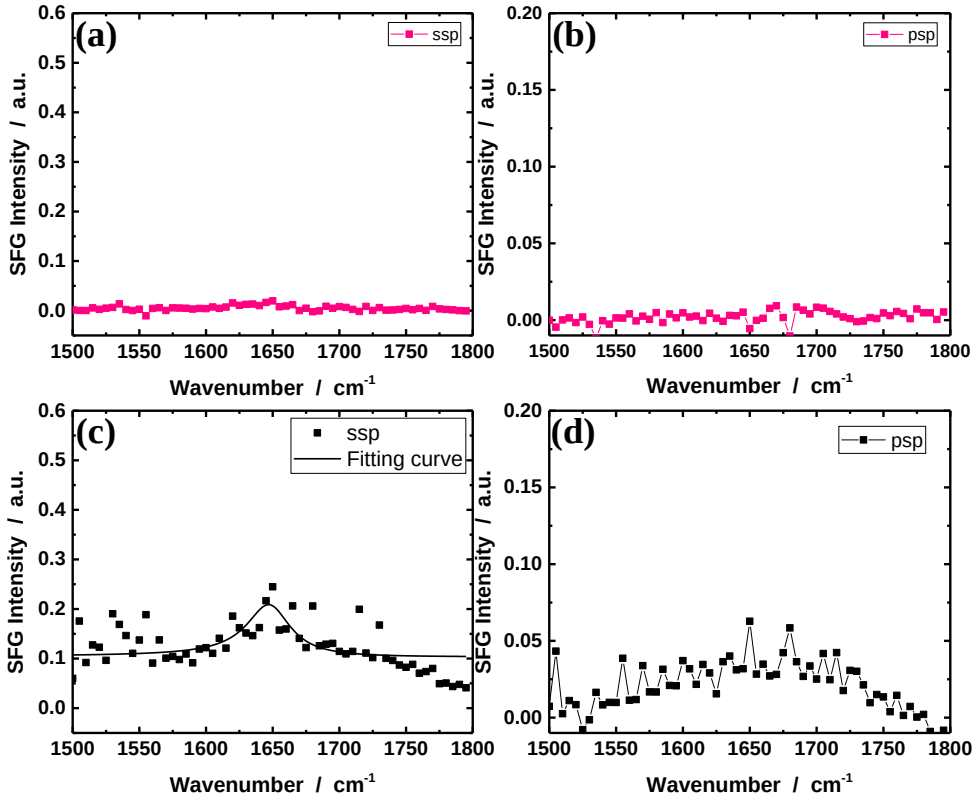

Figure 6.7 Non-chiral (a, c) and chiral (b, d) SFG spectra collected from the interface between silicone oil (with protein) and buffer solution containing 0.2% (a) (b) PS20 or (c) (d) PS80 in the bulk.

Similar to the previous experiments to replace protein solution, here the buffer solution containing surfactant in contact with silicone oil was replaced by a buffer solution (with no surfactant) and the process was repeated for three times. SFG spectra were then collected from the silicone oil/buffer solution interface after the system reached equilibrium (Figure 6.8), SFG signals were similar to what were observed before the buffer washes. No SFG protein signals were detected from the interface between silicone oil and buffer (used to wash the silicone oil surface originally in contact with a buffer containing PS20). For the interface between silicone oil and buffer (used to wash the silicone oil surface originally in contact with a buffer containing PS80), weak SFG alpha helical signal

of protein at the interface was detected (Figure 6.8c), indicated by a single peak at 1650 cm^{-1} observed by ssp SFG. For the same interface, no SFG beta-sheet signal was detected. This indicates that the influence of surfactant on interfacial proteins is irreversible and stable. There is no interfacial protein structural change after buffer washing.

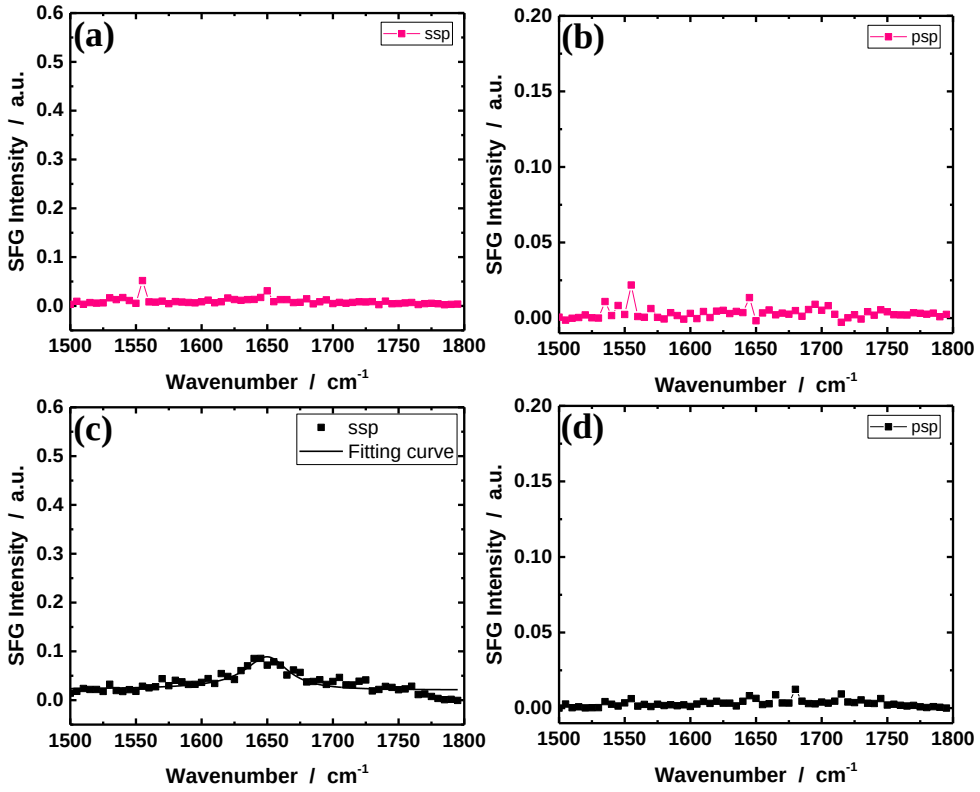

Figure 6.8 Non-chiral (ssp, a, c) and chiral (psp, b, d) SFG spectra collected from the silicone oil/buffer solution interface after replacing the buffer containing PS20 (a, b) or PS80 (c, d).

From the above buffer (without surfactants) washing experiments, we believed that after exposure to a surfactant solution, the originally adsorbed proteins on the silicone oil surface were mainly removed by surfactants. Protein reorientation to a random orientation should not be a dominating process. Otherwise after washing the interface three times with

buffer without containing surfactants, the protein orientations should recover to those before surfactant contact, which was not observed here. Here we concluded that surfactants could remove the originally adsorbed proteins at the silicone oil interface, while PS20 has a stronger effect than PS80. It has been extensively demonstrated in the literature that surfactants could effectively remove adsorbed proteins on hydrophobic surfaces.[2] Here silicone oil surface is hydrophobic, therefore it is feasible to remove the adsorbed fusion proteins on silicon oil surfaces. As discussed above, the different result obtained here compared to those published in ref.12 should be due to the different surfactant concentrations used in the experiments. More detailed concentration dependent surfactant effect will be investigated in the future.

6.3.3.2 Protein Adsorption at Surfactant Pre-Adsorbed Silicone-oil Surfaces

Our above research indicated that surfactants could interact with and remove protein molecules at the silicone surface. However, we do not know whether those proteins removed by the surfactants denatured or not. Here we studied protein behaviors at the silicone oil surface with pre-adsorbed surfactant molecules. We hope that the pre-adsorbed surfactants can minimize or prevent protein adsorption to the surface so that proteins could hold their native structure in solution. After a layer of silicone oil was prepared on a substrate surface, the silicone oil surface was placed in a 0.2 % PS20 or 0.2 % PS80 buffer solution for 20 mins. SFG spectra were then collected from the silicone oil/surfactant solution interface (Figure 6.9). For the ssp spectrum collected from the silicone oil/PS20 solution interface, a single peak at 1710 cm^{-1} was detected (Figure 6.9a). This signal is contributed by the C=O stretching mode of PS20, indicating the ordered PS20 molecules

on the silicone oil surface. Since carbonyl groups are not chiral, no SFG signals were observed in the psp SFG spectrum (Figure 6.9b). For the silicone oil/PS80 solution interface, no SFG signal was observed in ssp or psp SFG spectra (Figures 6.9c and d). PS80 molecules are more randomly distributed on the silicone oil surface as compared to PS20.

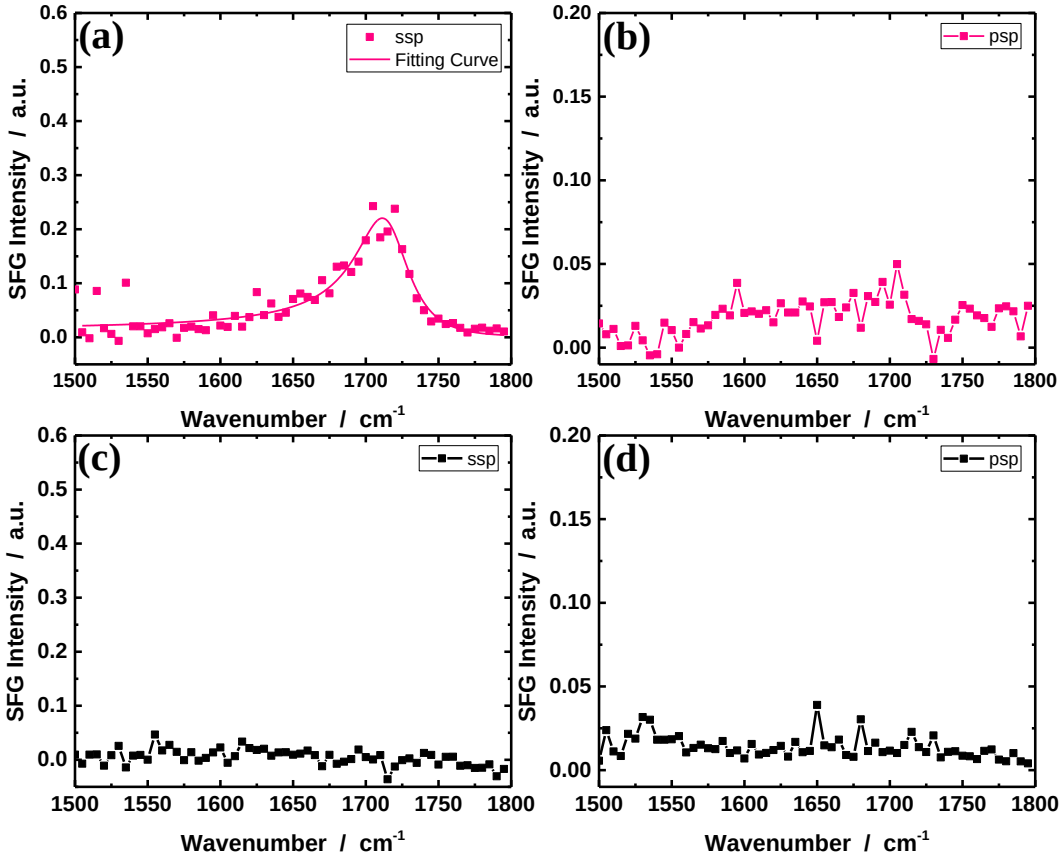

Figure 6.9 Non-chiral (ssp, a, c) and chiral (psp, b, d) SFG spectra collected from interfaces between silicone oil and buffer solution containing 0.2% (a) (b) PS20 or (c) (d) PS80.

After contacting the silicone oil surface with a surfactant solution for 20 mins, the surfactant solution was replaced by a buffer solution with no surfactant and this process was repeated for three times to remove loosely bound surfactant molecules on the silicone

oil surface. SFG spectra were then collected from the silicone oil (with pre-adsorbed surfactant)/buffer solution interface and no SFG signal change was observed (data not shown). Protein solution (1.0 mg/ml) was then placed in contact with the silicone oil surface (with pre-adsorbed surfactant) for 30 mins. This process was monitored by time-dependent SFG signal at 1650 cm^{-1} *in situ* (data not shown), only weak SFG signal was observed. After 30 mins, the SFG signal had no further change. SFG spectra were then collected from the silicone oil (with pre-adsorbed surfactant)/protein solution interface (Figure 6.10). For the PS20 case, a weak SFG peak at 1710 cm^{-1} was observed, showing the presence of PS20 at the interface. For both PS20 and PS80 cases, extremely weak signal at 1650 cm^{-1} was observed in the ssp spectra (Figure 6.10a and c), and no signal was detected in the chiral psp spectra. We believe that the pre-adsorbed surfactants can greatly reduce the adsorption of protein molecules to the silicone oil interface. However, they could not completely prevent the protein adsorption. Weak SFG signal contributed from the alpha helical secondary structure was detected for both cases. The absence of beta-sheet detection in the chiral spectra may be due to the fact that the signal is too weak to be seen (buried in the noise).

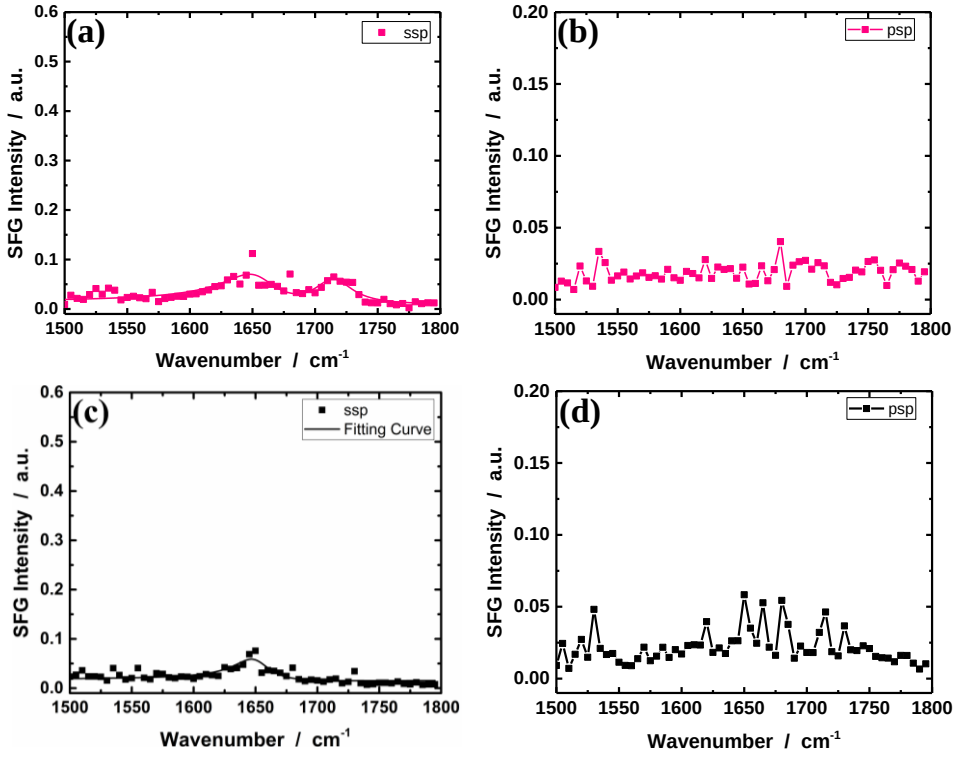

Figure 6.10 Non-chiral (ssp, a, c) and chiral (psp, b, d) SFG spectra collected from silicone oil (with pre-adsorbed (a) (b) PS20 and (c) (d) PS80)/protein solution interfaces.

Surfaces were then washed as what was done previously: the protein solution was replaced by buffer and this process was repeated for three times. SFG spectra were then collected from the silicone oil/buffer interface (Figure 6.11). SFG spectra exhibited no change, indicating that the small amount of protein adsorbed on surfactant pre-adsorbed silicone oil surface is mainly irreversible and stable. This also shows that the above weak signal is not due to the random orientation of the adsorbed proteins. Instead, the weak signal is due to the small amount of proteins, showing that pre-adsorbed surfactants could greatly reduce the protein adsorption to the silicone oil interface.

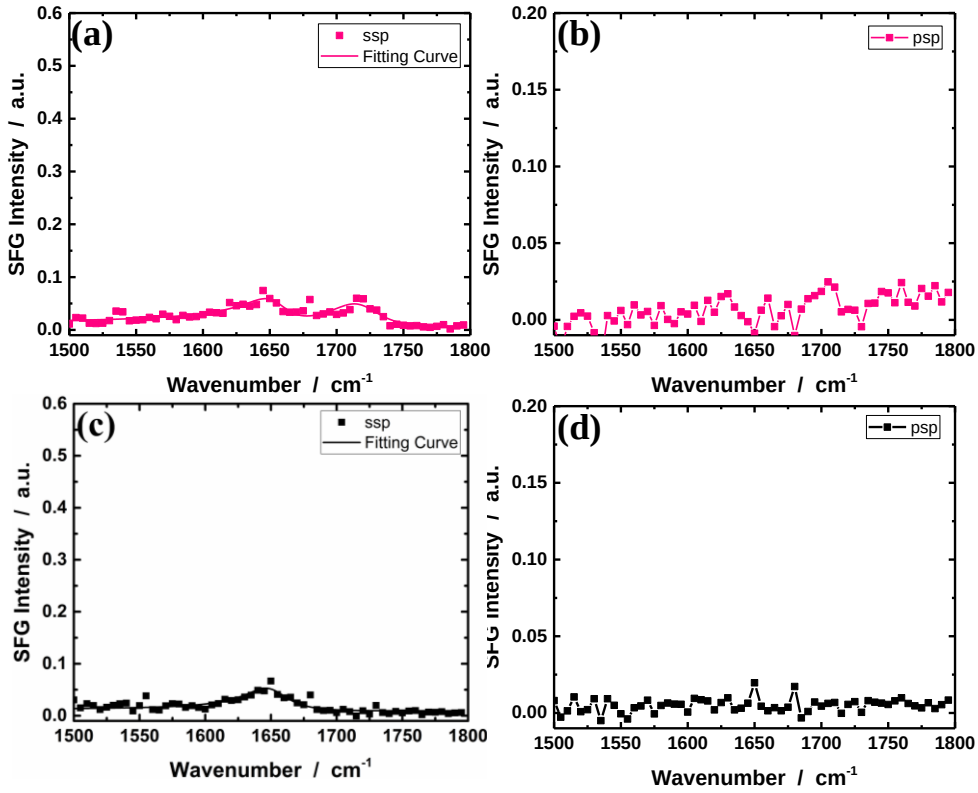

Figure 6.11 Non-chiral (ssp, a, c) and chiral (psp, b, d) SFG spectra collected from silicone oil (with pre-adsorbed surfactant)/buffer solution interface after the protein solution was replaced by buffer and washes three times. Pre-adsorbed (a) (b) PS20 and (c) (d) PS80 cases were investigated.

6.3.3.3 Co-adsorption of Protein and Surfactant Solution

As we presented in the previous section, pre-adsorbed surfactant could reduce the protein interfacial adsorption. This may happen via a different interfacial interaction (previously protein-silicone interaction but now surfactant-protein interaction) or a bulk interaction (e.g., form a protein/surfactant complex). Nevertheless, the protein-surfactant interaction is crucial. To better understand the effect of surfactant – protein interaction on protein adsorption, here we studied interactions between silicone oil and a mixture of protein (1.0 mg/ml) and 0.2% surfactant (PS20 or PS80) buffer solution.

Such a mixture solution was placed in contact with a silicone oil surface. The time-dependent SFG signal showed that the interface reached equilibrium after 30 mins (not shown), and then SFG spectra were collected from silicone oil/protein + surfactant mixture solution interfaces, shown in Figure 6.12. After contacting the mixture of protein and PS20 buffer solution, a single peak at 1710 cm^{-1} was observed, from PS20 molecules in the ssp SFG spectrum, indicating that PS20 molecules are ordered at the interface. Almost no SFG amide I signals of alpha helical or beta-sheet structures were observed, indicating that the presence of PS20 in protein solution reduced or prevented protein adsorption onto the silicone oil surface. Moreover, consistent with what was observed before, in the presence

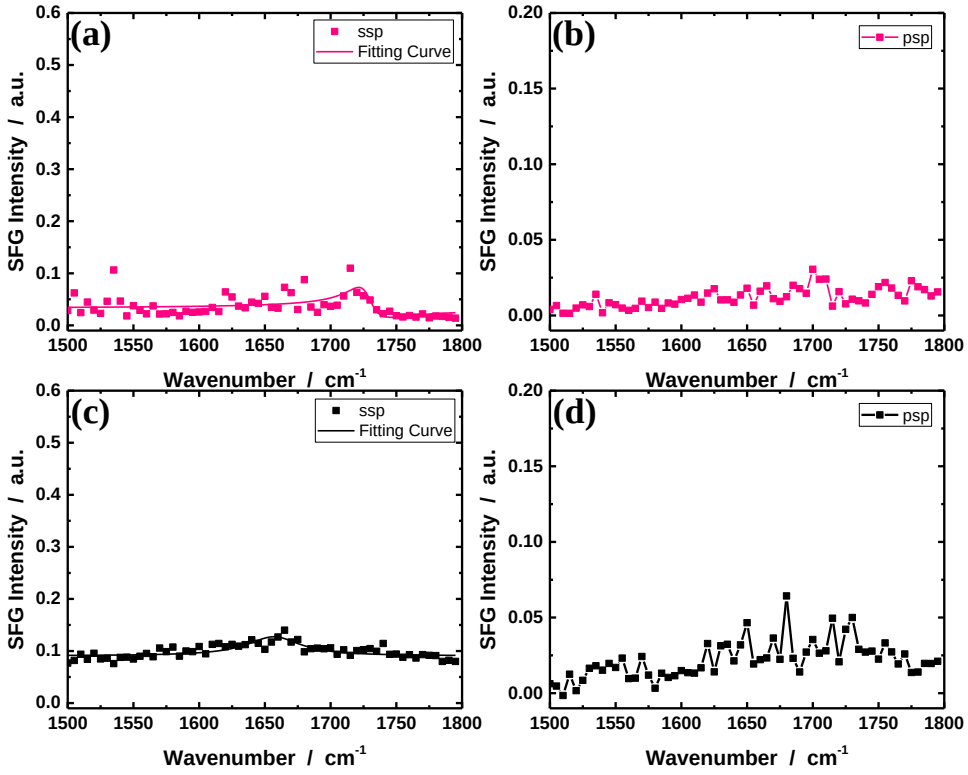

Figure 6.12 Non-chiral (ssp, a, c) and chiral (psp, b, d) SFG spectra collected from silicone oil/protein + 0.2% (a) (b) PS20 and (c) (d) PS80 surfactant mixture solution interfaces.

of surfactants, no beta-sheet conformation was found in the psp spectrum. However, after contacting the silicone oil surface with a mixture of protein and PS80 buffer solution, a small peak centered at 1650 cm^{-1} was observed, shown in Figure 6.12c, but much weaker compared to what was observed previously. Similar to the results from the protein/PS20 mixture, no signal from beta-sheet conformation of protein at the interface was observed in the chiral SFG psp spectrum. This shows that PS20 in the protein solution could more effectively reduce the protein adsorption to the silicone oil interface, consistent with our results above on surfactant replacement of originally adsorbed proteins.

These surfaces were then washed as what was done previously, with a buffer for three times. After these washes, SFG signals were collected from the silicone oil/buffer interfaces. Almost no change in SFG spectra was observed, indicating that the previous silicone oil/protein-surfactant mixture solution interfaces are stable, and the addition of surfactants to the protein solutions reduced/minimized protein adsorption to the silicone oil interface.

6.4 CONCLUSION

In this chapter, we investigated the molecular behavior of proteins at silicone oil interfaces. It was found that the fusion protein studied here aggregated to the silicone oil/protein solution interface with ordered alpha helical and beta-sheet secondary structural domains. The adsorbed proteins at the silicone oil interfaces are stable with a steady structure because buffer washes could not alter the SFG signal collected from the interfacial proteins. The effects of surfactants including PS20 and PS80 on the protein molecular

behaviors at the silicone oil interface were examined in detail. We introduced the surfactants into the system using three different methods: (1) Adsorbed proteins on silicone oil were placed in contact with buffer solutions containing surfactants; (2) Pre-adsorbed surfactants on silicone oil surface were placed in contact with protein solutions; and (3) Surfactants were mixed into the protein solutions and then contacted with silicone oil. In all three methods, surfactants could greatly reduce the silicone oil-protein interaction, leading to substantially less adsorption of protein molecules to the silicone oil interface. The PS20 surfactant has a better protein adsorption reduction effect compared to PS80.

It has been shown previously that surfactants could influence the protein adsorption at the silicone oil interfaces. The surfactant effect can be caused by a faster adsorption of the surfactants to the interface (to reduce interfacial protein adsorption), a stronger interaction between the proteins and surfactants in solution, and/or a stronger interface-surfactant interaction than the interface-protein interaction. It is known that PS80 is more surface active (due to its long and unsaturated chain) and may have a weak protein interaction than PS20.[2] Here the more reduced protein adsorption effect to silicone oil surface for PS20 observed in the mixed solution adsorption experiment may be because the protein – surfactant interaction in solution plays a major role, instead of the fast adsorption of the surfactant to the interface. Also the fact that PS20 has a stronger effect to reduce the pre-adsorbed protein on the silicone oil surface may also be because of a stronger interaction between the protein and PS20, which leads to an easier removal of the protein from the interface. The similar effect on protein adsorption reduction at the interface was observed for pre-adsorbed PS20 and PS80, because the overall interaction

between surfactants and proteins are both very weak (much weaker than the silicone oil – surfactant interactions), leading to no observed difference (while the slight difference in protein interaction of PS20 vs. PS80 does not play a role).

In this chapter we applied SFG to directly investigate the molecular behavior of proteins at buried interfaces *in situ*, which has not been probed before. Our studies can provide molecular level information about protein structure and monitor the protein behavior using molecular signatures or vibrational fingerprints.

6.5 REFERENCES

1. M. C. Manning, K. Patel and R. T. Borchardt, *Pharmaceutical research*, 1989, **6**, 903-918.
2. H. J. Lee, A. McAuley, K. F. Schilke and J. McGuire, *Advanced drug delivery reviews*, 2011, **63**, 1160-1171.
3. M. Soderquist and A. Walton, *Journal of Colloid and Interface Science*, 1980, **75**, 386-397.
4. J. D. Andrade, *Plenum Press*, 1985, 470.
5. P. Roach, D. Farrar and C. C. Perry, *Journal of the American Chemical Society*, 2005, **127**, 8168-8173.
6. K. Nakanishi, T. Sakiyama and K. Imamura, *Journal of Bioscience and Bioengineering*, 2001, **91**, 233-244.
7. R. K. Bernstein, *Diabetes care*, 1987, **10**, 786-787.
8. L. S. Jones, A. Kaufmann and C. R. Middaugh, *Journal of pharmaceutical sciences*, 2005, **94**, 918-927.
9. R. Thirumangalathu, S. Krishnan, M. S. Ricci, D. N. Brems, T. W. Randolph and J. F. Carpenter, *Journal of pharmaceutical sciences*, 2009, **98**, 3167-3181.
10. J. S. Bee, T. W. Randolph, J. F. Carpenter, S. M. Bishop and M. N. Dimitrova, *Journal of pharmaceutical sciences*, 2011, **100**, 4158-4170.
11. S. Mollmann, U. Elofsson, J. Bukrinsky and S. Frokjaer, *Pharmaceutical research*, 2005, **22**, 1931-1941.

12. N. Dixit, K. M. Maloney and D. S. Kalonia, *International journal of pharmaceutics*, 2012, **429**, 158-167.

13. J. Li, S. Pinnamaneni, Y. Quan, A. Jaiswal, F. I. Andersson and X. Zhang, *Pharmaceutical research*, 2012, **29**, 1689-1697.

14. N. B. Bam, J. L. Cleland, J. Yang, M. C. Manning, J. F. Carpenter, R. F. Kelley and T. W. Randolph, *Journal of pharmaceutical sciences*, 1998, **87**, 1554-1559.

15. Y. Shen, *Nature*, 1989, **337**, 519-525.

16. Y. Li, S. Wei, J. Wu, J. Jasensky, C. Xi, H. Li, Y. Xu, Q. Wang, E. N. G. Marsh, C. L. Brooks III and Z. Chen, *The Journal of Physical Chemistry C*, 2015, **119**, 7146-7155.

17. Z. Chen, Y. Shen and G. A. Somorjai, *Annual review of physical chemistry*, 2002, **53**, 437-465.

18. X. Chen, M. L. Clarke, J. Wang and Z. Chen, *International Journal of Modern Physics B*, 2005, **19**, 691-713.

19. J. Wang, M. A. Even, X. Chen, A. H. Schmaier, J. H. Waite and Z. Chen, *Journal of the American Chemical Society*, 2003, **125**, 9914-9915.

20. J. Wang, X. Chen, M. L. Clarke and Z. Chen, *Proceedings of the National Academy of Sciences of the United States of America*, 2005, **102**, 4978-4983.

21. X. Chen, J. Wang, J. J. Sniadecki, M. A. Even and Z. Chen, *Langmuir*, 2005, **21**, 2662-2664.

22. M. L. Clarke, J. Wang and Z. Chen, *The Journal of Physical Chemistry B*, 2005, **109**, 22027-22035.

CHAPTER 7 Conclusion and Outlook

This dissertation studied the chemical immobilization of biomolecules including peptides and proteins on solid surfaces which has been widely used in many important applications such as antibacterial materials, antifouling coatings, catalysis, drug delivery, biosensors, biochips and biofuel cells. The performance of such surfaces with immobilized biomolecules is largely affected by properties of solid supports, tethering sites of biomolecules, immobilization methods, biomolecule orientations after surface immobilization, and the surrounding environment, which have not been thoroughly investigated previously. This dissertation focuses on the study of structure-property relation of surface immobilized biomolecules by systematically studying the molecular structure (conformation and orientation) of surface immobilized biomolecules under a variety of different conditions and properties of these surface immobilized biomolecules. The knowledge obtained in this study will allow for better designing and engineering of biomolecule immobilized surfaces with optimized performance and activity.

Methods of maintaining the structure and function of proteins and peptides under harsh conditions were also developed in this thesis. For example, approaches to maintain the conformation, orientation, and function of surface immobilized biomolecules, including peptides and proteins, at low humidity conditions, were explored. For peptides and proteins at interfaces, removal of bulk water in the environment often destroys the

native structures of these biological molecules and reduces their functions, especially at ambient or higher temperatures. This substantially limits the utility of bio-composite materials in non-aqueous environments (e.g., in air). This work provides important guidance to develop strategies to retain the structures/functions of biomolecule immobilized surfaces under harsh conditions.

In order to have a better understanding of the molecular behaviors of biomolecules on surfaces/at interfaces, sum frequency generation vibrational spectroscopy (SFG) was applied in this dissertation to study several different biomolecule systems, with peptide/protein molecules immobilized/adsorbed at different surfaces/interfaces under different conditions, aiming to elucidate the structure-function relationships of these interfacial biomolecules. Previously, surface sensitive techniques, including SPR, XPS, AFM, ATR-FTIR, have all been widely applied to study the interfacial biomolecules. However, such methods either require special sample preparation or instrument operational conditions (such as high vacuum, require extensive labeling), or cannot provide detailed, molecular-level structural information of the molecules of interest at the surface/interface *in situ* at ambient conditions. With the combined use of SFG and the above mentioned analytical tools, the research presented in this thesis provided detailed, molecular-level structural information of surface/interface biomolecules *in situ*, and correlated such structure to the performance or activity of such biomolecules, leading to a better understanding of the molecular behaviors of biomolecules at surfaces/interfaces,

In Chapter 2, AMPs chemically immobilized onto surfaces through different termini were examined in detail. Peptides immobilized via different termini adopt similar

secondary structures but different orientations in phosphate buffer solution. Such a difference in orientation lead to varied antimicrobial efficiencies of the peptides examined by anti-bacterial tests. With the help of MD simulations, we could identify the amino residues that have stronger interactions with the substrate surface. After mutating these amino acids, we were able to vary peptide orientation after surface immobilization. Such an orientation of the new (mutant) peptide could be predicted and validated by SFG study. In general, this chapter made the following two breakthroughs: (1) Surface orientations of the immobilized peptides are well correlated to their antimicrobial activities; (2) A general method of combined MD simulation/SFG study was developed to tune the peptide sequence and control its orientation after surface immobilization.

Chapter 3 moves on to the study of more complicated systems of surface immobilized biomolecules: enzymes. We found that enzymes with neighboring immobilization sites adopt similar conformation and orientation after surface immobilization. Also, the enzymatic activity is lower when the immobilization site is close to the enzyme active site. For such a case, an increase in the enzymatic activity was successfully achieved by designing a new underlying surface with higher hydrophilicity, through reducing the interaction of this underlined substrate surface with enzymes. The weakened enzyme-surface interaction leads to more flexibility of the surface immobilized biomolecules (with a broader orientation distribution). The work in this chapter demonstrated that the desired orientation of surface immobilized enzymes can be achieved by site specific engineering and surface immobilization. It also indicates that by making the surface more hydrophilic, the activity of immobilized enzyme can be enhanced.

Chapter 4 and Chapter 5 developed strategies using hydro-mimetic functionalities to retain the conformation and orientation of surface immobilized biomolecules in the absence of bulk water. It was found that spin-coated sucrose can retain both conformation and orientation of immobilized peptides and proteins in air. Moreover, the orientation of surface immobilized peptides can be controlled and step-wisely varied by tuning the concentration of the sucrose solution used for coating. However, the antimicrobial activity of the immobilized peptides and the enzymatic activity of the immobilized enzymes could not be tested because the bacteria or substrate molecules were blocked by such a sucrose coating created on top of the peptides and proteins in air. To address this issue, hydro-mimetic sugar molecules were chemically attached to either immobilized peptides or substrate surfaces (CVD polymer surfaces). Using such methods, we successfully enhanced the antimicrobial activity of immobilized AMPs in the absence of bulk water. The activity increase is likely due to the correct structure and orientation retained by the tethered (or co-immobilized) sugar molecules. The detailed mechanism is under the current investigation.

Other than surface immobilization, Chapter 6 studied the conformation of protein molecules adsorbed at silicone oil surfaces. It was the very first time that SFG was applied to study pharmaceutical related fusion proteins at a solid/liquid interface. It was found that the fusion protein we studied tends to aggregate at silicone oil/protein solution (or buffer) interface with both ordered alpha helical and beta sheet domains. Interestingly, nonionic surfactants could effective minimize or even prevent the protein aggregation to the silicone

oil surface. This result is very important since protein drug molecules could denature and lose activity after the surface aggregation.

In summary, the research reported in this dissertation made important contribution in the following two aspects: (1) A combined study using SFG, CD, ATR-FTIR, and MD simulations was successfully performed to study bio-interfaces. SFG can provide detailed structural (e.g., conformational and orientational) information of biomolecules at interfaces *in situ*. However, SFG studies also have limitations. By combining several analytical tools, we are able to obtain a more complete picture of the molecular behaviors of biomolecules at interfaces and found that their functions are directly related to the structures which are mediated by biomolecule sequence, tethering site, underlying surface properties, and the surrounding environment. MD simulation results are able to provide a more detailed understanding on the experimental results. At the same time, MD simulations could predict peptide interfacial structure and its relationship with peptide sequence, which could be validated by SFG and CD experiments; (2) The successful use of hydro-mimetic groups to retain the structure of immobilized peptides and enhance their activity in the absence of bulk water. This provides important fundamental information and insights for the future design of hydro-mimetic materials for the preservation of enzyme structure and improvement of enzyme activity under non-aqueous conditions.

In the future, further research could be carried out to provide in-depth understanding of peptides and proteins at interfaces:

(1) In this thesis, we only studied the structures (e.g., conformations and orientations) of surface immobilized peptides in different environments. However, the detailed mechanism of how such immobilized AMPs with different structures lead to varied activities has not been elucidated. To further understand such a mechanism, studying peptide structure dynamically is very important. The surface immobilized peptide structure during the peptide-bacteria interaction should be investigated in real time in the future, which will help understand the detailed mechanism of how AMPs tethered on surface disrupt bacterial cell membranes and will provide valuable information for designing effective antimicrobial surfaces.

(2) We designed strategies to use hydro-mimetic functionalities to enhance the anti-bacterial activity of surface immobilized peptides in air. However, for certain cases (e.g., direction immobilization of hydro-mimetic molecules to surface immobilized peptides), no structural difference was observed from surface immobilized peptides with or without attached hydro-mimetic molecules. Therefore the antimicrobial activity enhancement mechanism is unclear. It may be because the peptides with hydro-mimetic molecules attached have different structures from those without hydro-mimetic molecules only when they are interacting with bacteria. Experiments that will study such real time interactions should be performed using the method developed in (1). Such in-depth understanding will help further develop water-free biologics with hydro-mimetic molecules.

(3) We found that a hydrophilic surface has the ability to reduce surface-enzyme interactions in order to enhance the enzymatic activity of the immobilized enzymes. In the

future, a systematic study of the effects of surface properties on immobilized enzyme structures and activities can be investigated.

(4) In this thesis, coarse grained MD simulations were successfully applied to study and predict the structure and orientation of surface immobilized biomolecules in aqueous buffer solution. However, as we discussed, the structure and function of immobilized biomolecules in harsh conditions in the absence of bulk water are very important. Such simulation methodologies can be optimized to study surface immobilized biomolecules under such conditions (e.g., in the absence of bulk water). This will provide guidance for water-free experiments and help understand the protein behavior under non-aqueous conditions.

(5) Molecular dynamics simulations can be used to study interactions between hydro-mimetic molecules and surface immobilized peptides, providing further understanding on how hydro-mimetic functionalities help to retain the interfacial peptide/proteins structures and enhance their functions.

(6) Fusion protein adsorbed at silicone oil surfaces were studied in this thesis. SFG can also be applied to study more pharmaceutical related protein therapeutics, such as antibodies in the future.